DEPARTMENT OF THE INTERIOR
U.S. GEOLOGICAL SURVEY

Capillary Correction for Acid-Etch Inclinometry in Boreholes for Glass Tubes Ranging in Diameter from 6 – 25 mm and Over a Temperature Range of 4 – 80 °C Including Statistical Analysis of the Data

by

T. C. Urban[1] and W. H. Diment[1]

Open-File Report 89-632

[1] U.S. Geological Survey, Denver, Colorado 80225

TABLE OF CONTENTS

ABSTRACT

An old technique for measuring the inclination of a borehole is to lower a suitably encased glass tube partially filled with a dilute aqueous solution of hydrofluoric acid, let it sit until a line is etched on the interior of the tube, retrieve the tube, and measure the dip angle of the line etched into the tube. This angle is a measure of the inclination of the borehole at the depth of measurement. And, were it not for capillary forces at the meniscus between liquid and gas, the measured, apparent angle would be a true measure of the inclination. Correction for capillarity is known to be significant at room temperature for tubes about 25 mm in diameter. The correction is zero at 0 and 90 degree true angles and reaches a maximum at 45 true degrees.

We determined corrections at 4°, 10°, 22°, 40°, 60°, and 80 °C for nominal tube diameters of 6, 10, 13, 16, 19, 20, and 25 mm for the purpose of extending the technique to hot, small-diameter boreholes. We plotted the etched angle versus the true inclination at 5-degree intervals for each temperature and found statistically that an arc of a circle of radius R, where R is a function of both temperature (T) and tube diameter (D), fitted the data. For each tube diameter $(\partial R/\partial T)_D$ is positive and nearly constant for all tube diameters at temperatures above 40 °C. Below 40 °C this derivative is nonconstant and decreasing with tube diameter. $(\partial R/\partial D)_T$ is nearly a constant over the range of diameters although alternative curves could be used to fit the data.

INTRODUCTION

Sophisticated equipment exists for the measurement of the inclination and azimuth with depth in large diameter boreholes. Our interest is in determining the inclination of relatively shallow (usually less than 800 m deep) boreholes of small diameter (< 8 cm) in geothermal areas. Often these boreholes penetrate altered volcanic rocks of high plasticity which remain open only through insertion of small diameter tubing, sometimes threaded through stuck drill pipe (e.g., Benoit, 1984; Urban, *et al.*, 1987). So the effective opening may be less than 5 cm in diameter, or even less in the case of kinked holes, which may be common in areas of active hydrothermal alteration, tectonic deformation, and landslides.

Certainly, high-tech devices could be constructed to measure the inclination and azimuth in such holes, but they would have to be thin, capable of withstanding ambient temperatures of about 200 °C and operative in steel casing, tubing, or drill rod.

Lacking such devices, we resorted to acid-etch inclinometry which has long been used in the mining industry, where glass tubes of about 25 mm diameter are commonly used and where corrections for capillarity have been measured near room temperature. Although the equipment is inexpensive, there is a bit of art involved in both field and laboratory. Many useful rules-of-thumb as to technique and interpretation have been developed over the years (e.g., Cumming, 1951; Cumming and Wicklund, 1980; Peele, 1941; Staley, 1964). We make no attempt to repeat them here, except to emphasize that this is a highly empirical technique and procedures followed in the laboratory should be followed as closely as possible in the field in order to achieve reliable results.

THEORY

General method of least squares curve fitting. In analyzing data, the two basic methods of curve fitting involve either fitting a curve through every point or fitting a curve which does not pass through every point but preserves the essential characteristics of the data. An interpolation formula is the most likely method used in the former case. However, if the number of points is large, the uncertainties in the data are large, or there are theoretical grounds for using a specific functional form, then the latter method is more appropriate. Since we have assumed a functional form for our analysis, the method of least squares will be used rather than a interpolating formula.

The method of least squares is based on the assumption that the observed values are distributed about the true values. That is to say, if the experiment were repeated many times and the average values calculated, then the average value would converge to the true value. This assumption will hold insofar as systematic errors, errors that cause the observed values to be consistently larger or smaller than the true values, do not affect the experiment. In our analysis we will assume that the distribution is normal although it would not necessarily have to be (Wolberg, 1967, p. 30).

The residuals are defined as the difference between the observed (X_{ji}, Y_i) and calculated (x_{ji}, y_i) values:

$$R_{y_i} = Y_i - y_i \tag{1}$$

$$R_{x_{ji}} = X_{ji} - x_{ji}. \tag{2}$$

The weights are defined as the reciprocals of the squares of the uncertainties:

$$w_{y_i} = \frac{1}{{\sigma_{y_i}}^2} \tag{3}$$

$$w_{x_{ji}} = \frac{1}{{\sigma_{x_{ji}}}^2}, \tag{4}$$

also known as statistical weighting (Wolberg, 1967, p. 32). The weighted sum of the squares of the residuals is S:

$$S = \sum_{i=1}^{n} \left[w_{y_i} R_{y_i}^2 + \sum_{j=1}^{m} w_{x_{ji}} R_{x_{ji}}^2 \right]. \tag{5}$$

If the functional relationship between the dependent (η_i) and independent (ξ_{ji}) variables is

$$\eta_i = f\left(\xi_{1i}, \xi_{2i} \ldots, \xi_{mi}; \alpha_1, \alpha_2, \ldots, \alpha_p\right), \tag{6}$$

then the method of least squares determines the α_i such that S is minimized. For the calculated variables

$$y_i = f\left(x_{1i}, x_{2i} \ldots, x_{mi}; A_1, A_2, \ldots, A_p\right), \tag{7}$$

Solution for the general case of one independent variable. Some simplifications are in order for our application. Since p and m = 1 in equation 5:

$$S = \sum_{i=1}^{n} \left[w_{y_i} R_{y_i}^2 + w_{x_i} R_{x_i}^2 \right]. \tag{8}$$

and

$$y_i = f\left(x_i; A_1\right). \tag{9}$$

Wolberg (1967, p. 39-45) describes a method of determining A_1. We can denote

$$F^i = y_i - f\left(x_i; A_1\right) \tag{10}$$

which implies

$$F^i = 0, i = 1, 2, \ldots, n. \tag{11}$$

Derivatives will be noted by subscripts

$$F_{x_i}^i = \frac{\partial F^i}{\partial x_i}, \quad F_{y_i}^i = \frac{\partial F^i}{\partial y_i}, \quad F_{A_1}^i = \frac{\partial F^i}{\partial A_1} \tag{12}$$

Because A_1 does not enter linearly in the functional form of the circle:

$$(x + A_1)^2 + (y - (90 + A_1))^2 = R^2 \tag{13}$$

the usual method of differentiating equation 8 and setting the derivatives equal to zero will not produce a solvable series of normal equations. Instead we must use a method called successive approximation (Hald, 1952, p. 652) to produce a linear function of the variables that can be solved by the normal equations. If A_{10} is the initial guess of A_1 then

$$B_1 = A_{10} - A_1 \tag{14}$$

can be made linear in the normal equations. Through the use of Lagrange multipliers it can be shown that the set of normal equations reduces to (Wolberg, 1967, p. 39-42)

$$B_1 \left[\frac{F_{A_1} F_{A_1}}{L}\right] = \left[\frac{F_{A_1} F_0}{L}\right] \tag{15}$$

where we have dropped the subscript i, the brackets [ ] denote the summation over i, the derivatives are defined by equation 12,

$$L_i = \sigma_{y_i}^2 + (F_{x_i} \cdot \sigma_{x_i})^2 \tag{16}$$

and

$$F_0^i = Y_i - f(X_i; A_{10}) . \tag{17}$$

Equation 15 may be simplified by using matrix notation

$$C_1 = \left[\frac{F_{A_1} F_{A_1}}{L}\right] \tag{18}$$

and

$$V_1 = \left[\frac{F_{A_1} F_0}{L}\right] . \tag{19}$$

Substituting into equation 15:

$$C_1 \cdot B_1 = V_1 \tag{20}$$

B_1 is solved by multiplying both sides by the inverse coefficient matrix C_1^{-1}

$$C^{-1} \cdot C \cdot B = C^{-1} \cdot V \tag{21}$$

where we have dropped the subscripts. Although not necessary, we have kept the matrix notation since equation 21 is applicable to p variables, $A_1, \ldots, A_p$ as well as to one variable.

The general procedure is to start with an initial guess A_{10} in equation 17, solve equation 21, use equation 14 to determine A_1 and which becomes, therefore, a new A_{10} and repeat the process until B_1 is reduced to a suitably small value, ϵ. For example,

$$\left|\frac{B_1}{A_1}\right| < \epsilon \tag{22}$$

is one criterion that we have used, although others can be chosen. The advantage of the matrix notation will become evident later when the variances of A_1 and f are calculated.

In addition to calculating the least squares fit for A_1 in equation 13, some test needs to be devised in order to determine whether two circles are really different with different sets of data at different diameters or temperatures.

Statistical analysis. The problem at hand is to decide whether the two circles are identical or not, that is, does the small portion of the two circles represent the same theoretical regression line. To do this we will test the hypothesis

$$H_0 : \alpha_1 = \alpha_2 \tag{23}$$

against the alternative

$$H_1 : \alpha_1 \neq \alpha_2 \tag{24}$$

where the α_i's are the absolute values of the coordinate of the center of the circle $(-\alpha_i, 90+\alpha_i)$.

Variance test of coordinate. If we are to do this we first have to consider the problem of testing the hypothesis

$$H_0 : \sigma^2_{\alpha_1} = \sigma^2_{\alpha_2} \tag{25}$$

against

$$H_1 : \sigma^2_{\alpha_1} \neq \sigma^2_{\alpha_2} \tag{26}$$

under the assumption that α_1 and α_2 are normally distributed. This may be done since the parameters, A_1 and A_2, determined by the least-square analysis are normally distributed about the true parameters, α_1 and α_2, with the least possible standard deviation, σ_i's, (Wolberg, 1967, p. 27-28). It is necessary to establish the equality of the two variances in order to apply the t distribution to test the difference between the two coordinates, that is, $H_0 : \alpha_1 = \alpha_2$ above. If the alternative hypothesis, $H_1 : \sigma_{\alpha_1} \neq \sigma_{\alpha_2}$, is found to be the case but the values of σ_1 and σ_2 are known, then only an approximate Student t distribution can be determined.

The determination of the equality of variances will be based on the following theorem (Hoel, 1962, p. 285):

"Theorem H: If u and v possess independent χ^2 distributions with ν_1 and ν_2 degrees of freedom, respectively, then

$$F = \frac{u/\nu_1}{v/\nu_2} \tag{27}$$

has the F distribution with ν_1 and ν_2 degrees of freedom given by

$$f(F) = CF^{\frac{1}{2}(\nu_1-2)}(\nu_2+\nu_1 F)^{-\frac{1}{2}(\nu_1+\nu_2)} \tag{28}$$

where C is given by..."

$$C = \frac{\nu_1^{\frac{\nu_1}{2}}\nu_2^{\frac{\nu_2}{2}}\Gamma\left(\frac{\nu_1+\nu_2}{2}\right)}{\Gamma\left(\frac{\nu_1}{2}\right)\Gamma\left(\frac{\nu_2}{2}\right)}. \tag{29}$$

Hald (1952, p. 374-387) discusses this theorem as the v^2-distribution. Let $s^2_{A_1}$ and $s^2_{A_2}$ be the sample variances. Then since $n_{A_1}s_{A_1}/\sigma^2_{A_1}$ and $n_{A_2}s^2_{A_2}/\sigma^2_{A_2}$ possess independent χ^2 distributions (Hoel, 1962, Theorem 1, p. 268),

$$\frac{u}{\nu_{A_1}} = \frac{n_{A_1}s^2_{A_1}}{(n_{A_1}-1)\sigma^2_{A_1}} \tag{30}$$

and

$$\frac{v}{\nu_{A_2}} = \frac{n_{A_2}s^2_{A_2}}{(n_{A_2}-1)\sigma^2_{A_2}} \tag{31}$$

will satisfy Theorem 4 and

$$F = \frac{n_{A_1}s^2_{A_1}/(n_{A_1}-1)}{n_{A_2}s^2_{A_2}/(n_{A_2}-1)} \tag{32}$$

will possess the F distribution with $n_{A_1} - 1$ and $n_{A_2} - 1$ degrees of freedom. This states that the value of F used in testing $H_0 : \sigma^2_{A_1} = \sigma^2_{A_2}$ is the ratio of the unbiased estimates of the two variances. It should be noted that this test is independent of population parameters (Hoel, 1962, p. 286).

Student's t-test for coordinate. The next step in the analysis is to test the hypothesis $H_0 : \alpha_1 = \alpha_2$. For this a Student's t test will be used. The simplist formulation involves the assumption of equal variances, which is tested by the F distribution above. If the F test shows that the assumption of equal variances is reasonable, then a significant t value when testing $H_0 : \alpha_1 = \alpha_2$ may not be attributed to $\sigma^2_{A_1} \neq \sigma^2_{A_2}$. It, however, is not the case, if $\sigma^2_{A_1} \neq \sigma^2_{A_2}$ that a significant t value is due to the inequality of the variances. Our starting point for the t test will be the following theorem (Hoel, 1962, p. 273-4):

"Theorem 3: If u is normally distributed with zero mean and unit variance and v^2 has a χ^2 distribution with ν degrees of freedom, and u and v are independently distributed, then the variable

$$t = \frac{u\sqrt{\nu}}{v} \tag{33}$$

has a Student's t distribution with ν degrees of freedom given by

$$f(t) = c\left(1 + \frac{t^2}{\nu}\right)^{-\frac{1}{2}(\nu+1)} \tag{34}$$

where constant c is given in ..."

$$c = \frac{\Gamma\left(\frac{\nu+1}{2}\right)}{\sqrt{\pi\nu}\,\Gamma\left(\frac{\nu}{2}\right)}. \tag{35}$$

One variable that satisfies the properties of u in Theorem 3 is (Hald, 1952, p.388; Wolberg, 1967, p.20; Hoel, 1962, p.274)

$$u = \frac{\bar{x} - \mu}{\sigma/\sqrt{n}}. \tag{36}$$

For v^2 we may use ns^2/σ^2 which also satisfies the requirements of Theorem 3 (Hoel, 1962, p. 268). For these variables the x's are normally distributed with mean μ and variance σ^2 and $\bar{x}$ and s^2 are their sample estimates based on a random sample of size n. In the case of immediate interest

$$u = \frac{(A_1 - A_2) - (\alpha_1 - \alpha_2)}{\sigma_{A_1 - A_2}}. \tag{37}$$

Also,

$$v^2 = \frac{n_1 S_{A_1}^2 + n_2 S_{A_2}^2}{\sigma^2} \tag{38}$$

satisfies the requirements of Theorem 3 with $\nu = n_1 + n_2 - 2$ degrees of freedom, since $\frac{n_1 s_{A_1}^2}{\sigma^2}$ and $\frac{n_2 s_{A_2}^2}{\sigma^2}$ possess independent χ^2 distributions with $n_1 - 1$ and $n_2 - 1$ degrees of freedom. Now

$$\begin{aligned} u &= \frac{(A_1 - A_2) - (\alpha_1 - \alpha_2)}{\sigma_{A_1 - A_2}} \\ &= \frac{(A_1 - A_2) - (\alpha_1 - \alpha_2)}{\sqrt{\frac{\sigma^2}{n_1} + \frac{\sigma^2}{n_2}}} \\ &= \frac{(A_1 - A_2) - (\alpha_1 - \alpha_2)}{\sigma\sqrt{\frac{1}{n_1} + \frac{1}{n_2}}} \end{aligned} \tag{39}$$

with $\sigma_{A_1}^2 = \sigma_{A_2}^2 = \sigma^2$ (Wolberg, 1967, p.22). Therefore,

$$t = \frac{(A_1 - A_2) - (\alpha_1 - \alpha_2)}{\sqrt{n_1 s_{A_1}^2 + n_2 s_{A_2}^2}} \sqrt{\frac{n_1 n_2 (n_1 + n_2 - 2)}{n_1 + n_2}} \tag{40}$$

will have student's t distribution with $n_1 + n_2 - 2$ degrees of freedom. Then, to test the hypothesis $H_0 : \alpha_1 = \alpha_2$, one merely calculates the value of t and compares it to a table of values to see if the sample value of t numerically exceeds the critical value.

If the sample variances are not the same, that is $\sigma_{A_1}^2 \neq \sigma_{A_2}^2$ but the values of σ_{A_1} and σ_{A_2} are known, then one can test the hypothesis $H_0 : \alpha_1 = \alpha_2$ by the standard normal variable (Hoel, 1962, p. 298):

$$\begin{aligned} \tau &= \frac{(A_1 - A_2) - (\alpha_1 - \alpha_2)}{\sigma_{A_1 - A_2}} \\ &= \frac{(A_1 - A_2) - (\alpha_1 - \alpha_2)}{\sqrt{\frac{\sigma_{A_1}^2}{n_1} + \frac{\sigma_{A_2}^2}{n_2}}} \end{aligned} \tag{41}$$

Since the values of the variances are seldom known, they are replaced by their estimated values, $s_{A_1}^2$ and $s_{A_2}^2$.

The variable

$$t = \frac{(A_1 - A_2) - (\alpha_1 - \alpha_2)}{\sqrt{\frac{s_{A_1}^2}{n_1} + \frac{s_{A_2}^2}{n_2}}} \tag{42}$$

can be shown to possess an approximate Student's t distribution (Hoel, 1962, p.279). The number of degrees of freedom necessary to make this variable an approximate t variable is given by

$$\nu = \frac{\left(\frac{s_{A_1}^2}{n_1} + \frac{s_{A_2}^2}{n_2}\right)^2}{\frac{\left(\frac{s_{A_1}^2}{n_1}\right)^2}{n_1+1} + \frac{\left(\frac{s_{A_2}^2}{n_2}\right)^2}{n_2+1}} - 2 \tag{43}$$

which is usually not an integer. One merely chooses the nearest integer value in looking up critical values of t. A similar relationship is determined by Hald (1952, p. 397-398).

Student's t-test for function. Although the Student t-test for the coordinate, A, where the center of the circle is $(-A, 90 + A)$ may or may not show that two curves have the same center, a further test is required in order to distinguish between regression lines for two distinctly different temperatures. The reason for this is that all of the curves, even those for different tube sizes, go through the points (0,0) and (90, 90). That is to say, at 0 and 90 degree dip of the tube the true and apparent angles are the same. A further test can be made at 45 degrees which is the angle of maximum departure. If a t-test indicates that there is significance at this angle, then one can conclude that the two regression lines represent different theoretical regression lines. Let f(x;A) represent the least squares regression line, $\gamma(x; A)$ is the theoretical regression line, and the unbiased estimate of σ_f is denoted as s_f. Then as before we intend to test the hypothesis

$$H_0 : \gamma(x; \alpha_1) = \gamma(x; \alpha_2) \tag{44}$$

against the alternative hypothesis

$$H_1 : \gamma(x; \alpha_1) \neq \gamma(x; \alpha_2). \tag{45}$$

To simplify notation we will drop the paratheses and use subscripts to denote the reference to the different functions, that is $f_1 = f(x; A_1)$, $\gamma_1 = \gamma(x; A_1)$, etc. In order to establish a t-test, we have to assume that the Y_i values $Y_i = f(x_i; A_j)$ are normally distributed about the true values, η_i and that the values of $\sigma_{x_{ji}}$ can be neglected (Wolberg, 1967, p. 66). Then we can define a variable u which is normally distributed with zero mean and unit variance:

$$\begin{aligned} u &= \frac{(f_1 - f_2) - (\gamma_1 - \gamma_2)}{\sigma_{f_1 - f_2}} \\ &= \frac{(f_1 - f_2) - (\gamma_1 - \gamma_2)}{\sigma\sqrt{\frac{1}{n_1} + \frac{1}{n_2}}}. \end{aligned} \tag{46}$$

For v^2 we can use ns_f^2/σ_f^2 which has a χ^2 distribution with n-1 degrees of freedom. Since u and v^2 satisfy Theorem 3, the variable

$$\begin{aligned} t &= \frac{u\sqrt{\nu}}{v} \\ &= \frac{(f_1 - f_2) - (\gamma_1 - \gamma_2)}{\sqrt{n_1 s_{f_1}^2 + n_2 s_{f_2}^2}} \sqrt{\frac{n_1 n_2 (n_1 + n_2 - 2)}{n_1 + n_2}} \end{aligned} \tag{47}$$

has a Student's t distribution with $n_1 + n_2 - 2$ degrees of freedom for equal variances.

If the F test indicates that the variances are not equal, but σ_1 and σ_2 are known, then

$$\begin{aligned} \tau &= \frac{(f_1 - f_2) - (\gamma_1 - \gamma_2)}{\sigma_{f_1 - f_2}} \\ &= \frac{(f_1 - f_2) - (\gamma_1 - \gamma_2)}{\sqrt{\frac{\sigma_{f_1}^2}{n_1} + \frac{\sigma_{f_2}^2}{n_2}}}. \end{aligned} \tag{48}$$

Since the values of the variances are seldom known, they are replaced by their estimated values s_1 and s_2. The variable

$$t = \frac{(f_1 - f_2) - (\gamma_1 - \gamma_2)}{\sqrt{\frac{s_{f_1}^2}{n_1} + \frac{s_{f_2}^2}{n_2}}} \tag{49}$$

can be shown to possess an approximate Student's t distribution (Hoel, 1962, p.279). The number of degrees of freedom necessary to make this variable an approximate t variable is given by

$$\nu = \frac{\left(\frac{s_{f_1}^2}{n_1} + \frac{s_{f_2}^2}{n_2}\right)^2}{\frac{\left(\frac{s_{f_1}^2}{n_1}\right)^2}{n_1+1} + \frac{\left(\frac{s_{f_2}^2}{n_2}\right)^2}{n_2+1}} - 2 \tag{50}$$

which is usually not an integer. The nearest integer value is chosen in looking up the critical value for t.

Comparison of two linear regression lines. In the preceding discussion, we considered various tests that can be used to show that two circles as determined by their respective regression lines are the same or are significantly different. In this section we will further examine tests but from a slightly different perspective. If it is possible to transform the regression curve to that of a straight line, then the theory of linear regression may be applied to the transformed observations. Simply stated (Hald, 1952, p. 558):

If the points (x_i, y_i) can be transformed to $(g(x_i), f(y_i))$and are grouped about a straight line such that f(y) is normally distributed with a mean value

$$\alpha + \beta \left(g(x) - \overline{g(x)} \right) \tag{51}$$

and variance σ^2. then the theory of linear regression may be applied to the transformed observations. We will discuss the means of transforming equation 13 later. For now we will assume that such a transformation exists and fulfills the criteria above. Hald (1952, p. 571-579) gives tests for comparing two linear regression lines and the following summarizes that presentation.

After transformation, the two regression lines are

$$Y_1 = \overline{y_1} + b_1 (x - \overline{x_1}) \tag{52}$$

$$Y_2 = \overline{y_2} + b_2 (x - \overline{x_2}) . \tag{53}$$

where b_i is the slope of the regression line.

As above, the first step is to determine whether the variances are the same or there is a significant difference in variances. That is, we need to test the hypothesis

$$H_0 : \sigma_1^2 = \sigma_2^2 \tag{54}$$

against the hypothesis

$$H_1 : \sigma_2^2 \neq \sigma_2^2 \tag{55}$$

If the test hypothesis H_o is found to be true, then a t-test will be used to compare the slopes of the two regression lines. If the hypothesis H_1 is found to be true, then an approximate t-test will be developed.

Again to test H_o and H_1 we use the variance ratio, v^2, as in equation 27. In this case

$$v^2 = s_1^2 / s_2^2 \tag{56}$$

is calculated and compared to the theoretical value for ν_1 and ν_2 degrees of freedom.

Case 1. If the two variances, s_1^2 and s_2^2, do not differ significantly as shown by equation 56, then the pooled estimate s^2 of the theoretical variance σ^2 is

$$s^2 = \frac{(n_1 - 2) s_1^2 + (n_2 - 2) s_2^2}{n_1 + n_2 - 4} \tag{57}$$

Because of the way we will later define the transformation from a circle to a straight line, two variables in equations 52 and 53 are the same. That is $\overline{y_1} = \overline{y_2}$ and $b_1 = b_2 = -1$. This results in the hypothesis $\beta_1 = \beta_2$ not being rejected and, therefore, a common slope weighted by the reciprocal values of the variances as weights, that is,

$$\bar{b} = \frac{b_1 \sum (x_i - \overline{x_1})^2 + b_2 \sum (x_i - \overline{x_2})^2}{\sum (x_i - \overline{x_1})^2 + \sum (x_i - \overline{x_2})^2} \tag{58}$$

$$= b_1 = b_2 = -1. \tag{59}$$

By the addition theorem for the normal distribution $\bar{b}$ is normally distributed about β with variance

$$V\{\bar{b}\} = \frac{\sigma^2}{\sum (x_i - \overline{x_1})^2 + \sum (x_i - \overline{x_2})^2}. \tag{60}$$

We next calculate $\hat{b}$ which denotes the slope of the straight line connecting the points $(\overline{x_1}, \overline{y_1})$ and $(\overline{x_2}, \overline{y_2})$; that is,

$$\hat{b} = \frac{\overline{y_1} - \overline{y_2}}{\overline{x_1} - \overline{x_2}} = 0. \tag{61}$$

It should be noted that $\bar{b}$ has been calculated from the variation within sets and is stochastically independent of $\hat{b}$ which is based on the variation between sets (Hald, 1952, p. 573.). The slope $\hat{b}$ will only deviate randomly from $\bar{b}$ if the two theoretical regression lines are identical. The variance of $\hat{b}$ is

$$V\left\{\hat{b}\right\} = \frac{\sigma^2}{(\overline{x_1} - \overline{x_2})^2}\left(\frac{1}{n_1} + \frac{1}{n_2}\right) \tag{62}$$

and we have

$$V\left\{\hat{b} - \bar{b}\right\} = \sigma^2\left(\frac{1}{(\overline{x_1} - \overline{x_2})^2}\left(\frac{1}{n_1} + \frac{1}{n_2}\right) + \frac{1}{\sum (x_i - \overline{x_1})^2 + \sum (x_i - \overline{x_2})^2}\right). \tag{63}$$

If the two theoretical regression lines are identical, then

$$u = \frac{\hat{b} - \bar{b}}{\sqrt{V\left\{\hat{b} - \bar{b}\right\}}} \tag{64}$$

will be normally distributed with mean O and variance 1 and the quantity will have a t-distribution when σ is replaced by s. Therefore, by applying a t-test it will be possible to test the hypothesis of the identity of the two theoretical regression lines, $\beta_1 = \beta_2$.

Case 2. The variances s_1^2 and s_2^2 differ significantly as shown by the variance ratio (equation 56). If the test hypothesis is correct, $H_0 : \beta_1 = \beta_2$ then the difference $b_1 - b_2$ is normally distributed about 0 with variance

$$V\{b_1 - b_2\} = \frac{\sigma_1^2}{\sum (x_i - \overline{x_1})^2} + \frac{\sigma_2^2}{\sum (x_i - \overline{x_2})^2}. \tag{65}$$

This means that the quantity

$$u = \frac{b_1 - b_2}{\sqrt{V\{b_1 - b_2\}}} \tag{66}$$

is normally distributed about 0 with unit variance. If the estimates s_1^2 and s_2^2 are substituted for σ_1^2 and σ_2^2, then

$$t = \frac{b_1 - b_2}{\sqrt{\frac{s_1^2}{\sum (x_i - \overline{x_1})^2} + \frac{s_2^2}{\sum (x_i - \overline{x_2})^2}}} \tag{67}$$

which is distributed approximately as t with ν degrees of freedom determined by

$$\frac{1}{\nu} = \frac{c^2}{\nu_1} + \frac{(1-c)^2}{\nu_2} \tag{68}$$

where

$$c = \frac{\frac{s_1^2}{\sum (x_i - \overline{x_1})^2}}{\frac{s_1^2}{\sum (x_i - \overline{x_1})^2} + \frac{s_2^2}{\sum (x_i - \overline{x_2})^2}}. \tag{69}$$

Now the value $b_1 - b_2 = 0$ and, therefore, $t = 0$. Thus, the hypothesis $\beta_1 = \beta_2$ is not rejected. The common slope is

$$\overline{b} = -1 \tag{70}$$

since

$$\overline{b} = \frac{b_1 \frac{\sum (x_i - \overline{x_1})^2}{\sigma_1^2} + b_2 \frac{\sum (x_i - \overline{x_2})^2}{\sigma_2^2}}{\frac{\sum (x_i - \overline{x_1})^2}{\sigma_1^2} + \frac{\sum (x_i - \overline{x_2})^2}{\sigma_2^2}}.$$

But

$$b_1 = b_2 \Rightarrow \overline{b} = b_1 = b_2 = -1.$$

According to the addition theorem for the normal distribution (Hald, 1952, p. 214-216)

$$V\{\bar{b}\} = \frac{1}{\frac{\sum(x_i-\bar{x_1})^2}{\sigma_1^2} + \frac{\sum(x_i-\bar{x_2})^2}{\sigma_2^2}} \tag{71}$$

Since σ_1^2 and σ_2^2 are usually unknown, they are replaced by s_1^2 and s_2^2, the estimates. In order to test the identity of the regression lines, the slope $\bar{b}$ is compared with the slope $\hat{b}$ $(= 0)$, equation 61. The variance of $\hat{b}$ is

$$V\left\{\hat{b}\right\} = \frac{1}{(\bar{x_1} - \bar{x_2})^2}\left(\frac{\sigma_1^2}{n_1} + \frac{\sigma_2^2}{n_2}\right). \tag{72}$$

Therefore,

$$V\left\{\hat{b} - \bar{b}\right\} = \frac{1}{(\bar{x_1} - \bar{x_2})^2}\left(\frac{\sigma_1^2}{n_1} + \frac{\sigma_2^2}{n_2}\right) + \frac{1}{\frac{\sum(x_i-\bar{x_1})^2}{\sigma_1^2} + \frac{\sum(x_i-\bar{x_2})^2}{\sigma_2^2}}. \tag{73}$$

If the test hypothesis $H_0 : \beta_1 = \beta_2$ is correct, then the quantity

$$u = \frac{\hat{b} - \bar{b}}{\sqrt{V\left\{\hat{b} - \bar{b}\right\}}} \tag{74}$$

is normally distributed with mean 0 and variance 1. Replacing σ_1^2 and σ_2^2 by s_1^2 and s_2^2, we have

$$t \cong \frac{\hat{b} - \bar{b}}{\sqrt{V\left\{\hat{b} - \bar{b}\right\}}} \tag{75}$$

which is approximately normally distributed for large values of ν_1 and ν_2.

INCLINOMETER TUBES

Properties. If the size of the drill hole or casing in which the inclination is to be measured is quite large, then the choice of the size of the glass tubes and accompanying pressure case is of no great concern. However, many geothermal, heat flow, or mining exploration holes are quite small and may have casings in them as small as $1\frac{1}{4}$ in or less in nominal diameter. For such small holes or casing, the tube size becomes a significant consideration, that is, if you can't get it down the hole, you can't make the measurement. For this reason, we have used a 16 mm culture tube in a 1 inch outside diameter pressure case for a number of years. Until recently, most of these measurements were obtained in holes of low to moderate (15-30°C) temperatures. Since these holes were very nearly vertical, a few calibration points at room temperature sufficed. It was only when the temperature at the point of measurement significantly departed from room temperature that we decided to expand the range of temperatures and the angles at which calibrations were obtained. Comparison of our results to those supplied by industry and to Cumming (1951, p.341) indicated that tube diameter would also need to be examined. Thus, we chose to calibrate a range of tubes from a nominal 6 mm to 25 mm outside diameter.

The tubes used to measure inclination are known as culture tubes as opposed to test tubes. The difference is that a test tube has a belled or flaired lip while a culture tube does not. Culture tubes are manufactured from long tube stock which is cut to length. One end is then melted to form a rounded bottom while the other is fused to form a bead around the opening to eliminate any sharp edges. The consequence of this manufacturing process is a tube which ranges in cross-section from circular to slightly elliptical, even if the initial tube stock is perfectly circular. The tubes that we used in this study are listed in tables 1-7. In these tables we have tabulated the major (2a) and minor (2b) axes, the foci, eccentricity (e.g., Thomas, 1962, p. 473-482), and the diameter of the equivalent circle ($2\sqrt{ab}$) for the outside and inside diameters of the tubes. A histogram of the inside and outside diameters of the 16- and 25-mm tubes (fig. 1) illustrates that (1) the diameters can vary by almost 0.5 mm (table 8) and (2) the wall thickness of the 25 mm tubes is greater than that of the 16 mm tubes, which can be derived from table 8. The mean values of the inside and outside diameters are listed in table 9 along with their respective standard deviations. With the exception of the 16- and 25-mm tubes, the remainder were selected, but only selected to be circular or nearly circular (tables 1-7). The standard deviations are all roughly comparable and we suspect that some of the lower deviations on the selected tubes may be coupled to the small sample size.

The eccentricities of the tubes used are listed in tables 1-7 and histograms of the inside- and outside-diameter eccentricities are plotted in figure 2. The means and their standard deviations for the 16- and 25-mm tubes are listed in Table 10. In this table, the zero eccentricities have been ignored in the calculation of the means and, hence, the difference in the number of values used for the outside and inside eccentricities (table 10). From an examination of the numbers, it is fairly obvious that they are quite small. That is to say, even for the 16- and 25-mm tubes, the cross sections of the outside and inside of the tubes are nearly circular for most of the tubes. For example, for an eccentricity of 0.1 implies that the difference between the length of the major and minor axes (2a-2b) is only about 0.5 % of the major axis (2a). Nevertheless, it appears that for even relatively small eccentricities ($\approx$ 0.1), an error in the apparent angle of a half a degree or more may be introduced by the ellipticity. Since culture tubes are relatively inexpensive, it seems only prudent to measure the tubes before they are used and select only those that are circular or nearly so in order to reduce one source of possible error.

Initially a random sample of tubes was used (tables 4 and 7) in the case of the 16- and 25-mm tubes. This resulted in some scatter in the calibrations due to the ellipticity of the tubes. Subsequent calibrations of the 6, 10, 13, 19, and 20 mm tubes were conducted on selected tubes, that is, on tubes that were circular or as close to circular as possible. This is reflected in the tables (tables 1, 2, 3, 5, and 6) by the zero or near zero eccentricity.

Chemical composition and physical properties. We chose soda-lime glass culture tubes for our measurements. The glass is relatively soft and etches nicely with dilute hydrofluoric (HF) acid solutions (4 %). The tubes were manufactured by Kimble Glass of Vineland, New Jersey, under their EXAX trademark. The average chemical composition is listed in table 11 (Paul Abendroth, Kimble Glass, personal commun.). The glass the tubes are manufactured from is known as R-6 glass (Kimble, 1988, p. 10A-11A). It has a density of 2.53 gm/cm^3, a coefficient of expansion of 93×10^{-7}/°C, thermal conductivity of 2.4 millical/cm·sec·°C at 0 °C, and Young's modulus of 10.9×10^4 psi (Kimble, 1988, p. 10A-11A).

We were unable to obtain the chemical composition of the nominal 20 mm borosilicate culture tubes. However, in general, the SiO_2 content is about the same or only slightly higher than the soda-lime glass that we used. The main differences are a higher B_2O_3 (10-20%) and lower Na_2O (4% or less) in the borosilicates (e.g., see Ratcliffe, 1963). Borosilicate glass is significantly more resistant to etching by dilute hydrofluoric acid solutions; PYREX^{TM} is even more so. Thus, unless a specific size tube is available only in borosilicate composition, soda-lime glass tubes are preferable since the etch times are shorter and weaker acids can be used.

Test stand. The test stand used in calibrating the culture tubes is shown in figure 3. The tube is held in place in a V-shaped tray with a thumb screw. The thumb screw is attached to the tray with a piece of thin aluminum sheetmetal, in order to allow for thermal expansion which, in a rigidly clamped system, could break the tube. The V-shaped tray was mounted on a Starrett Company model 361 protractor and aligned along the edge such that a reading of 90 degrees on the protractor corresponded to a vertical tube. The protractor was mounted perpendicularly to a triangular-shaped baseplate. Leveling screws, with locking nuts at each corner facilitated leveling the apparatus. The level of the base plate was checked with a machinist level.

Temperatures. The procedure for etching a tube is to fill it approximately half full of HF acid, plug the tube with a cork or rubber stopper, and mount the tube in the tray of the test stand (fig. 3); the angle having been previously set to the appropriate value for the calibration. The acid used is a dilute 4% aqueous solution of 48% HF acid and distilled water. For example, 500 ml of 4% acid consists of 41.7 ml of 48% HF and 458.3 ml of distilled water.

For room-temperature calibrations ($\approx$ 22 °C), the test stand can be leveled and used on the lab bench. However, variations in air temperature in the lab can be several degrees Celsius. With the exception of the 4 °C calibration, the 10°, 22°, 40°, 60° and 80 °C calibrations were run in a temperature-controlled water bath. The 4 °C calibration was obtained in a refrigerator. To facilitate insertion and removal of the test stand from the bath, a withdrawal rod and knob were mounted on the base of the test stand (fig. 3). In order to simplify leveling, the water bath was leveled so as to make the inside, bottom of the bath level. The leveling screws on the test stand were then adjusted to set the

^{TM} PYREX is a trademark of Corning Glass Works

base plate horizontal. In this manner we could insert and retrieve the test stand without continuous releveling. Both the test stand and the bath were checked several times a day to guard against unexpected shifts in the bath or stand baseplate from the horizontal. Temperatures in the bath were controlled to ± 0.2 °C and were monitored with a digital thermometer.

The temperature of the dilute acid when used at room temperature, the temperature at which it is mixed, causes no problems when etching a line in the tubes. However, as the temperature increases significantly from $\approx$ 22 °C, bubbles form as dissolved air outgases from the solution. The formation of bubbles at the meniscus can result in a band being etched instead of a sharp line. Boiling of the acid at high temperatures can produce similar results. To minimize this effect, the dilute HF acid was placed in a bell jar and evacuated. Evacuation for about 15 minutes usually was sufficient to remove most of the air. When air is reintroduced into the bell jar, some air undoubtedly is dissolved in the acid. The amount of air going back into solution, however, is small compared to that in the pre-evacuated acid solution. The evacuation procedure had the desired result of decreasing significantly bubble production, especially at higher temperatures.

The time required to etch a line in the wall of a tube varied considerably with temperature. Table 12 is a list of average times for all diameter tubes and for soda-lime and borosilicate glass. As in all of our tests, these times are based upon the use of a 4% hydrofluoric acid solution. The factors that enter into the etch time include (1) the strength of the acid, (2) the temperature at which the acid is etching the line, (3) the hardness of the glass, (4) the chemical composition of the glass, (5) the size of the tube, that is, surface area, and (6) the age of the acid. The last item, age of the acid, appears to be related to the reaction of the acid with the air above it in the bottle, although we do not know if this is a true chemical reaction or simply outgasing of HF. What we have observed is that freshly prepared, dilute HF acid is more reactive, that is, it will etch lines quicker than acid that is a year old or older. Needless-to-say, there may be other factors affecting the etch time. The numbers in table 12 work quite nicely, but depending upon the tubes used, may require more or less time to etch with 4% HF solution.

EXPERIMENTAL PROCEDURES

Angle measurement. Reading the angle etched on the wall of a tube is not a trivial matter. People consistently either overread or underread the angle (Cumming, 1951, p. 337). Because of this bias in one direction or another, it seems only reasonable that the person doing the calibrating also do the reading of the field tubes.

From a side view, the line etched appears as a straight line. This straight line is deceiving. In fact, careful measurement will show that the ends of the "straight" line are curved upward, more so on the top side of the tube than on the bottom. Although this is not readily apparent in most tubes at high dip (near 90 degrees, a vertical hole), it is readily seen at very small dip angles (near 0 degrees, a horizontal hole). As the tube size decreases, the departure from linearity decreases. We used this fact to establish a measurement criteria that was consistent across the range of tubes used in this study.

We first assumed that the line was straight and extrapolated it to the outside wall of the tube. For most tubes and angles, this was relatively simple and straightforward. Second, for the tubes that had low dip angles (say 10-20 degrees) or the line exhibited some curvature, we also assumed that the line was straight. This assumption is a reasonable approximation because more than half the line about the center of the line is quite straight with most of the curvature near or at the end points. Again, we extrapolated the line to the outside wall. This is tricky and usually required repeated measurements to establish confidence in the measurement. The physical setup used to measure the angle is illustrated in figure 4. The extrapolated points were measured with the vertical caliper (vernier height gage). The point was transferred to the caliper measuring edge by the cross-hair of the transit. For stability, the tube-mount (dividing head) and the vertical caliper were placed on a granite surface block. The small size of the granite surface block precluded positioning the transit on it also. This was found not to be a problem as long as the transit was level. To insure that the cross-hair was horizontal at all times, the level of the transit was checked before and after each reading. The distance between the two vertical measurements, $\triangle z$, was recorded and, along with the measured outside diameter, D, of the tube, provided the two numbers required to determine the dip angle, $\alpha = \tan^{-1}(D/\triangle z)$. The window shown in figure 4 is part of the "art" in this measurement. A suitable source of diffuse light is required in order to observe the line etched in the wall of the tube. Although different light sources were tried, we found that sunlight reflected from an adjacent building and transmitted through the window worked best.

The measurement configuration shown in figure 4 is unsuitabe for use in the field. Where a field measurement is required, good results can be obtained using a graphical method. We simply align the etchline along the horizontal lines on graph paper and, using a straightedge, draw a line parallel to the axis of the tube. This is easily accomplished by resting the tube on the straight edge. Using a protractor, we measure the angle between the horizontal line and the drawn line. The accuracy of this method is limited to about 0.5 degrees at best. The large diameter tubes are easier to read than the smaller ones.

Apparent angles of 16- and 25-mm tubes. Using the apparatus in figures 3 and 4, we measured the apparent angles for 16- and 25-mm tubes over a range from 5 to 85 degrees dip. There is no difference between the true and apparent angles at 0 and 90 degrees dip. The results are listed in table 13 for temperatures of 4°, 22°, and 80 °C. The 5 degree values were discarded because, at this low angle, the etch line intersected the end of the tube and the stopper, preventing a complete ellipse from being etched and virtually making it impossible to extrapolate a straight line to the wall of the tube.

As we mentioned above, the data when plotted appeared nearly symmetrical about the diagonal line relating true angle to apparent angle. We, therefore, selected to fit the data in table 13 to an arc of a circle for each temperature.

General method of least squares curve fitting - application to circle. An examination of a plot of true angle versus the apparent angle (e.g., fig. 15) suggests that (1) the data may be adequately fit using a circle and (2) the circle must pass through (0, 0) and (90, 90). The second point constrains the circle to pass through those points and to lie along a 45 degree line (fig. 5). Therefore, the coordinates of the center of the circle are $(-A, 90 + A)$, and $R^2 = A^2 + (90 + A)^2$ in equation 13. In order to apply equation 8, equation 13 is solved for y:

$$y_i = 90 + A - \sqrt{A^2 + (90 + A)^2 - (x_i - A)^2}. \tag{76}$$

The negative sign before the square root signifies that the portion of the arc of the circle that we are interested in is in the fourth quadrant. We have also dropped the subscript 1 in A_1 since there is only one constant. The derivatives are

$$F_A{}^i = \frac{\partial F^i}{\partial A} = -1 + \frac{A + 90 - x_i}{\sqrt{A^2 + (90 + A)^2 - (x_i + A)^2}} \tag{77}$$

$$F_{x_i}{}^i = \frac{\partial F^i}{\partial x_i} = \frac{-x_i + A}{\sqrt{A^2 + (90 + A)^2 - (x_i + A)^2}}. \tag{78}$$

If the initial estimate or guess for A is A_{10}, then F_0^i is defined by equation 17. The weights are defined by equation 16, where $\sigma_{y_i} = \sigma_{x_i} = 0.5$ that is, we assumed an experimental error of 0.5 degrees. By using the method of successive approximation defined by equations 14 through 21, we were able to determine a value for A and, thus, for R, the radius of the arc of the circle. A C-program, listed in the Appendix, is the one we used to determine the least-squares fit and all the statistics, which we will discuss shortly.

As can be seen from the constants we used in the program, the iterations continued until $B < 1 \times 10^{-5}$ that is until the correction was small (equation 14). The criteria for convergence, equation 22, was used initially but was subsequently dropped when it became apparent that we were having convergence problems. We subsequently used $B < \epsilon$ directly in all of our calculations.

Least squares convergence. There is always the possibility in nonlinear least-squares analysis that the A_k values may not converge. Wolberg (1967, p. 48-53) discussed convergence for the nonlinear case. No solution will exist, for example, if (1) any of the partial derivatives or F_o become unbounded for one of the data points, (2) one of the derivatives was zero for all n data points, or (3) two or more of the partial derivatives, F_{A_k}, were highly correlated, yielding a singular matrix (that is, the determinant is zero) for which no solution is obtainable. For the circle we obtained convergence but at a very slow rate. In general, the closer our initial guess to the final value, the quicker convergence was achieved.

Initially we suspected convergence might be a problem because of the large number of iterations required before our criterion, equation 22, was met. When we plotted the results of each iteration, for example Figure 6 (A16.C4a), we found that for only one computer run the values, A, were indeed converging, but very slowly. The problem stemmed, in part, from our criterion, $B < \epsilon$. If each iteration approached the final value monotonically, then $B < \epsilon$ is quite satisfactory. However, for an oscillation $B < \epsilon$ can be achieved at a maximum or minimum of the oscillations where B is changing very slowly. We found this to be the case for both the 16- and 25-mm tubes at 4°, 22°, and 80 °C (figs. 6 through 11).

As we stated earlier, the closer our initial guess is to the final value, the faster the rate of convergence. So we added a second criterion for convergence. Our final value for A after the first computer run was rounded to three decimal places and used as an initial guess for a second computer run. The second run converged at a faster rate. The results of the second computer run were used as the initial guess for the third computer run. And so forth until the end result for the value of A did not change. Usually this involved about eight computer runs of the program in the Appendix. Figures 7 through 11 show the results of the first two computer runs. Correction factors B for the first computer run are shown in figures 12 and 13 for 16- and 25-mm tubes at 4°, 22°, and 80 °C.

As a final test, we calculated the average for each run. This indicated that the A-values were indeed oscillating about the final value. Indeed, even after the first computer run (for example A16.C4a of table 14), the mean value $\overline{A}$ is very close to the final value of A. Tables 14 through 19 also list the minimum and maximum as well as the number of iterations for each run.

If convergence is a problem, one method to force convergence is to divide the correction factor, B, in equation 14 by a constant before adding it to the initial guess A_{10}. The value of the constant is quite arbitrary but usually a number between 2 and 10 is used. We tested the effect of such a scheme on the least-squares fit to the nominal 16 mm tubes at 4 °C. The results are shown in table 20 and figure 14. Table 20 is similar to tables 14 through 19 except that B was divided by 3. The effect on the first computer run is shown in figure 14 (A16.C4a1) and should be compared to figure 6 (A16.C4a). The number of iterations for the computer run is down by a factor of about 2 (tables 14 and 20), but the total number of runs is about the same and actually increases in some cases. Figure 14 (A16.C4a2) illustrates the output as per figure 14 (A26.C4a1) except that B was divided by 10 instead of 3. As can be seen in comparing figures 14 (A16.C4a2) and 6 (A16.C4a), the number of iterations in this case is the same but the number of cycles is reduced in figure 14. We concluded that dividing the correction, B, by a constant on the order of 3 will reduce the number of iterations, which may be of interest to those using a microcomputer to do the least-squares calculations. For a minicomputer or mainframe computer, which are significantly faster, the reduction in the number of iterations is not that significant and is probably not worth the experimentation required to select the best constant to divide into B.

Results of final least-squares calculation. The final iteration results for the 16- and 25-mm tubes at 4°, 22°, and 80 °C are listed in tables 21 through 26 and plotted as true angle versus apparent angle in figures 15 and 16.

In the least-squares fit, the value of A was determined from which the value for the radius of the arc of the circle was calculated. The uncertainty in A, s_A, and the small value of S in the χ^2 comparison indicate that the fit to an arc of a circle is quite good. Examination of figures 15 and 16 tend also to confirm this. The deviations between measured and calculated angles are also small and are at or within the experimental error of 0.5 degrees or less. The results are presented for the 99% confidence interval. The determination of the uncertainty in A and the function at 45 degrees are also presented in the tables and will be considered in the following paragraphs.

In the above discussions, we have avoided any mention of how to determine the uncertainty in A, s_A. From the method of determining of the least square parameter, A, the value of s_A^2 can be calculated (Wolberg 1967, p. 60) as

$$s_A{}^2 = \frac{S}{n-1} C_{11}{}^{-1} \tag{79}$$

where S is the weighted sum of the squares of the residuals, n-1 is the number of degrees of freedom, and C_{11}^{-1} is the element of the inverse coefficient matrix determined in the general least-squares method above. If the experiment is repeated many times, the value of S will be distributed according to the χ^2 distribution with n-1 degrees of freedom (Wolberg, 1967, p. 60).

Since we will be comparing the curves for 16- and 25-mm tubes at 4°, 22°, and 80 °C to each other, we will need to have a measure of the confidence interval of the function. For the confidence interval we will need the uncertainty in the function, s_f. Wolberg (1967, p. 64-68) gives the general method of determining s_f. For our purposes a much simpler expression will suffice:

$$s_f{}^2 = \frac{S}{n-1} F_A{}^2 C_{11}{}^{-1} \tag{80}$$

where S and $C_{11}{}^{-1}$ were defined above and F_A is given by equation 77. By combining equations 79 and 80, we obtain

$$s_f{}^2 = s_A{}^2 F_A{}^2. \tag{81}$$

Thus, s_f is dependent on s_A and by reducing the uncertainty in A, we can reduce the error in f. Although we theoretically could reduce this to a very small value if systematic errors do not affect the experiment, there is a practical limit as to the minimum value of s_f.

Examination of equation 77 also indicates that when the apparent angle is 0 or 90 degrees, the value for F_A goes to zero. Equations 80 and 81, therefore, also go to zero. This is not surprising since at 0 and 90 degrees the true and apparent angles are equal and there is no correction.

A few words concerning significant figures are in order. We have reported all values to 3 decimal places. In fact, the measurements are only accurate to 3 or 4 significant figures. The uncertainties in table 21 through 26 confirm this also. We have kept the additional decimal places in order (1) to force convergence in the least-squares sense, (2) to reduce errors in calculating the value of the radius, R, due to squaring of terms, and (3) to enhance the visual appearance of the results in various plots (e.g., fig. 21). Keeping the additional digits prevents jagged- or step-type plots and prevents the calculated curve, in figure 15 for example, from being offset from the data points in the worst case.

Statistical analysis of least-squares curves. The results of the least-squares fits to the data for the 16- and 25-mm tubes have been shown in figures 15 and 16. Composite plots for these tubes are shown in figures 18 and 19. Although it is apparent that there is some separation in the curves, the question remains as to whether there is any real difference among the three curves at temperatures of 4°, 22°, and 80 °C for 16- and 25-mm tubes, respectively.

As we stated earlier, the true and apparent angles are equal at 0 and 90, that is there is no capillarity correction. Departing from 0 and 90, the correction increases, reaching a maximum at 45 degrees. The first test will be on the coordinate, A, as determined from the least-squares fit to the circle and the second test will be on the functional value at 45 degrees. We will do these tests on adjacent temperature curve, say 4° and 22 °C and 22° and 80 °C, and if they are found to be mutually exclusive, then we can assume that 4° and 80 °C curves are different since the functions are monotonic. The results of these calculations are summarized in table 27. In order to make table 27 more meaningful, we will examine the 16 mm tubes at 4° and 22 °C in detail, using the data from the first two lines in table 27. The results we will show are presented in the third line. Subsequent sets of three lines in table 27 follow the same pattern.

For the 16 mm tubes at 4° and 22 °C, the first hypothesis is $H_0 : \sigma^2_{A_1} = \sigma^2_{A_2}$ (equation 25) against the hypothesis $H_1 : \sigma^2_{A_1} \neq \sigma^2_{A_2}$ under the assumption that the true coordinates, α_1 and α_2 are normally distributed. This follows from the least-squares analysis. Then (equation 32):

$$F = \frac{18(0.437)^2/17}{17(0.300)^2/16}$$
$$= 2.11$$

will satisfy an F distribution with $f_1 = 17$ and $f_2 = 16$ degrees of freedom. Since $F < F_{0.95}(17, 16) = 2.29$, the variances do not differ significantly. Therefore, we can test the hypothesis $H_0 : \alpha_1 = \alpha_2$ that the coordinates are the same by a t-test (equation 40).

$$t = 172.69,$$

and the number of degrees of freedom

$$f = 33.$$

Since for $f = 33$ the Student's t-value, $t(5\%) = 2.036$, implies that t is significant. Thus, the two centers are not the same. We now need to test the function at 45 degrees to determine if we have the same functional value, that is, we will test the hypothesis $H_0 : \gamma(x; A_1) = \gamma(x; A_2)$ (equation 44). Since f is our function as determined by the least-squares analysis, we will let $f_1 = f(x; A_1)$ and $f_2 = f(x; A_2)$ in order to shorten our notation. We then will test the hypothesis $H_0 : \sigma^2_{f_1} = \sigma^2_{f_2}$.

From equation 32, $F = 1.19$ for 17 and 16 degrees of freedom. Since $F_{0.95}(17, 16) = 2.29$, the variances do not differ significantly. Therefore, we can test by equation 47: $t_f = 179.05$. Since the Student's t- value (5%) is 2.036 for 33 degrees of freedom, the two functions are not the same and $H_1 : \gamma_1 \neq \gamma_2$. All of the above follows for the various cases by the application of equations 23 through 50. Table 27 summarizes these calculations for the 16- and 25-mm tubes. In all cases the curves are found to be distinct, in other words, hypotheses H_1 (equations 24 and 45) are found to hold for all the curves in figures 18 and 19.

Transformation of arc of circle to straight line. As an alternative to the statistical analysis on the arc of the circle presented in the previous section, if it is possible to transform the function, that is the arc of the circle, into a straight line, then comparison of two such lines is fairly standard and applies to the results of the arc of the circle equally as well (equation 51). In this section we shall present one method of converting (x,y) into (g(x),f(y)) that satisfies equation 51.

In equation 76, if the expression containing the square root can be transformed into another variable, say x_1, then a linear function in x_1 would satisfy the conditions of equation 51. Although this transformation is not necessarily one-to-one, we can make it unique (1) by restricting the square root to only negative values, as we did in equation 76, and (2) by defining the function only over the restricted interval [0, 90].

With these restrictions, the transformed equation becomes

$$y_1 = \alpha_0 + \beta_0 x_1 \tag{82}$$

where $y_1 = y$, $\alpha_0 = 90 + A$, $\beta_0 = -1$ and

$$x_1 = \sqrt{A^2 + (90 + A)^2 - (x + A)^2}. \tag{83}$$

In order to put equation 81 in terms similar to that of equation 51, we need to determine $\overline{x_1}$, the average value of x_1. From the mean-value theorem for integrals (Taylor, 1955, p.52-53):

$$\overline{x_1} = \frac{1}{b - a} \int_a^b x_1 \, dx_1 \tag{84}$$

where upon substitution of x = 0,90 into equation 83 and integrating equation 84, we obtain $\overline{x_1} = 45 + A$. By including this expression for $\overline{x_1}$ into equation 82, we obtain

$$y_1 = 45 - (x_1 - (45 + A)), \tag{85}$$

on the closed interval $[A, 90 + A]$. In examining equation 85 in light of equation 52, it becomes apparent that $\overline{Y_1} = 45 = \overline{y}$ and $\overline{x_1} = 45 + A = \overline{x} + A$.

Statistical analysis for straight line for transformed arcs of circles for 16- and 25-mm tubes. The arcs of circles relating true-to-apparent angle of the etch lines were transformed as in the previous section. This resulted in a family of straight lines with a slope of −1, apparent angle ranging from A to 90+A, and true angle ranging from 0 to 90 for each of the 16- and 25-mm tubes at 4°, 22°, and 80 °C. The analysis of these lines is covered by equation 52 through 75 for various cases. For example, the parameters for the 16 mm tubes at 22 °C are $A_1 = 118.716$, $s_1 = 0.437$, $ssdx_1 = 12458.84$, $n_1 = 18$, and at 80 °C are $A_2 = 139.474$, $s_2 = 0.374$, $ssdx_2 = 12506.73$, $n_2 = 18$. Now, if the hypothesis H_0 (equation 54) is found to be true, then we can use a t-test. Using the variance ratio test (equation 56) $v^2 = 1.37$. The variances, thus, do not differ significantly since $F_{0.95}(16, 16) = 2.33$ for

16 and 16 degrees of freedom. Then the pooled estimate (equation 57) of the theoretical variance is $s^2 = 0.165$. The common slope weighted by the reciprocal values of the variances as weights is $\overline{b} = -1$ (equation 59). By the addition theorem for the normal distribution $\overline{b}$ is normally distributed about the true slope with variance $V\{\overline{b}\} = 6.609 \times 10^{-6}$ (equation 60). The uncertainty in $\overline{b} = 2.57 \times 10^{-3}$. The slope, $\widehat{b}$, of the straight line connecting $(\overline{x_1}, \overline{y_1})$ and $(\overline{x_2}, \overline{y_2})$ is zero by equation 61. Since $\overline{b}$ has been calculated from the variation within sets, it is stochastically independent of $\widehat{b}$ which is based on the variation between sets. The slope $\widehat{b}$ will only deviate randomly from $\overline{b}$ if the two theoretical regression lines are identical. The variance of $\widehat{b}$ is $V\left\{\widehat{b}\right\} = 4.255 \times 10^{-5}$ (equation 62). The difference between the two slopes, $\overline{b} - \widehat{b}$, is -1. The variance is (equation 63). If we apply a t-test, we find that $t = -142.6$, for 32 degrees of freedom (equation 64). Since this is significant ($t_{5\%} = -2.040$) the two lines are not the same. These results are summarized in table 28. In addition, table 28 summarizes the calculations for the 16 mm tubes at 4° and 22 °C and the 25 mm tubes at 4° and 22 °C, and 22° and 80 °C. Comparison of 4° and 80 °C is not necessary since the curves are monotonic.

The conclusion that can be reached from this analysis is that these curves are indeed distinct. Obviously as the temperature difference decreases, at some ΔT the analysis will indicate that there is effectively no difference between the curves. However, the value of ΔT where the curves become effectively similar itself is temperature-dependent as can be surmised from figure 21 which illustrates that the radius of the arc of the circle for a given tube is nonlinear with temperature.

GEOMETRICAL CONSIDERATIONS

Circle radius as function of true and apparent angle. If the arc of a circle can be utilized to describe the relationship between the line etched on the wall of the culture tube and the true dip angle, then a simple function can be obtained that relates the difference between the two angles to the circle radius. We will use the true angle at 45 degrees because (1) the arc is symmetrical about 45 degrees, (2) the geometry is simpler, and (3) the maximum departure of the apparent angle occurs at 45 degrees.

The geometry needed for the derivation is shown in figure 20. In this diagram, C is the difference between the true and apparent angle, O is the center of the circle $(-A, 90 + A)$, R is the radius of the circle, and $\ell/2$ is $45\sqrt{2}$. The line $\overline{OP}$ is perpendicular to the chord $\overline{\emptyset \cdot P \cdot 90}$ and $\overline{OP}$ is along the diagonal of the square, that is, $\overline{OP}$ is inclined 45 degrees from the horizontal.

From elementary geometry (Eves, 1963, p. 107),

$$(2R - d)\cdot d = (\ell/2)\cdot(\ell/2) = C\cdot\overline{PN}. \tag{86}$$

Hence, $\overline{PN} = \frac{(\ell/2)^2}{C}$. Now, $\overline{PL} = \frac{\overline{PN}-C}{2}$ and $\cos 45 = \frac{\overline{PL}}{OP} = \frac{\overline{PL}}{R-d}$. Therefore, $R - d = \frac{\overline{PL}}{\cos 45} = \frac{2\overline{PL}}{\sqrt{2}} = \overline{PL}\sqrt{2}$. Substituting for $\overline{PL}$ yields

$$R - d = \frac{(\ell/2)^2 - C^2}{2C}\sqrt{2} \tag{87}$$

Now expanding equation 86 and completing the squares results in

$$d^2 - 2Rd + R^2 = R^2 - (\ell/2)^2$$

$$\text{or} \quad (d - R)^2 = (R - d)^2 = R^2 - (\ell/2)^2. \tag{88}$$

From equations 87 and 88

$$(R - d)^2 = \left(\frac{(\ell/2)^2 - C^2}{2C}\sqrt{2}\right)^2$$

$$= R^2 - (\ell/2)^2$$

or

$$R^2 = \left(\frac{(\ell/2)^2 - C^2}{2C}\sqrt{2}\right)^2 + (\ell/2)^2$$

Expanding and collecting terms

$$R^2 = \frac{(\ell/2)^4 + C^4}{2C^2}$$

and since $\ell/2 = 45\sqrt{2}$,

$$R = \frac{\sqrt{4\cdot 45^4 + C^4}}{\sqrt{2}C} \tag{89}$$

Equation 89 allows us to calculate the circle radius only knowing the difference between the true and apparant angles.

Having established that the data could be represented by an arc of a circle and deriving equation 89, we obtained culture tubes with nominal diameters of 6, 10, 13, 19, and 20 mm with the objective of obtaining values for the radius, R, at temperatures of 4°, 10°, 22°, 40°, 60°, and 80 °C based on measurements at 45 true degrees. The measured angles are listed in table 29 along with those obtained for the 16- and 25-mm tubes at 45 degrees. The radii of the arc of the circle for all of the tubes at various temperatures are listed in table 30 and their corresponding coordinates, |A|, in table 31.

Figure 21 is a plot of the radii from table 30 as a function of temperatures. As the nominal tube diameter decreases from 25 mm to 6 mm, the curves tend to flatten and the change with temperature decreases. As can be observed from figure 20, the minimum value for R is 90, because the arc of the circle is required to go through 0 and 90 degrees. Since the 6 mm tubes are close to this value (fig. 21 and table 30), we etched the 6 mm tubes at angles other than 45 degrees. Inspection of a partially filled 6 mm tube with colored water indicated that fluid tended to behave as in a larger tube for dip angles greater than about 45 degrees. At a dip angle of zero, however, the fluid would remain in the tube and not run out. Angles etched at room temperature (fig. 22 and table 32) showed that above 45 degrees the etch angle followed the arc of the circle as predicted from the radius at 45 degrees. Below 45 degrees, however, the apparent angle decreased only slightly with decreasing true angle. For example, at a true angle of 10 degrees, the measured apparent angle was 66.4 degrees, whereas the predicted value, based on the arc of the circle at 45 degrees, of the apparent angle was 33.7 degrees. The inside diameter of the 6 mm tubes is only about 4.5 mm (table 9). This small diameter apparently is on the verge of becoming a capillary tube in which the meniscus does not change with dip.

Although this ended our experiments with the 6 mm tubes, a few comments or speculations are in order. At 22 °C, the breakover point, that is the point where the apparent angle departs from the arc determined at 45 degrees, is approximately 40 degrees or so (fig. 22). Although we do not have data on the surface tension of 4% HF acid solution, the surface tension of water and many dilute, aqueous solutions tends to decrease with increasing temperature. If the 4% HF solution follows this pattern, then the breakover point should decrease as temperature increases. Measurements at a true angle of 45 degrees at 4 °C, however, do not indicate any radical departure in the radius (fig. 21) when compared to higher-temperature measurements. This would tend to indicate that the breakover point may be at 45 degrees or less for all temperatures in the 6 mm tubes. For true dip angles greater than 45 degrees, the 6 mm tubes appear to follow the arc of a circle and can be used as inclinometer tubes, although this should be only done after further calibration and with some caution. We have not tried to replicate the results below a true angle of 45 degrees for the 6 mm tubes (fig. 22) but suspect that problems of threshold gradients and capillary hysteresis (Olsen, 1965) would be involved.

The next larger diameter tube we used was 10 mm, which exhibited some of the same tendency to act as a capillary tube at low dip angles. Although we did not etch any tubes at angles other than at a true angle of 45 degrees, we suspect that these 10 mm tubes will also break away from the arc of the circle but at some dip angle less than that of the 6 mm tubes, that is, at a true angle less than about 40 degrees. Again, there undoubtedly is a temperature dependence and we would expect that the effect would be most noticeable at low temperatures.

For 13 mm and larger tubes, the fluid ran out of the tube when it was placed in a horizontal position (0 degrees true angle). We, therefore, doubt that these tubes would suffer from this limitation. Indeed, the 16 mm tubes do not exhibit any such behavior even at 10 degree dip and 4 °C temperature.

Radius of arc of circle versus tube diameter. An examination of figure 21 indicates some irregularities in the curves relating circle radius to temperature. In addition to the dependence of the circle radius on temperature, there appears to be a functional relationship of radius to tube diameter. If this is indeed the case, then one might be able to devise a correction in order to "smooth" the curves in figure 21.

As a first attempt, we plotted the circle radius against inside tube diameter at constant temperature (fig. 23). The points on each plot were fit to a straight line by a least-squares method (Nielsen, 1964, p. 269). When the intercept, R_o, for zero inside tube diameter is plotted as a function of temperature (fig. 24), R_o takes on a minimum at 22 °C, increasing towards lower and higher temperatures. The slope (fig. 24) on the other hand increases for all temperatures, but appears to be approaching an asymptote at higher temperatures. This is also discernable from figure 21 since the change in radius at higher temperatures decreases.

We have been unable to assign any physical significance to the values of R_o especially since a radius of 90 is the minimum in order for the circle to pass through 0 and 90 degrees. Therefore, we made no attempt to fit any functional form to R_o or the slope in figure 24. The straight lines plotted in figure 23 would have to terminate at a radius of 90, which is at an inside diameter of approximately 4 mm. Since this is near the inside diameter of the 6 mm tubes and since the 6 mm tubes at some temperatures and angles behave similarly to capillary tubes, these plots (fig. 23) may be indicating that tubes with inside diameters less that about 4 mm behave as capillary tubes. On the other hand, the low R_o's may just be suggesting that the function, a straight line, is not a correct representation of the data.

When we use the straight lines of figure 23 to correct figure 21 (table 33) we see that for 6 and 10 mm tubes, the correction results in a less regular relationship between circle radius and temperature (fig. 25). As the diameter increases, however, the relationship improves. This at least suggests that some sort of correction may be feasible, but possibly with a different functional form.

Since we have no theoreticial basis for selecting any particular function, we chose the power series as a likely candidate. The second degree equation, constrained to pass through radius 90 at zero inside tube diameter, deviated too far from the data for the 25 mm tubes. In addition, the points suggested an inflection point may occur between 10 and 15 mm inside diameter. The third degree equation seemed to be the next logical choice. the least-squares fit to the third-degree equation was constrained to pass through radius 90 at 0 mm inside tube diameter and the slope, $(\partial R/\partial D)_T$ where D is the inside tube diameter, was set to zero at 0 mm inside tube diameter. The constraints were applied using Lagrangian multipliers (Nielsen, 1964, p. 169-170; Apostol, 1957, p. 152-157).

The results of fitting the third degree equation are shown in figure 26. The intercept, R_0, is 90 in all cases and the linear or first degree term, R_1, is zero as a consequence of requiring $(\partial R/\partial D)_T = 0$ at 0 mm inside tube diameter. The second-degree term, R_2, increases with temperature (fig. 27), while the third-degree term, R_3, decreases with temperature. In both cases the points appear to be approaching an asymptote as would be expected due to the decrease of $(\partial R/\partial T)_D$, where T is temperature, with increasing temperature (fig. 21).

The least-squares fit to the third degree equation is reasonable at all temperatures (fig. 26). Applying these curves to the data of figure 21 produces a series of curves (fig. 28; table 34) which are much improved over figure 25 at the small tube diameters but much worse for the 25 mm tubes. The third degree equation fit is quite good for the 25 mm tubes. The radii in figure 28 are a bit low at 40° and 60 °C and contribute to the appearance of a sag in the curve. In examining R_2 and R_3 (fig. 27), it is apparent that the 40° and 60 °C values for R_2 and R_3 are offset somewhat from the trend as established by the points at other temperatures. In Figure 26, the general character of the 40°, 60°, and 80 °C curves is different than that of the 4°, 10°, and 22 °C curves by being more pronounced in its curvature at larger tube diameters.

One possible explanation for the variation in shape of the 25 mm curve may be in the nature of the meniscus. At one extreme is the 6 mm tube which, under certain conditions, may operate as a capillary tube. This, as well as most of the tubes used in this study, would fall into the small or narrow tube category. By this we mean a vertical tube of circular cross-section such that the curvature of the meniscus is approximately spherical (Rayleigh, 1915, p. 185). In a large or wide tube, the meniscus is not spherical and can be described by two radii of curvature r_1 and r_2 (Landau and Lifshitz, 1959, p. 230), where r_1 is the central curvature and r_2 is the peripheral curvature. If $r_1 = r_2$ then we have the narrow tube. If $r_1 = r_2 = \infty$ then the surface is a plane. Now, if the 25 mm tubes are very near or at the transition from the narrow tube to the wide tube, then one would expect to encounter some deviations from a smooth curve as the transition occurred. For example, one explanation of figure 28 is that for the 25 mm tubes at or below room temperatures, the tube behaves as a narrow tube while for temperatures greater than 22 °C, the tube behaves as a transition or even a wide tube. Although Rayleigh (1915) discusses the narrow and wide tube, he gives no criteria given as to where the transition occurs. Temperature dependency is not addressed in his analysis. In addition, all the tubes are assumed to be vertical and perfectly circular. For the inclined tube the meniscus is no longer circular but elliptical with a large surface area and since the surface tension decreases with temperature, the tube may effectively become a wide tube at higher temperatures. Given the test apparatus (fig. 3) and the test procedure, we have no way of confirming this conjecture. Finally, it is quite obvious that all the above supposition may not be valid if the cubic equation (fig. 26) does not adequately describe the data.

Circle radius, temperature and tube diameter. Culture tubes are manufactured in a wide variety of length, diameters and wall thicknesses. Although we have attempted to cover the range of most standard sizes, there are undoubtedly others that we have not examined. In order to generalize figure 21, we plotted the values for circle radius as a function of temperature and tube inside diameter and contoured the radii (fig. 29). The original machine contours were quite ragged due to the small data set and the accompanying literal interpolation of the computer program. Since we were attempting to generalize in figure 29, we "smoothed" the contours by hand and only included lines at a radius interval of 50. The regularity of the pattern, "smoothed" or otherwise, allows for easy interpolation to various tube diameters at specific temperatures.

NOTES ON CAPILLARITY

There is a vast literature on capillarity and surface tension. References to some of it can be found in advanced texts by Adams(1941), Adamson(1967), Landau and Lifshitz(1959), and Partington(1951), each of whom view the subject in a somewhat different manner.

As to the mathematical aspects of the problem, Partington(1951, p.135) opined: "The subject has been a favorite field for the pure mathematician, who has added little to the results of Laplace[1806]." This does not mean that the mathematics are simple. They are not (e.g., Landau and Lifshitz, 1959, p.233), and treatment of real problems usually involve series approximations.

We take note of the capillary constant ($a = \sqrt{2\sigma/g\rho}$) where σ is the surface tension (dyne/cm=erg/cm^2), g is the acceleration due to gravity (cm/sec^2) and ρ is density (gm/cm^3). "The shape of the fluid surface is determined by this quantity alone. If the capillary constant is large compared with the dimension of the medium, we may neglect gravity in determining the shape of the surface" (Landau and Lifshitz, 1959, p.233). The capillarity constant for pure water at 20 °C is 0.3857 cm (Dorsey, 1940, p.514) and the variation with temperature is about -3.8×10^{-4} cm/ °C. These numbers indicate (1) the capillary constant (length) is close to the inside diameter of our smallest tubes (0.45 cm) and we might expect complications from the passage from domains dominated by gravity to those dominated by surface tension. Actually all of the tubes (6 – 25 mm O.D.) show the influence of both, and it is not until a diameter of about 50 mm is reached that a partially flat surface is reached (Raleigh, 1916). Just how the concept of length is to be incorporated into the analysis of data from inclined tubes is beyond us. (2) The capillary constant varies with temperature (fig. 30). Although the variation is small ($\sim$ 10% over the range of interest), it may influence $(\partial R/\partial D)_T$ and $(\partial R/\partial T)_D$ but we are not sure how. We note, however, that these two derivatives are nearly constant above about 40 °C and that this is also so of da/dT (fig. 30). The reason is that above 40 °C both $d\sigma/dT$ and $d\rho/dT$ are nearly constant. Laplace noted that $\sigma \approx \sigma_o(1 - \gamma T)$ and that $\rho \approx \rho_o(1 - \gamma T)$ and the rate of decrease with temperature (γ) for both σ and ρ is approximately the same (Partington, 1951, p.140). If this were strictly so the capillary constant would indeed be a constant for a given liquid. For water neither σ nor ρ vary linearly with T. ρ progressively departs from linearity below 40 °C and accounts for the variation in a.

In the world of real tubes and real aqueous solutions, additional factors may be significant. Atmospheric contamination reduces surface tension and increases the contact angle between the meniscus and the tube (Olsen, 1965). Etching takes place not only at the meniscus but along the entire length of the tube exposed to acid. Tube diameter was uniformly greater (as measured with a telescoping gage) below the meniscus than above after etching but we could not measure the amount with the instruments available. The solution was cloudy and sometimes a precipitate was observed after etching. If part of the colloidal precipitate enters the meniscus or floats on top of it, surface tension could be affected. Indeed oils have been placed on the meniscus in order to reduce the capillary correction, but the results have been difficult to replicate, and are extremely sensitive to the thickness of the film of oil (Cumming, 1951, p.345). If a contaminated meniscus is a problem with a 4% HF solution, it means that the relation between the area of the meniscus to volume of solution should be explored. This varies with inclination of the tube, of course. We do not have the means to pursue this matter further.

The question arises as to the variation of surface tension with concentration and temperature in aqueous solutions. Although the surface tension of nonaqueous/nonpolar solutions often exhibit an approximately linear dependence on mole fraction, aqueous solutions, however, often show pronounced nonlinearity with concentration (Reid and Sherwood, 1966, p.387). A good example of this is the nonlinearity of H_2O and H_2SO_4 mixtures both with respect to concentration and temperature (Washburn, et al., 1928, p.464). Unfortunately we do not have the same information at hand for aqueous HF solutions. The surface tension of pure HF at 20 °C is 10.41 dyne/cm, and its rate of change with temperature is $-0.07867\,\text{dyne/cm}\cdot{}^\circ\text{C}$ (Dean, 1985, p.10-100). But we do not know what happens as a function of concentration. Perhaps the point is moot. When the solute lowers the surface tension of the pure solvent the solute tends to pass into the surface, so that the surface concentration is larger than that in the bulk of the liquid, whereas, if the solute increases the surface tension, the concentration of the surface layer is less than that of the bulk of the solution (Partington, 1951, p.197 and references cited therein). The difference in the concentration in the surface (C_s) and in the bulk of the fluid (C) is given by Gibb's equation (for dilute solutions): $C_s - C = -(RT)\cdot d(\ln\sigma)/dC$, where R is the gas constant per mole, T is temperature, and σ is the surface tension (Partington, 951, p.197). Thus, the relation between concentration at the meniscus and that in the body of the fluid is complicated and may change with time as the acid is expended.

The examples in the two preceding paragraphs are intended to illustrate the complexity of capillarity and to show that optimal use of acid-etch inclinometry requires careful technique and standardization. The examples also illustrate why we are reluctant to assign physical significance to $(\partial R/\partial T)_D$ and $(\partial R/\partial D)_T$.

ACKNOWLEDGEMENTS

We thank H.W. Olsen and H.S. Swolfs for rigorous reviews of the manuscript and H.W. Olsen for broadening our knowledge of the literature on capillarity. Figures 3 and 4 were drawn by R.J. Ricotta.

Table 1. Major and minor axis (mm), foci, eccentricity (ECCEN) and diameter of equivalent circle (DIA E.C. in mm) for the outside and inside diameters of 6 mm nominal outside diameter inclinometer tubes.

OUTSIDE DIAMETER					INSIDE DIAMETER				
MINOR AXIS	MAJOR AXIS	FOCI	ECCEN	DIA E.C.	MINOR AXIS	MAJOR AXIS	FOCI	ECCEN	DIA E.C.
6.07	6.07	0.00	0.000	6.07	4.45	4.45	0.00	0.000	4.45
6.12	6.12	0.00	0.000	6.12	4.42	4.42	0.00	0.000	4.42
6.05	6.05	0.00	0.000	6.05	4.22	4.22	0.00	0.000	4.22
6.08	6.08	0.00	0.000	6.08	4.61	4.61	0.00	0.000	4.61
6.06	6.06	0.00	0.000	6.06	4.39	4.39	0.00	0.000	4.39
6.06	6.06	0.00	0.000	6.06	4.53	4.53	0.00	0.000	4.53
6.06	6.06	0.00	0.000	6.06	4.43	4.43	0.00	0.000	4.43

Table 2. Major and minor axis (mm), foci, eccentricity (ECCEN) and diameter of equivalent circle (DIA E.C. in mm) for the outside and inside diameters of 10 mm nominal outside diameter inclinometer tubes.

OUTSIDE DIAMETER					INSIDE DIAMETER				
MINOR AXIS	MAJOR AXIS	FOCI	ECCEN	DIA E.C.	MINOR AXIS	MAJOR AXIS	FOCI	ECCEN	DIA E.C.
10.34	10.34	0.00	0.000	10.34	8.56	8.56	0.00	0.000	8.56
10.12	10.12	0.00	0.000	10.12	8.41	8.41	0.00	0.000	8.41
10.25	10.25	0.00	0.000	10.25	8.50	8.50	0.00	0.000	8.50
10.27	10.27	0.00	0.000	10.27	8.57	8.57	0.00	0.000	8.57
10.35	10.35	0.00	0.000	10.35	8.62	8.62	0.00	0.000	8.62
10.11	10.11	0.00	0.000	10.11	8.42	8.42	0.00	0.000	8.42

Table 3. Major and minor axis (mm), foci, eccentricity (ECCEN) and diameter of equivalent circle (DIA E.C. in mm) for the outside and inside diameters of 13 mm nominal outside diameter inclinometer tubes.

OUTSIDE DIAMETER					INSIDE DIAMETER				
MINOR AXIS	MAJOR AXIS	FOCI	ECCEN	DIA E.C.	MINOR AXIS	MAJOR AXIS	FOCI	ECCEN	DIA E.C.
12.70	12.73	0.44	0.069	12.71	10.97	10.97	0.00	0.000	10.97
12.70	12.70	0.00	0.000	12.70	10.95	10.95	0.00	0.000	10.95
12.73	12.73	0.00	0.000	12.73	10.95	10.95	0.00	0.000	10.95
12.70	12.70	0.00	0.000	12.70	10.97	10.97	0.00	0.000	10.97
12.69	12.69	0.00	0.000	12.69	10.95	10.95	0.00	0.000	10.95
12.73	12.73	0.00	0.000	12.73	10.97	10.97	0.00	0.000	10.97

Table 4. Major and minor axis (mm), foci, eccentricity (ECCEN) and diameter of equivalent circle (DIA E.C. in mm) for the outside and inside diameters of 16 mm nominal outside diameter inclinometer tubes.

OUTSIDE DIAMETER					INSIDE DIAMETER				
MINOR AXIS	MAJOR AXIS	FOCI	ECCEN	DIA E.C.	MINOR AXIS	MAJOR AXIS	FOCI	ECCEN	DIA E.C.
15.60	15.60	0.00	0.000	15.60	14.02	14.02	0.00	0.000	14.02
15.45	15.60	0.68	0.088	15.57	14.05	14.05	0.00	0.000	14.05
15.62	15.62	0.00	0.000	15.62	14.06	14.06	0.00	0.000	14.06
15.70	15.80	0.89	0.112	15.75	14.20	14.20	0.00	0.000	14.20
15.72	15.80	0.79	0.101	15.76	14.17	14.17	0.00	0.000	14.17
15.67	15.71	0.56	0.071	15.69	14.19	14.19	0.00	0.000	14.19
15.75	15.82	0.74	0.094	15.78	14.22	14.22	0.00	0.000	14.22
15.57	15.62	0.62	0.080	15.59	14.05	14.05	0.00	0.000	14.05
15.54	15.60	0.68	0.088	15.57	14.00	14.00	0.00	0.000	14.00
15.57	15.65	0.79	0.101	15.61	14.05	14.05	0.00	0.000	14.05
15.62	15.74	0.97	0.123	15.68	13.98	14.16	1.13	0.159	14.07
15.63	15.74	0.93	0.118	15.68	14.07	14.16	0.80	0.113	14.11
15.62	15.68	0.69	0.087	15.65	14.01	14.12	0.88	0.125	14.06
15.58	15.62	0.56	0.072	15.60	13.97	14.05	0.75	0.107	14.01
15.66	15.71	0.63	0.080	15.68	14.03	14.10	0.70	0.100	14.06
15.57	15.66	0.84	0.107	15.61	13.97	14.08	0.88	0.125	14.02
15.57	15.67	0.88	0.113	15.62	14.00	14.07	0.70	0.100	14.03
15.58	15.66	0.79	0.101	15.62	14.00	14.05	0.59	0.084	14.02
15.60	15.67	0.74	0.094	15.63	14.00	14.07	0.70	0.100	14.03
15.66	15.68	0.40	0.050	15.67	14.03	14.11	0.75	0.106	14.07
15.63	15.68	0.63	0.080	15.65	14.00	14.08	0.75	0.106	14.04
15.54	15.65	0.93	0.118	15.59	13.94	14.07	0.95	0.136	14.00
15.54	15.58	0.56	0.072	15.56	13.94	14.02	0.75	0.107	13.98
15.67	15.71	0.56	0.071	15.69	14.05	14.12	0.70	0.099	14.08
15.60	15.62	0.40	0.051	15.61	14.02	14.05	0.46	0.065	14.03
15.57	15.67	0.88	0.113	15.62	13.97	14.10	0.96	0.135	14.03
15.63	15.72	0.84	0.107	15.67	14.02	14.12	0.84	0.119	14.07
15.63	15.66	0.48	0.062	15.64	14.05	14.12	0.70	0.099	14.08
15.62	15.67	0.63	0.080	15.64	14.02	14.12	0.84	0.119	14.07
15.60	15.67	0.74	0.094	15.63	14.01	14.10	0.80	0.113	14.05
15.65	15.75	0.89	0.113	15.70	14.01	14.15	0.99	0.140	14.08
15.56	15.62	0.68	0.088	15.59	14.00	14.05	0.59	0.084	14.02
15.53	15.63	0.88	0.113	15.58	13.97	14.06	0.79	0.113	14.01
15.71	15.86	1.09	0.137	15.78	14.10	14.22	0.92	0.130	14.16
15.65	15.72	0.74	0.094	15.68	14.07	14.12	0.59	0.084	14.09
15.71	15.74	0.49	0.062	15.72	14.11	14.15	0.53	0.075	14.13
15.58	15.63	0.62	0.080	15.60	13.98	14.10	0.92	0.130	14.04
15.62	15.67	0.63	0.080	15.64	14.01	14.08	0.70	0.100	14.04
15.63	15.65	0.40	0.051	15.64	14.06	14.08	0.38	0.053	14.07
15.52	15.63	0.93	0.118	15.57	13.94	14.02	0.75	0.107	13.98
15.49	15.54	0.62	0.080	15.51	13.94	14.00	0.65	0.092	13.97

Table 4 (continued). Major and minor axis (mm), foci, eccentricity (ECCEN) and diameter of equivalent circle (DIA E.C. in mm) for the outside and inside diameters of 16 mm nominal outside diameter inclinometer tubes.

OUTSIDE DIAMETER					INSIDE DIAMETER				
MINOR AXIS	MAJOR AXIS	FOCI	ECCEN	DIA E.C.	MINOR AXIS	MAJOR AXIS	FOCI	ECCEN	DIA E.C.
15.63	15.70	0.74	0.094	15.66	14.02	14.10	0.75	0.106	14.06
15.53	15.61	0.79	0.101	15.57	13.94	14.02	0.75	0.107	13.98
15.49	15.62	1.01	0.129	15.55	13.92	14.03	0.88	0.125	13.97
15.67	15.71	0.56	0.071	15.69	14.08	14.12	0.53	0.075	14.10
15.71	15.82	0.93	0.118	15.76	14.14	14.20	0.65	0.092	14.17
15.58	15.63	0.62	0.080	15.60	14.01	14.07	0.65	0.092	14.04
15.58	15.63	0.62	0.080	15.60	14.02	14.07	0.59	0.084	14.04
15.52	15.57	0.62	0.080	15.54	13.91	13.98	0.70	0.100	13.94
15.43	15.52	0.83	0.108	15.47	13.87	13.97	0.83	0.119	13.92
15.62	15.79	1.16	0.146	15.70	14.06	14.24	1.13	0.158	14.15
15.63	15.70	0.74	0.094	15.66	14.06	14.14	0.75	0.106	14.10
15.51	15.56	0.62	0.080	15.53	13.93	14.00	0.70	0.100	13.96
15.65	15.68	0.48	0.062	15.66	14.08	14.12	0.53	0.075	14.10
15.66	15.75	0.84	0.107	15.70	14.02	14.15	0.96	0.135	14.08
15.61	15.66	0.63	0.080	15.63	14.02	14.12	0.84	0.119	14.07
15.61	15.70	0.84	0.107	15.65	13.98	14.10	0.92	0.130	14.04
15.56	15.67	0.93	0.118	15.61	13.96	14.11	1.03	0.145	14.03
15.70	15.71	0.28	0.036	15.70	14.10	14.14	0.53	0.075	14.12
15.57	15.60	0.48	0.062	15.58	13.98	14.06	0.75	0.107	14.02
15.49	15.67	1.18	0.151	15.58	13.88	14.11	1.27	0.180	13.99
15.57	15.62	0.62	0.080	15.59	13.97	14.06	0.79	0.113	14.01
15.75	15.82	0.74	0.094	15.78	14.15	14.22	0.70	0.099	14.18
15.54	15.66	0.97	0.124	15.60	13.96	14.08	0.92	0.130	14.02
15.61	15.71	0.88	0.113	15.66	14.00	14.15	1.03	0.145	14.07
15.48	15.57	0.84	0.107	15.52	13.87	14.00	0.95	0.136	13.93
15.49	15.65	1.12	0.143	15.57	13.91	14.12	1.21	0.172	14.01
15.48	15.66	1.18	0.151	15.57	13.89	14.10	1.21	0.172	13.99
15.62	15.77	1.08	0.138	15.69	14.03	14.19	1.06	0.150	14.11
15.62	15.66	0.56	0.071	15.64	14.02	14.08	0.65	0.092	14.05
15.71	15.79	0.79	0.101	15.75	14.12	14.22	0.84	0.118	14.17
15.54	15.67	1.01	0.129	15.60	13.97	14.07	0.84	0.119	14.02
15.63	15.80	1.16	0.146	15.71	14.06	14.24	1.13	0.158	14.15
15.56	15.58	0.39	0.051	15.57	13.96	14.01	0.59	0.084	13.98
15.43	15.51	0.79	0.101	15.47	13.87	13.97	0.83	0.119	13.92

Table 5. Major and minor axis (mm), foci, eccentricity (ECCEN) and diameter of equivalent circle (DIA E.C. in mm) for the outside and inside diameters of 19 mm nominal outside diameter inclinometer tubes.

OUTSIDE DIAMETER					INSIDE DIAMETER				
MINOR AXIS	MAJOR AXIS	FOCI	ECCEN	DIA E.C.	MINOR AXIS	MAJOR AXIS	FOCI	ECCEN	DIA E.C.
18.75	18.75	0.00	0.000	18.75	16.51	16.51	0.00	0.000	16.51
18.72	18.75	0.53	0.057	18.73	16.47	16.47	0.00	0.000	16.47
18.87	18.87	0.00	0.000	18.87	16.61	16.61	0.00	0.000	16.61
18.85	18.85	0.00	0.000	18.85	16.59	16.59	0.00	0.000	16.59
18.86	18.86	0.00	0.000	18.86	16.57	16.57	0.00	0.000	16.57
18.75	18.77	0.43	0.046	18.76	16.54	16.54	0.00	0.000	16.54

Table 6. Major and minor axis (mm), foci, eccentricity (ECCEN) and diameter of equivalent circle (DIA E.C. in mm) for the outside and inside diameters of 20 mm nominal outside diameter inclinometer tubes. Tubes are borosilicate glass.

OUTSIDE DIAMETER					INSIDE DIAMETER				
MINOR AXIS	MAJOR AXIS	FOCI	ECCEN	DIA E.C.	MINOR AXIS	MAJOR AXIS	FOCI	ECCEN	DIA E.C.
19.76	19.81	0.70	0.071	19.78	17.86	17.88	0.42	0.047	17.87
19.74	19.74	0.00	0.000	19.74	17.83	17.83	0.00	0.000	17.83
19.91	19.91	0.00	0.000	19.91	17.92	17.92	0.00	0.000	17.92
19.89	19.89	0.00	0.000	19.89	17.93	17.93	0.00	0.000	17.93
19.76	19.83	0.83	0.084	19.79	17.88	17.91	0.52	0.058	17.89
19.76	19.76	0.00	0.000	19.76	17.87	17.87	0.00	0.000	17.87
19.89	19.89	0.00	0.000	19.89	17.96	17.96	0.00	0.000	17.96
19.72	19.77	0.70	0.071	19.74	17.86	17.91	0.67	0.075	17.88
19.81	19.89	0.89	0.090	19.85	17.93	17.96	0.52	0.058	17.94
19.71	19.71	0.00	0.000	19.71	17.82	17.82	0.00	0.000	17.82
19.76	19.80	0.63	0.064	19.78	17.88	17.88	0.00	0.000	17.88
19.76	19.76	0.00	0.000	19.76	17.96	17.96	0.00	0.000	17.96

Table 7. Major and minor axis (mm), foci, eccentricity (ECCEN) and diameter of equivalent circle (DIA E.C. in mm) for the outside and inside diameters of 25 mm nominal outside diameter inclinometer tubes.

OUTSIDE DIAMETER					INSIDE DIAMETER				
MINOR AXIS	MAJOR AXIS	FOCI	ECCEN	DIA E.C.	MINOR AXIS	MAJOR AXIS	FOCI	ECCEN	DIA E.C.
25.54	24.64	1.11	0.090	24.59	21.87	22.00	1.19	0.109	21.93
24.54	24.64	1.11	0.090	24.59	21.87	22.00	1.19	0.109	21.93
24.59	24.59	0.00	0.000	24.59	22.02	22.02	0.00	0.000	22.02
24.56	24.66	1.11	0.090	24.61	21.97	22.07	1.05	0.095	22.02
24.60	24.68	0.99	0.080	24.64	22.00	22.14	1.24	0.112	22.07
24.64	24.66	0.50	0.040	24.65	22.02	22.05	0.57	0.052	22.03
24.50	24.54	0.70	0.057	24.52	21.87	22.00	1.19	0.109	21.93
24.50	24.50	0.00	0.000	24.50	21.92	21.92	0.00	0.000	21.92
24.65	24.73	0.99	0.080	24.69	22.02	22.17	1.29	0.116	22.09
24.71	24.77	0.86	0.070	24.74	22.12	22.23	1.10	0.099	22.17
24.56	24.59	0.61	0.049	24.57	21.95	22.01	0.81	0.074	21.98
24.49	24.51	0.49	0.040	24.50	21.84	21.95	1.10	0.100	21.89
24.49	24.54	0.78	0.064	24.51	21.89	22.01	1.15	0.104	21.95
24.66	24.66	0.00	0.000	24.66	22.10	22.10	0.00	0.000	22.10
24.46	24.54	0.99	0.081	24.50	21.86	22.00	1.24	0.113	21.93
24.59	24.61	0.50	0.040	24.60	22.02	22.05	0.57	0.052	22.03
24.49	24.54	0.78	0.064	24.51	21.87	21.95	0.94	0.085	21.91
24.71	24.74	0.61	0.049	24.72	22.15	22.16	0.33	0.030	22.15
24.46	24.59	1.26	0.103	24.52	21.88	21.98	1.05	0.095	21.93
24.82	24.87	0.79	0.063	24.84	22.17	22.23	0.82	0.073	22.20
24.54	24.59	0.78	0.064	24.56	21.95	22.02	0.88	0.080	21.98
24.61	24.64	0.61	0.049	24.62	22.05	22.12	0.88	0.079	22.08
24.66	24.74	0.99	0.080	24.70	22.05	22.15	1.05	0.095	22.10
24.49	24.49	0.00	0.000	24.49	21.95	21.95	0.00	0.000	21.95
24.61	24.61	0.00	0.000	24.61	22.02	22.02	0.00	0.000	22.02
24.68	24.68	0.00	0.000	24.68	22.11	22.11	0.00	0.000	22.11
24.79	24.79	0.00	0.000	24.79	22.10	22.14	0.67	0.060	22.12
24.40	24.45	0.78	0.064	24.42	21.82	21.91	0.99	0.091	21.86
24.46	24.52	0.86	0.070	24.49	21.87	21.97	1.05	0.095	21.92
24.49	24.60	1.16	0.094	24.54	21.89	22.07	1.41	0.127	21.98
24.54	24.54	0.00	0.000	24.54	21.95	21.95	0.00	0.000	21.95
24.63	24.63	0.00	0.000	24.63	21.98	22.06	0.94	0.085	22.02
24.49	24.59	1.11	0.090	24.54	21.92	22.00	0.94	0.085	21.96
24.56	24.61	0.78	0.064	24.58	21.95	22.00	0.74	0.067	21.97
24.66	24.69	0.61	0.049	24.67	22.02	22.10	0.94	0.085	22.06
24.56	24.66	1.11	0.090	24.61	21.87	22.02	1.28	0.117	21.94
24.66	24.71	0.79	0.064	24.68	22.07	22.12	0.74	0.067	22.09
24.74	24.82	1.00	0.080	24.78	22.12	22.17	0.74	0.067	22.14
24.68	24.71	0.61	0.049	24.69	22.05	22.10	0.74	0.067	22.07
24.54	24.54	0.00	0.000	24.54	21.95	22.00	0.74	0.067	21.97
24.61	24.61	0.00	0.000	24.61	21.97	22.07	1.05	0.095	22.02

Table 7 (continued). Major and minor axis (mm), foci, eccentricity (ECCEN) and diameter of equivalent circle (DIA E.C. in mm) for the outside and inside diameters of 25 mm nominal outside diameter inclinometer tubes.

OUTSIDE DIAMETER					INSIDE DIAMETER				
MINOR AXIS	MAJOR AXIS	FOCI	ECCEN	DIA E.C.	MINOR AXIS	MAJOR AXIS	FOCI	ECCEN	DIA E.C.
24.36	24.42	0.86	0.070	24.39	21.79	21.84	0.74	0.068	21.81
24.37	24.49	1.21	0.099	24.43	21.74	21.95	1.51	0.138	21.84
24.56	24.61	0.78	0.064	24.58	21.89	22.02	1.19	0.109	21.95
24.74	24.79	0.79	0.063	24.76	22.10	22.15	0.74	0.067	22.12
24.54	24.54	0.00	0.000	24.54	21.97	21.97	0.00	0.000	21.97
24.56	24.56	0.00	0.000	24.56	22.00	22.02	0.47	0.043	22.01
24.59	24.64	0.78	0.064	24.61	22.02	22.12	1.05	0.095	22.07
24.47	24.47	0.00	0.000	24.47	21.84	21.89	0.74	0.068	21.86
24.75	24.78	0.61	0.049	24.76	22.15	22.15	0.00	0.000	22.15
24.78	24.78	0.00	0.000	24.78	22.14	22.20	0.82	0.073	22.17
24.60	24.60	0.00	0.000	24.60	21.98	22.01	0.57	0.052	21.99
24.70	24.70	0.00	0.000	24.70	22.12	22.12	0.00	0.000	22.12
24.60	24.64	0.70	0.057	24.62	22.00	22.07	0.88	0.080	22.03
24.65	24.65	0.00	0.000	24.65	22.02	22.11	1.00	0.090	22.06
24.68	24.68	0.00	0.000	24.68	22.05	22.07	0.47	0.043	22.06
24.54	24.54	0.00	0.000	24.54	21.97	22.05	0.94	0.085	22.01
24.56	24.64	0.99	0.081	24.60	21.97	22.05	0.94	0.085	22.01
24.61	24.69	0.99	0.080	24.65	22.00	22.12	1.15	0.104	22.06
24.47	24.47	0.00	0.000	24.47	21.87	21.92	0.74	0.068	21.89
24.54	24.54	0.00	0.000	24.54	21.97	22.00	0.57	0.052	21.98
24.45	24.45	0.00	0.000	24.45	21.95	21.95	0.00	0.000	21.95
24.57	24.57	0.00	0.000	24.57	21.97	21.97	0.00	0.000	21.97

Table 8. Minimum (MIN), maximum (MAX), and difference (MAX − MIN) of outside and inside diameters (DIAMETER) of nominal 16 and 25 mm tubes used in this study. The tubes are manufactured from soda-lime glass.

NOMINAL TUBE (mm)	DIAMETER	MIN (mm)	MAX (mm)	MAX - MIN (mm)
16	Inside	13.92	14.22	0.30
16	Outside	15.47	15.78	0.31
25	Inside	21.81	22.20	0.39
25	Outside	24.39	24.84	0.45

Table 9. Mean outside (M.O.D.) and inside (M.I.D.) diameters of tubes and their standard deviations. The tubes are soda-lime glass except for the borosilicates indicated by a B.

NOMINAL TUBE (mm)	N	M.O.D. (mm)	M.I.D. (mm)
6	7	6.07±0.02	4.45±0.12
10	6	10.24±0.10	8.51±0.09
13	6	12.71±0.02	10.96±0.01
16	75	15.63±0.07	14.05±0.07
19	6	18.80±0.06	16.55±0.05
20B	12	19.80±0.07	17.90±0.05
25	63	24.62±0.10	22.01±0.09

Table 10. Mean outside (M.O.E.) and inside (M.I.E.) eccentricity of tubes and their standard deviations. The tubes are soda-lime glass.

NOMINAL TUBE (mm)	N (MOE/MIE)*	M.O.E.	M.I.E.
16	73/65	0.096±0.026	0.113±0.027
25	39/51	0.069±0.017	0.084±0.023

* Number of eccentricity values for outside (MOE) and inside (MIE) excluding zero eccentricity.

Table 11. Average chemical composition of EXAX^{TM*} brand culture tubes.

CHEMICAL COMPOSITION	AVERAGE %
SiO_2	68
B_2O_3	2
Al_2O_3	3
CaO	5
MgO	4
Na_2O	15
K_2O	1
BaO	2

* EXAX is trademark of Kimble Glass.

Table 12. Average etch times for all tubes as a function of temperature.

TEMPERATURE (°C)	TIME (min)
4	106
10	65
22	42
40	31
60	25
80	21

Table 13. Measured apparent angle of 16 and 25 mm nominal, outside-diameter inclinometer tubes for various true angles at 4°, 22°, and 80°C.

TRUE ANGLE	16mm			25mm		
	4°C	22°C	80°C	4°C	22°C	80°C
90	90	90	90	90	90	90
85	87.02	86.94	87.14	—	86.56	86.00
80	84.52	83.77	83.45	—	82.65	82.50
75	81.71	80.55	80.36	—	78.75	79.00
70	78.05	77.15	76.53	—	75.00	74.50
67.5	—	—	—	73.33	—	—
65	—	73.25	73.00	—	70.70	70.00
60	71.30	70.07	68.62	—	66.40	66.00
55	66.84	65.37	64.49	—	61.60	62.00
50	63.53	61.10	60.40	—	57.52	56.50
45	59.02	56.74	55.84	53.50	52.55	52.50
40	53.52	52.51	50.84	—	47.50	47.50
35	49.01	47.51	45.95	—	42.50	42.00
30	43.39	42.05	40.66	—	37.37	37.00
25	37.49	36.58	34.71	—	31.50	30.98
22.5	—	—	—	29.33	—	—
20	31.42	29.19	28.50	—	26.00	26.00
15	25.00	23.18	22.68	—	19.50	19.50
10	17.75	15.93	16.00	—	13.50	13.50
0	0	0	0	0	0	0

Table 14. Number of points, average value, minimum and maximum value of absolute value of X−coordinate for 16mm nominal, outside-diameter inclinometer tubes at 4°C. Values are calculated from least squares fits of calibration data to a circle. Each run lasted through N iterations until the correction factor was less than 1×10^{-5}.

FILE	N	A	$\overline{A}$	MIN	MAX
A16.C4a	2562	96.542	96.060	93.585533	97.914825
A16.C4b	312	95.950	96.055	95.735344	96.296028
A16.C4c	211	96.083	96.057	96.003639	96.127800
A16.C4d	168	96.063	96.057	96.039024	96.069702
A16.C4e	26	96.054	96.056	96.052345	96.059784
A16.C4f	26	96.058	96.056	96.055313	96.058350
A16.C4g	26	96.056	96.057	96.055687	96.057297
A16.C4h	12	96.056	96.057	96.056305	96.057014

FILE - Name of the individual file in which the X−coordinate from each iteration was stored for an individual run. The new starting value for each run was entered to only three decimal places.

N - Number of iterations of the least squares fit to a circle until the correction was less than 1×10^{-5}.

A - absolute value of calculated X−coordinate of center of circle when correction to A was less than 1×10^{-5} for each run of the designated FILE.

$\overline{A}$ - Average of all N points of file designated in list FILE.

MIN - Minimum value in file designated in list FILE.

MAX - Maximum value in file designated in list FILE.

Starting value of A was 100.0 for the initial guess of the least squares calculation.

Table 15. Number of points, average value, minimum and maximum value of absolute value of $X-$coordinate for 16 mm nominal, outside-diameter inclinometer tubes at 22°C. Values are calculated from least squares fits of calibration data to a circle. Each run lasted through N iterations until the correction factor was less than 1×10^{-5}.

FILE	N	A	$\overline{A}$	MIN	MAX
A16.C22a	4168	116.442	118.804	105.432434	129.611511
A16.C22b	371	118.220	118.726	117.561081	120.276886
A16.C22c	574	118.812	118.718	118.468864	119.049751
A16.C22d	211	118.693	118.716	118.653046	118.763878
A16.C22e	168	118.710	118.717	118.704880	118.732300
A16.C22f	26	118.719	118.717	118.713310	118.720970
A16.C22g	26	118.716	118.716	118.717781	118.717781
A16.C22h	12	118.716	118.717	118.716293	118.716965

FILE - Name of the individual file in which the $X-$coordinate from each iteration was stored for an individual run. The new starting value for each run was entered to only three decimal places.

N - Number of iterations of the least squares fit to a circle until the correction was less than 1×10^{-5}.

A - absolute value of calculated $X-$coordinate of center of circle when correction to A was less than 1×10^{-5} for each run of the designated FILE.

$\overline{A}$ - Average of all N points of file designated in list FILE.

MIN - Minimum value in file designated in list FILE.

MAX - Maximum value in file designated in list FILE.

Starting value of A was 150.0 for the initial guess of the least squares calculation.

Table 16. Number of points, average value, minimum and maximum value of absolute value of X-coordinate for 16 mm nominal, outside-diameter inclinometer tubes at 80 °C. Values are calculated from least squares fits of calibration data to a circle. Each run lasted through N iterations until the correction factor was less than 1×10^{-5}.

FILE	N	A	$\overline{A}$	MIN	MAX
A16.C80a	816	138.870	136.976	129.634613	142.646317
A16.C80b	2892	137.170	136.931	135.666763	137.874298
A16.C80c	259	136.986	136.930	136.770844	137.048950
A16.C80d	211	136.917	136.930	136.893112	136.957901
A16.C80e	26	136.936	136.931	136.923676	136.939087
A16.C80f	26	136.928	136.930	136.926407	136.933105
A16.C80g	26	136.931	136.930	136.929123	136.931747
A16.C80h	26	136.930	136.930	136.929749	136.930618
A16.C80i	12	136.930	136.930	136.930115	136.930420

FILE - Name of the individual file in which the X−coordinate from each iteration was stored for an individual run. The new starting value for each run was entered to only three decimal places.

N - Number of iterations of the least squares fit to a circle until the correction was less than 1×10^{-5}.

A - absolute value of calculated X−coordinate of center of circle when correction to A was less than 1×10^{-5} for each run of the designated FILE.

$\overline{A}$ - Average of all N points of file designated in list FILE.

MIN - Minimum value in file designated in list FILE.

MAX - Maximum value in file designated in list FILE.

Starting value of A was 150.0 for the initial guess of the least squares calculation.

Table 17. Number of points, average value, minimum and maximum value of absolute value of X-coordinate for 25 mm nominal, outside-diameter inclinometer tubes at 4 °C. Values are calculated from least squares fits of calibration data to a circle. Each run lasted through N iterations until the correction factor was less than 1×10^{-5}.

FILE	N	A	$\overline{A}$	MIN	MAX
A25.C4a	3795	190.637	191.561	186.372833	195.462128
A25.C4b	168	191.314	191.558	191.095261	192.168488
A25.C4c	501	191.506	191.553	191.434113	191.712418
A25.C4d	211	191.564	191.553	191.529587	191.584091
A25.C4e	26	191.548	191.552	191.545410	191.558380
A25.C4f	26	191.555	191.553	191.550446	191.556076
A25.C4g	26	191.552	191.553	191.551422	191.553909
A25.C4h	26	191.553	191.553	191.552429	191.553406
A25.C4i	4	191.553	191.553	191.552750	191.552841

FILE - Name of the individual file in which the $X-$coordinate from each iteration was stored for an individual run. The new starting value for each run was entered to only three decimal places.

N - Number of iterations of the least squares fit to a circle until the correction was less than 1×10^{-5}.

A - absolute value of calculated $X-$coordinate of center of circle when correction to A was less than 1×10^{-5} for each run of the designated FILE.

$\overline{A}$ - Average of all N points of file designated in list FILE.

MIN - Minimum value in file designated in list FILE.

MAX - Maximum value in file designated in list FILE.

Starting value of A was 200.0 for the initial guess of the least squares calculation.

Table 18. Number of points, average value, minimum and maximum value of absolute value of X-coordinate for 25 mm nominal, outside-diameter inclinometer tubes at 22 °C. Values are calculated from least squares fits of calibration data to a circle. Each run lasted through N iterations until the correction factor was less than 1×10^{-5}.

FILE	N	A	$\overline{A}$	MIN	MAX
A25.C22a	4384	221.265	218.614	203.408234	231.096390
A25.C22b	1113	218.110	218.537	216.761551	219.865540
A25.C22c	501	218.454	218.539	218.325058	218.824539
A25.C22d	211	218.559	218.539	218.496353	218.594254
A25.C22e	68	218.531	218.538	218.524200	218.548477
A25.C22f	26	218.541	218.538	218.534592	218.542862
A25.C22g	26	218.537	218.538	218.536209	218.539551
A25.C22h	26	218.539	218.538	218.537567	218.538864
A25.C22i	26	218.538	218.538	218.537537	218.538559
A25.C22j	4	218.538	218.538	218.538116	218.538208

FILE - Name of the individual file in which the $X-$coordinate from each iteration was stored for an individual run. The new starting value for each run was entered to only three decimal places.

N - Number of iterations of the least squares fit to a circle until the correction was less than 1×10^{-5}.

A - absolute value of calculated $X-$coordinate of center of circle when correction to A was less than 1×10^{-5} for each run of the designated FILE.

$\overline{A}$ - Average of all N points of file designated in list FILE.

MIN - Minimum value in file designated in list FILE.

MAX - Maximum value in file designated in list FILE.

Starting value of A was 250.0 for the initial guess of the least squares calculation.

Table 19. Number of points, average value, minimum and maximum value of absolute value of X–coordinate for 25 mm nominal, outside-diameter inclinometer tubes at 80 °C. Values are calculated from least squares fits of calibration data to a circle. Each run lasted through N iterations until the correction factor was less than 1×10^{-5}.

FILE	N	A	$\overline{A}$	MIN	MAX
A25.C80a	4186	229.058	230.948	220.220139	239.280960
A25.C80b	1833	231.184	230.917	229.982559	232.171310
A25.C80c	433	230.861	230.914	230.736343	231.048340
A25.C80d	211	230.928	230.916	230.888275	230.951324
A25.C80e	26	230.910	230.914	230.906631	230.921539
A25.C80f	26	230.917	230.915	230.912613	230.918625
A25.C80g	26	230.914	230.915	230.913956	230.916092
A25.C80h	26	230.916	230.915	230.914597	230.915970
A25.C80i	26	230.915	230.915	230.914627	230.915588
A25.C80j	4	230.915	230.915	230.915176	230.915298

FILE - Name of the individual file in which the X–coordinate from each iteration was stored for an individual run. The new starting value for each run was entered to only three decimal places.

N - Number of iterations of the least squares fit to a circle until the correction was less than 1×10^{-5}.

A - absolute value of calculated X–coordinate of center of circle when correction to A was less than 1×10^{-5} for each run of the designated FILE.

$\overline{A}$ - Average of all N points of file designated in list FILE.

MIN - Minimum value in file designated in list FILE.

MAX - Maximum value in file designated in list FILE.

Starting value of A was 250.0 for the initial guess of the least squares calculation.

Table 20. Number of points, average value, minimum and maximum value of absolute value of X—coordinate for 16 mm nominal, outside-diameter inclinometer tubes at 4 °C. Values are calculated from least squares fits of calibration data to a circle. Each run lasted through N iterations until the correction factor was less than 1×10^{-5}. The correction factor, however, was divided by 3 to force convergence.

FILE	N	A	$\overline{A}$	MIN	MAX
A16.C4a1	1499	96.584	96.060	94.291260	98.650963
A16.C4b1	133	96.192	96.054	95.808365	96.407578
A16.C4c1	503	96.082	96.056	95.992470	96.146828
A16.C4d1	37	96.066	96.056	96.044556	96.073540
A16.C4e1	11	96.052	96.055	96.052155	96.062874
A16.C4f1	11	96.059	96.057	96.053535	96.058800
A16.C4g1	11	96.055	96.056	96.055473	96.058205
A16.C4h1	11	96.057	96.057	96.055534	96.057373
A16.C4i1	10	96.056	96.057	96.056427	96.056870
A16.C4j1	11	96.057	96.057	96.056206	96.056900

FILE - Name of the individual file in which the X—coordinate from each iteration was stored for an individual run. The new starting value for each run was entered to only three decimal places.

N - Number of iterations of the least squares fit to a circle until the correction was less than 1×10^{-5}.

A - absolute value of calculated X—coordinate of center of circle when correction to A was less than 1×10^{-5} for each run of the designated FILE.

$\overline{A}$ - Average of all N points of file designated in list FILE.

MIN - Minimum value in file designated in list FILE.

MAX - Maximum value in file designated in list FILE.

Starting value of A was 100.0 for the initial guess of the least squares calculation.

Table 21. Inclinometer tube: 16mm @ 4 °C. Results of last calibration calculation including statistics and deviations between calculated and observed true angles.

$$(x + A)^2 + (y - (90 + A))^2 = R^2$$

$$R^2 = A^2 + (90 + A)^2$$

Number of data points = 17

A = 96.056
Uncertainty in A = 0.300
Student's t value for 16 degrees of freedom and $P_{0.005}$ = 2.921
99% confidence interval = 95.180 < A < 96.932
χ^2 value for 16 degrees of freedom and $P_{0.01}$ = 32.000
and S = 2.813 $\Longrightarrow$ THIS IS A GOOD FIT! since S < χ^2
Number of iterations = 12
R = 209.389
99% confidence interval = 208.209 < R < 210.567
Uncertainty of function at 45 true degrees = 2.912×10^{-2}

Deviations (d) at (true angles): $\bar{d}$ = 0.3

0.0(90.0)	0.6(85.0)	-0.1(80.0)	-0.4(75.0)	0.3(70.0)
-0.2(60.0)	0.5(55.0)	-0.5(50.0)	-0.4(45.0)	0.5(40.0)
-0.1(35.0)	0.1(30.0)	0.2(25.0)	0.1(20.0)	-0.2(15.0)
-0.3(10.0)	0.0(0.0)			

Table 22. Inclinometer tube: 16 mm @ 22 °C. Results of last calibration calculation including statistics and deviations between calculated and observed true angles.

$$(x + A)^2 + (y - (90 + A))^2 = R^2$$

$$R^2 = A^2 + (90 + A)^2$$

Number of data points = 18

A = 118.716
Uncertainty in A = 0.437
Student's t value for 17 degrees of freedom and $P_{0.005}$ = 2.898
99% confidence interval = 117.449 < A < 119.983
χ^2 value for 17 degrees of freedom and $P_{0.01}$ = 33.409
and S = 3.842 $\Longrightarrow$ THIS IS A GOOD FIT! since S < χ^2
Number of iterations = 12
R = 240.116
99% confidence interval = 238.389 < R < 241.845
Uncertainty of function at 45 true degrees = 3.187×10^{-2}

Deviations (d) at (true angles): $\bar{d}$ = 0.3

0.0(90.0)	0.2(85.0)	0.3(80.0)	0.3(75.0)	0.2(70.0)
0.5(65.0)	-0.3(60.0)	0.5(55.0)	0.4(50.0)	0.2(45.0)
-0.4(40.0)	-0.4(35.0)	-0.4(30.0)	-0.6(25.0)	0.4(20.0)
0.0(15.0)	0.1(10.0)	0.0(0.0)		

Table 23. Inclinometer tube: 16 mm @ 80 °C. Results of last calibration calculation including statistics and deviations between calculated and observed true angles.

$$(x + A)^2 + (y - (90 + A))^2 = R^2$$

$$R^2 = A^2 + (90 + A)^2$$

Number of data points = 18

A = 136.930
Uncertainty in A = 0.374
Student's t value for 17 degrees of freedom and $P_{0.005}$ = 2.898
99% confidence interval = 135.847 < A < 138.013
χ^2 value for 17 degrees of freedom and $P_{0.01}$ = 33.409
and S = 1.874 $\Longrightarrow$ THIS IS A GOOD FIT! since S < χ^2
Number of iterations = 12
R = 265.042
99% confidence interval = 263.555 < R < 266.529
Uncertainty of function at 45 true degrees = 2.220×10^{-2}

Deviations (d) at (true angles): $\overline{d}$ = 0.2

0.0(90.0)	-0.4(85.0)	0.3(80.0)	-0.2(75.0)	0.2(70.0)
-0.1(65.0)	0.4(60.0)	0.3(55.0)	0.0(50.0)	0.0(45.0)
0.1(40.0)	-0.1(35.0)	-0.2(30.0)	0.0(25.0)	0.1(20.0)
-0.3(15.0)	-0.5(10.0)	0.0(0.0)		

Table 24. Inclinometer tube: 25 mm @ 4 °C. Results of last calibration calculation including statistics and deviations between calculated and observed true angles.

$$(x + A)^2 + (y - (90 + A))^2 = R^2$$

$$R^2 = A^2 + (90 + A)^2$$

Number of data points = 5

A = 191.553

Uncertainty in A = 0.710

Student's t value for 4 degrees of freedom and $P_{0.005} = 4.604$

99% confidence interval = 188.285 < A < 194.821

χ^2 value for 4 degrees of freedom and $P_{0.01} = 13.277$

and S = 0.042 $\Longrightarrow$ THIS IS A GOOD FIT! since $S < \chi^2$

Number of iterations = 4

R = 340.536

99% confidence interval = 335.997 < R < 345.077

Uncertainty of function at 45 true degrees = 2.524×10^{-2}

Deviations (d) at (true angles): $\bar{d} = 0.1$

0.0(90.0)	0.0(67.5)	-0.1(45.0)	0.1(22.5)	0.0(0.0)

Table 25. Inclinometer tube: 25 mm @ 22 °C. Results of last calibration calculation including statistics and deviations between calculated and observed true angles.

$$(x + A)^2 + (y - (90 + A))^2 = R^2$$

$$R^2 = A^2 + (90 + A)^2$$

Number of data points = 18

A = 218.538

Uncertainty in A = 0.879

Student's t value for 17 degrees of freedom and $P_{0.005}$ = 2.898

99% confidence interval = 215.991 < A < 221.085

χ^2 value for 17 degrees of freedom and $P_{0.01}$ = 33.409

and S = 0.817 $\Longrightarrow$ THIS IS A GOOD FIT! since S < χ^2

Number of iterations = 4

R = 378.093

99% confidence interval = 374.543 < R < 381.644

Uncertainty of function at 45 true degrees = 2.526×10^{-2}

Deviations (d) at (true angles): $\overline{d}$ = 0.2

0.0(90.0)	-0.2(85.0)	0.0(80.0)	0.1(75.0)	-0.2(70.0)
0.0(65.0)	0.0(60.0)	0.4(55.0)	-0.2(50.0)	0.0(45.0)
0.1(40.0)	0.0(35.0)	-0.2(30.0)	0.1(25.0)	-0.2(20.0)
0.2(15.0)	0.0(10.0)	0.0(0.0)		

Table 26. Inclinometer tube: 25 mm @ 80 °C. Results of last calibration calculation including statistics and deviations between calculated and observed true angles.

$$(x + A)^2 + (y - (90 + A))^2 = R^2$$

$$R^2 = A^2 + (90 + A)^2$$

Number of data points = 18

A = 230.915

Uncertainty in A = 1.862

Student's t value for 17 degrees of freedom and $P_{0.005}$ = 2.898

99% confidence interval = 225.520 < A < 236.310

χ^2 value for 17 degrees of freedom and $P_{0.01}$ = 33.409
and S = 3.075 $\Longrightarrow$ THIS IS A GOOD FIT! since S < χ^2

Number of iterations = 4

R = 395.358

99% confidence interval = 387.830 < R < 402.890

Uncertainty of function at 45 true degrees = 4.888×10^{-2}

Deviations (d) at (true angles): $\overline{d}$ = 0.3

0.0(90.0)	0.5(85.0)	0.1(80.0)	-0.4(75.0)	0.1(70.0)
0.5(65.0)	0.1(60.0)	-0.4(55.0)	0.6(50.0)	-0.3(45.0)
-0.2(40.0)	0.1(35.0)	-0.2(30.0)	0.3(25.0)	-0.4(20.0)
0.0(15.0)	-0.2(10.0)	0.0(0.0)		

Table 27. Statistical analysis of circles relating true and apparent angles for curves at two different temperatures for tubes of the same diameter. The analysis follows that of p. 5–10.

TUBE SIZE	T (°C)	n	A	s_A	f (45°)	s_f	ANG	F_A	$F_{0.95}$	s_A's	t_A	ν_A	t_A (5%)	$True_A$	F_f	s_f's	t_f	ν_f	t_f (5%)	$True_f$
16	22	18	118.716	0.437	56.74	3.187×10^{-2}														
	4	17	96.056	0.300	59.02	2.912×10^{-2}														
							58	2.11	2.21	=	172.69	33	2.036	H_1	1.19	=	179.05	33	2.036	H_1
16	22	18	118.716	0.437	56.74	3.187×10^{-2}														
	80	18	136.930	0.374	55.84	2.220×10^{-2}														
							56	1.37	2.22	=	-130.56	34	2.034	H_1	2.06	=	-127.22	34	2.034	H_1
25	22	18	218.538	0.879	52.55	2.526×10^{-2}														
	4	5	191.553	0.710	53.50	2.524×10^{-2}														
							53	1.30	4.88	=	60.35	21	2.080	H_1	0.85	=	64.58	21	2.080	H_1
25	80	18	230.915	1.862	52.5	4.888×10^{-2}														
	22	18	218.538	0.879	52.55	2.526×10^{-2}														
							52	4.49	2.22	≠	25.50	25	2.060	H_1	3.74	≠	26.21	26	2.056	H_1

TUBE SIZE – nominal outside diameter of tube (mm).

T(°C) – Temperature of measurement.

n – number of points used to determine A.

A – Coordinate (center of circle [-A,90+A]).

s_A – uncertainty in A.

f (45°) – apparent angle at true angle of 45°.

s_f – uncertainty of function at 45 true degrees.

ANG – Approximate apparent angle at true angle of 45°.

F_A – variance ratio test (equation 32) - A.

$F_{0.95}$ – F-distribution at 95%.

s_A's – { = implies variances are equal. ≠ implies variances are NOT equal.

t_A – t-test { equation 40 - equal variances, or equation 42 - unequal variances.

ν_A – Number of degrees freedom - A { n_1+n_2-2 - equal variances, or equation 43 - unequal variances.

t_A(5%) – Student's t-distribution at 5% for ν_A degrees of freedom.

$True_A$ – { H_o : $A_1=A_2$, or H_1 : $A_1\neq A_2$.

F_f – Variance ratio test (equation 32 with s_f substituted for s_A

s_f's – { = implies variances are equal, or ≠ implies variances are NOT equal.

t_f – t-test { equation 47 - equal variances, or equation 49 - unequal variances.

ν_f – Number degrees of freedom - f { n_1+n_2-2 - equal variances, or equation 50 - unequal variances.

t_f(5%) – Student's t-distribution at 5% for ν_f degrees of freedom.

$True_f$ – { H_o : $f_1=f_2$, or H_1 : $f_1\neq f_2$.

Table 28. Statistical analysis of circles relating true and apparent angles that have been transformed into straight lines for curves at two different temperatures for tubes of the same diameter. The analysis follows that of p. 10–14 and Hald(1952, p. 571-579).

TUBE SIZE	T (°C)	n	A_o	s_{A_o}	ssdx	V^2	$F_{0.95}$	$True_{\sigma^2}$	s^2	$V\{\bar{b}\}$	$s_{\bar{b}}$	$V\{\hat{b}\}$	$V\{\bar{b}-\hat{b}\}$	t	ν	$t_{5\%}$	True
16	22	18	118.716	0.437	12458.84												
	4	17	96.056	0.300	12186.00												
						2.12	2.39	H_o	0.142	5.762×10^{-6}	2.40×10^{-3}	3.163×10^{-5}	3.739×10^{-5}	-163.5	31	-2.040	H_1
16	80	18	136.930	0.374	12506.73												
	22	18	118.716	0.437	12458.84												
						1.37	2.33	H_o	0.165	6.609×10^{-6}	2.57×10^{-3}	4.255×10^{-5}	4.92×10^{-5}	-142.6	32	2.038	H_1
25	4	5	191.553	0.710	5070.13												
	22	18	218.538	0.879	12580.41												
						1.53	3.69	H_o	0.730	4.136×10^{-5}	6.43×10^{-3}	2.562×10^{-4}	2.976×10^{-4}	57.97	20	2.086	H_1
25	22	18	218.538	0.879	12580.41												
	80	18	230.915	1.862	12493.16												
						4.49	2.33	H_1	—	5.029×10^{-5}	7.09×10^{-3}	1.538×10^{-3}	1.588×10^{-3}	-25.09	L*	-1.968	H_1

* L – Large values of ν.

TUBE SIZE – Nominal outside diameter of tube (mm).

T(°C) – Temperature of measurement.

n – number of points used to determine A_o.

s_{A_o} – uncertainty in A_o.

ssdx – $\sum_{1}^{n}(x_i - \bar{x})^2$.

V^2 – variance ratio test (equation 56).

$F_{0.95}$ – F distribution for $(n_1 - 2, n_2 - 2)$ degrees of freedom.

$True_{\sigma^2}$ – $\begin{cases} H_o : \sigma_1^2 = \sigma_2^2. \\ H_1 : \sigma_1^2 \neq \sigma_2^2. \end{cases}$

s^2 – pooled estimate of theoretical variance (equation 57).

$V\{\bar{b}\}$ – variance of $\bar{b}$ ($b_1 = b_2 = -1$, equation 59) – equation 60 or 71.

$s_{\bar{b}}$ – uncertainty in $\bar{b}$ ($s_{\bar{b}}^2 = V\{\bar{b}\}$).

$V\{\hat{b}\}$ – variance of $\hat{b}$ ($\hat{b} = 0$, equation 61) – equations 62 or 72.

$V\{\bar{b} - \hat{b}\}$ – variance of $\bar{b} - \hat{b}$ – equations 63 or 73.

t – t-test – equations 64 or 75.

ν – number of degrees of freedom: $n_1 + n_2 - 4$.

$t_{5\%}$ – Student's t-distribution at 5% level.

True – $\begin{cases} H_o : \text{Lines are same.} \\ H_1 : \text{Lines are NOT same.} \end{cases}$

Table 29. Measured apparent angle of nominal, outside-diameter inclinometer tubes at true angle of 45° for several temperatures.

T(°C)	6mm	10mm	13mm	16mm	19mm	20mmB**	25mm
4	75.23	65.10	61.37	59.02*	56.10	54.97	53.50*
10	74.48	64.63	60.49	57.50	55.67	54.56	52.98
22	73.51	64.00	59.68	56.74*	55.03	54.16	52.55*
40	73.46	63.59	58.95	56.04	54.59	53.80	52.46
60	72.59	62.88	58.51	56.01	54.42	53.61	52.36
80	71.74	62.34	58.25	55.84*	54.37	53.51	52.50*

* From Table 13. These values will not necessarily yield radii of Table 31 since radii of Tables 21 – 26 are based on least squares fit to data of Table 13. The remainder of apparent angles will yield radii of Table 31.

** B denotes bolosilicate. Remainder are soda-lime glass

Table 30. Radius of circle relating apparent angle to true angle for inclinometer tubes of different diameters at several different temperatures.

NOMINAL TUBE* (mm)	4 °C	10 °C	22 °C	40 °C	60 °C	80 °C
6	97.115	99.355	102.451	102.617	105.616	108.754
10	143.184	146.547	151.323	154.609	160.665	165.609
13	175.323	185.204	195.357	205.526	212.190	216.338
16	209.389	225.673	240.116	259.518	261.647	265.042
19	258.118	268.502	285.610	298.699	304.084	305.705
20B**	287.326	299.635	312.707	325.489	332.667	336.573
24***	—	—	351.371	—	—	—
25	340.536	358.914	378.093	383.921	389.136	395.358
30***	—	—	394.457	—	—	—

* NOMINAL TUBE - Nominal outside diameter of tube in millimeters.

** B denotes borosilicate glass tube. Remainder of tubes are soda-lime glass.

*** Calculated from data in Cumming (1951, p. 344); no temperature given but assumed approximately to be room temperature ($\approx$ 22 °C).

Table 31. Absolute value of $X-$coordinate of center of circle $(-A, 90+A)$ for inclinometer tubes of different diameters at several different temperatures.

NOMINAL TUBE* (mm)	4 °C	10 °C	22 °C	40 °C	60 °C	80 °C
6	6.872	8.951	11.772	11.922	14.601	17.360
10	45.696	48.344	52.079	54.634	59.315	63.112
13	70.517	77.985	85.603	93.186	98.134	101.206
16	96.056	108.099	118.716	132.904	134.456	136.930
19	131.883	139.450	151.879	161.363	165.258	166.430
20B**	153.124	162.040	171.490	180.713	185.887	188.700
24***	—	—	199.348	—	—	—
25	191.553	204.769	218.538	222.718	226.458	230.915
30***	—	—	230.269	—	—	—

* NOMINAL TUBE - Nominal outside diameter of tube in mm.

** B denotes borosilicate glass tube. Remainder of tubes are soda-lime glass.

*** Calculated from data in Cumming (1951, p. 344); no temperature given but assumed approximately to be room temperature ($\approx$ 22 °C).

Table 32. Apparent and true angles for 6mm inclinometer tubes at 22 °C.

APPARENT ANGLE	TRUE ANGLE
82.09	60
73.51*	45
69.92	30
67.95	20
66.44	10

* From Table 29.

Table 33. Inclinometer tube radius corrected by straight line interpolation. Nominal tube diameters are listed at the top of columns 2 through 8. Beneath these nominal diameters are listed the average values of the inside-tube diameter in mm. For the 16 mm tubes, the average diameter was 14.05 mm for 75 measurements, while that for the 25 mm tubes was 22.01 mm for 63 measurements.

Inclinometer tube radius corrected by straight line									
T (°C)	6 mm 4.5	10 mm 8.5	13 mm 11.0	16 mm 14.1	19 mm 16.5	20 mmB* 17.9	25 mm 22.0	R_0**	s**
4	88.70	145.34	180.74	224.64	258.62	278.44	336.50	24.98	14.16
10	91.64	151.68	189.20	235.73	271.76	292.77	354.31	24.09	15.01
22	92.19	156.95	197.42	247.61	286.47	309.13	375.51	19.33	16.19
40	98.75	164.83	206.13	257.34	296.99	320.12	387.85	24.41	16.52
60	101.44	168.28	210.05	261.85	301.96	325.35	393.86	26.24	16.71
80	105.45	172.69	214.71	266.82	307.17	330.70	399.62	29.80	16.81

* B represents Borosilicate tube. Remainder of tubes are soda-lime glass.

** R_0 & s are variables in least squares straight line ($R = R_0 + s \cdot x$) of Figure 23.

Table 34. Inclinometer tube radius (R) corrected by cubic line interpolation. Nominal tube diameters are listed at the top of columns 2 through 8. Beneath these nominal diameters are listed the average values of the inside-tube diameter (TD) in millimeters. For the 16 mm tubes, the average diameter was 14.05 mm for 75 measurements, while that for the 25 mm tubes was 22.01 mm for 63 measurements. The cubic equation was constrained by 1) TD=0, R=90; and 2) $\partial R/\partial(TD) = 0$ at TD=0.

Inclinometer tube radius corrected by cubic line							
T (°C)	6 mm 4.5	10 mm 8.5	13 mm 11.0	16 mm 14.1	19 mm 16.5	20 mmB* 17.9	25 mm 22.0
4	106.56	144.13	175.45	219.81	256.53	278.27	340.29
10	108.02	148.79	182.69	230.55	270.01	293.31	359.29
22	109.70	154.11	190.89	242.59	284.98	309.87	379.68
40	112.84	162.86	202.98	257.22	299.46	323.11	382.84
60	113.67	165.32	206.60	262.13	305.09	328.99	388.38
80	113.87	166.23	208.31	265.31	309.85	334.86	398.45

* B represents Borosilicate tube. Remainder of tubes are soda-lime glass.

Variables in least squares cubic line ($R = R_0 + R_1x + R_2x^2 + R_3x^3$) of Figure 26, where x=TD.

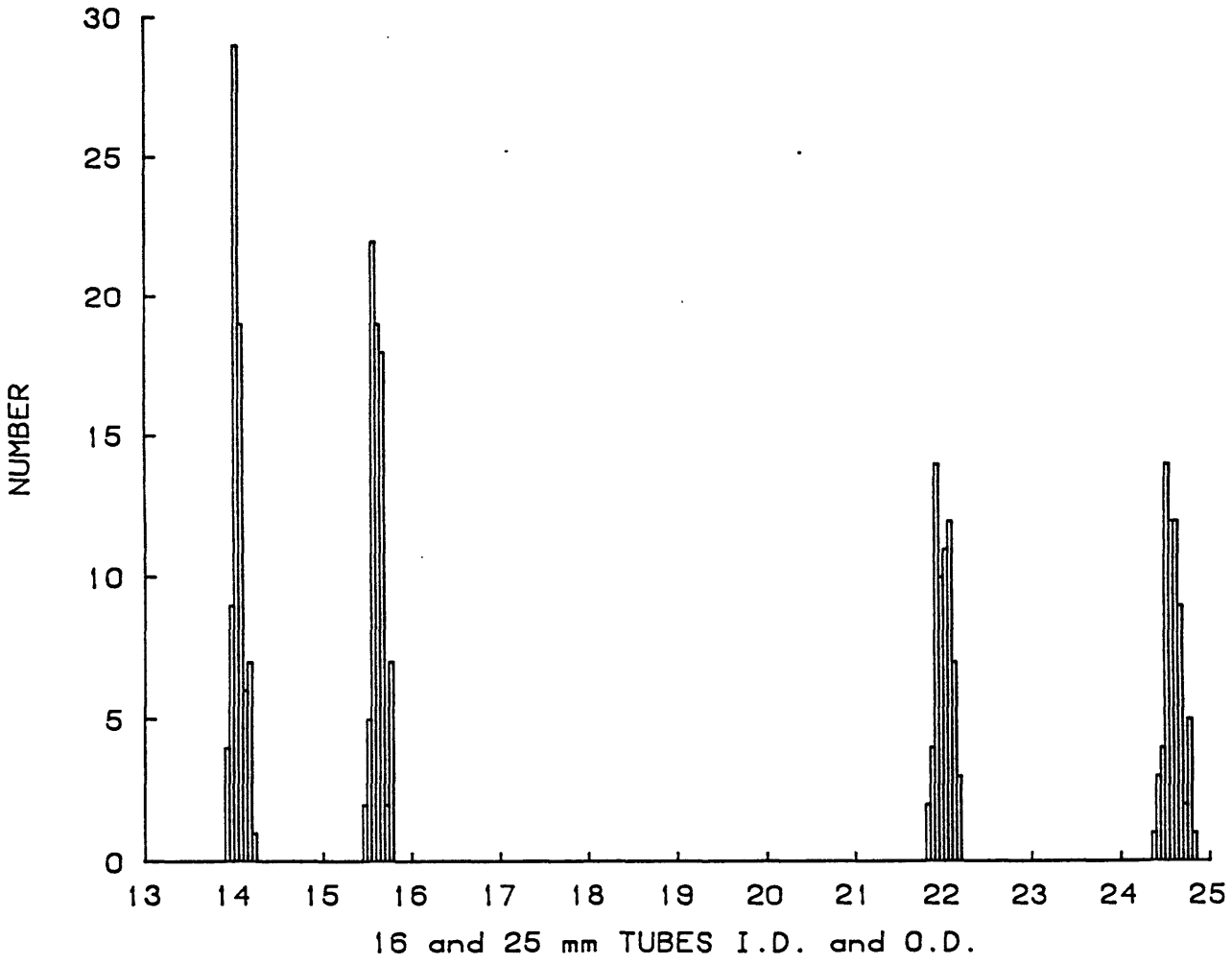

Figure 1. Histogram of 16- and 25-mm tube inside and outside diameters in millimeters.

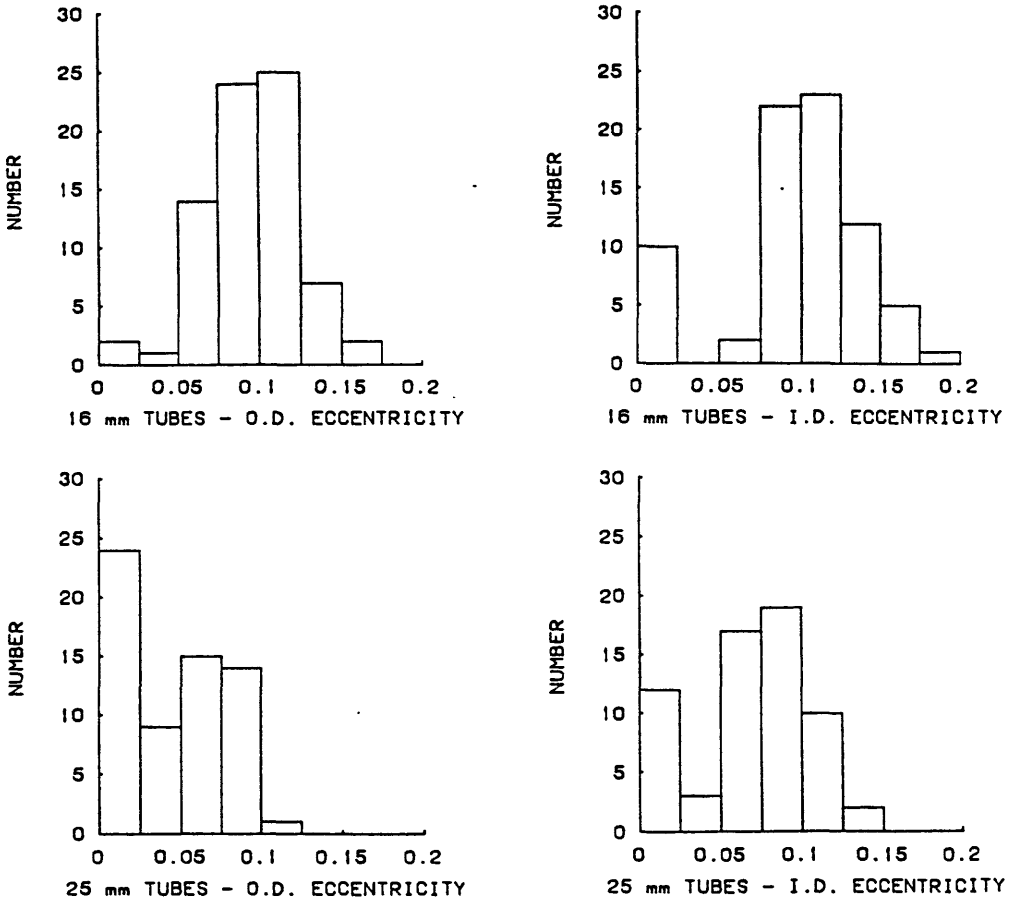

Figure 2. Histograms of eccentricities of 16- and 25-mm tubes used in this study.

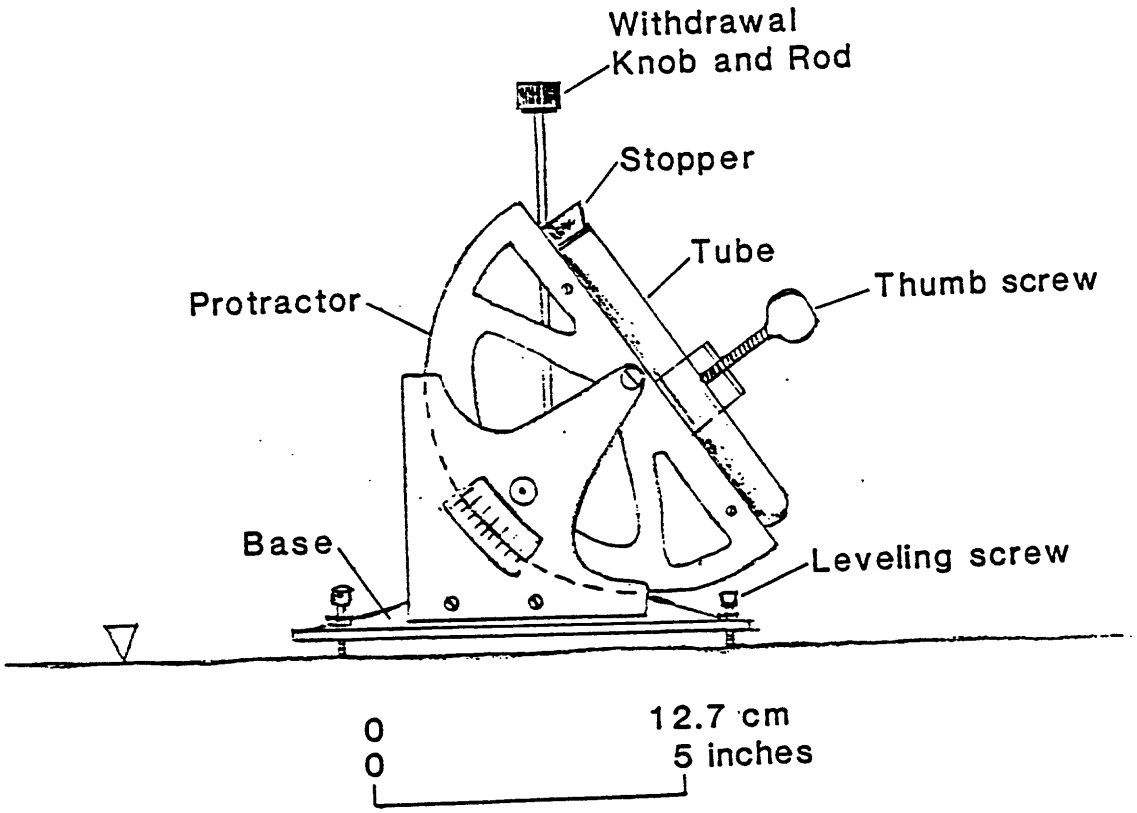

Figure 3. Inclinometer tube test stand.

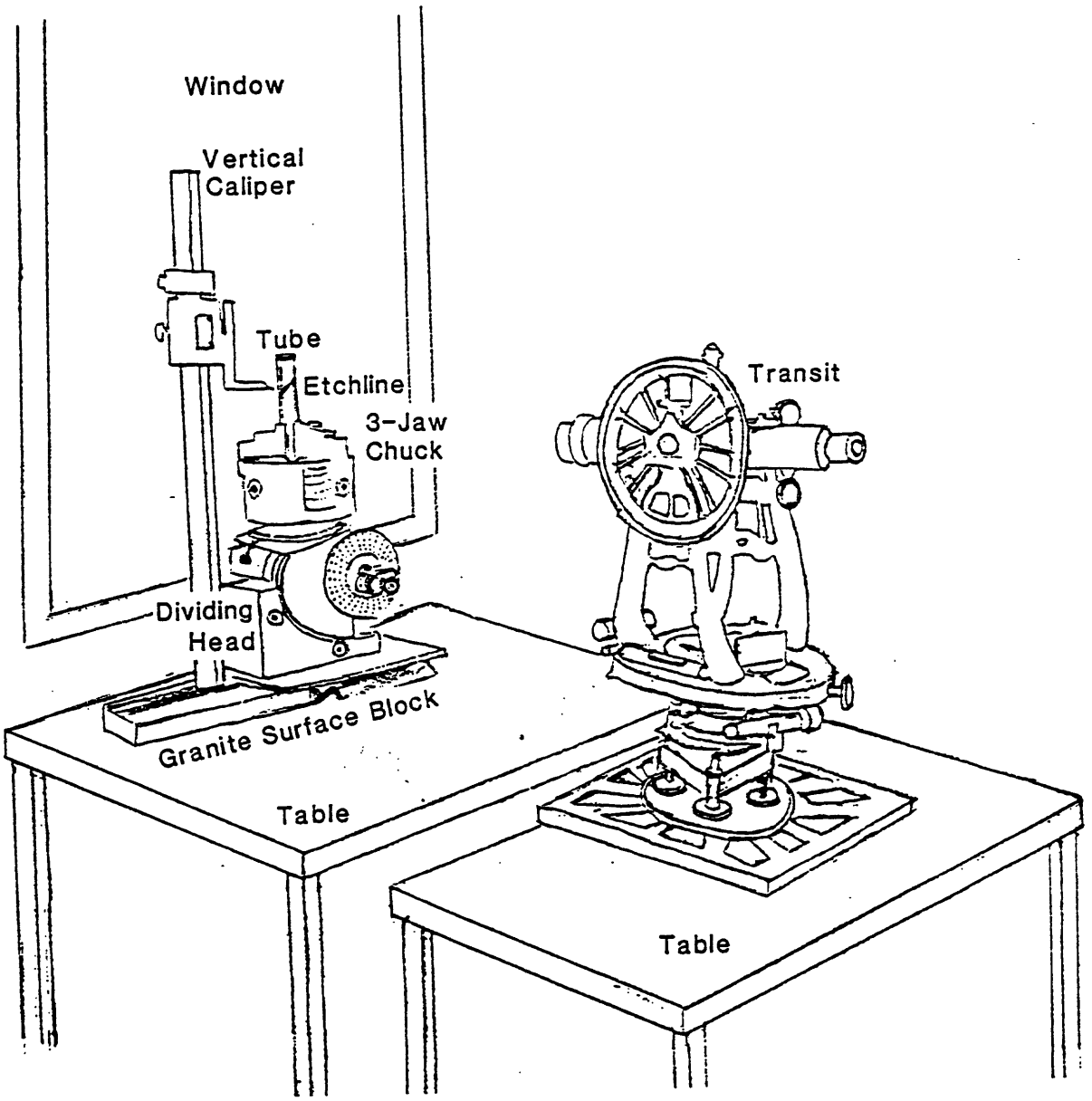

Figure 4. Apparatus to measure angle of etch line, including transit, vertical caliper, and dividing head holder. Spacing from the transit to the tube is 1 meter. Light from the window is the light source used to illuminate the etch line in the tube.

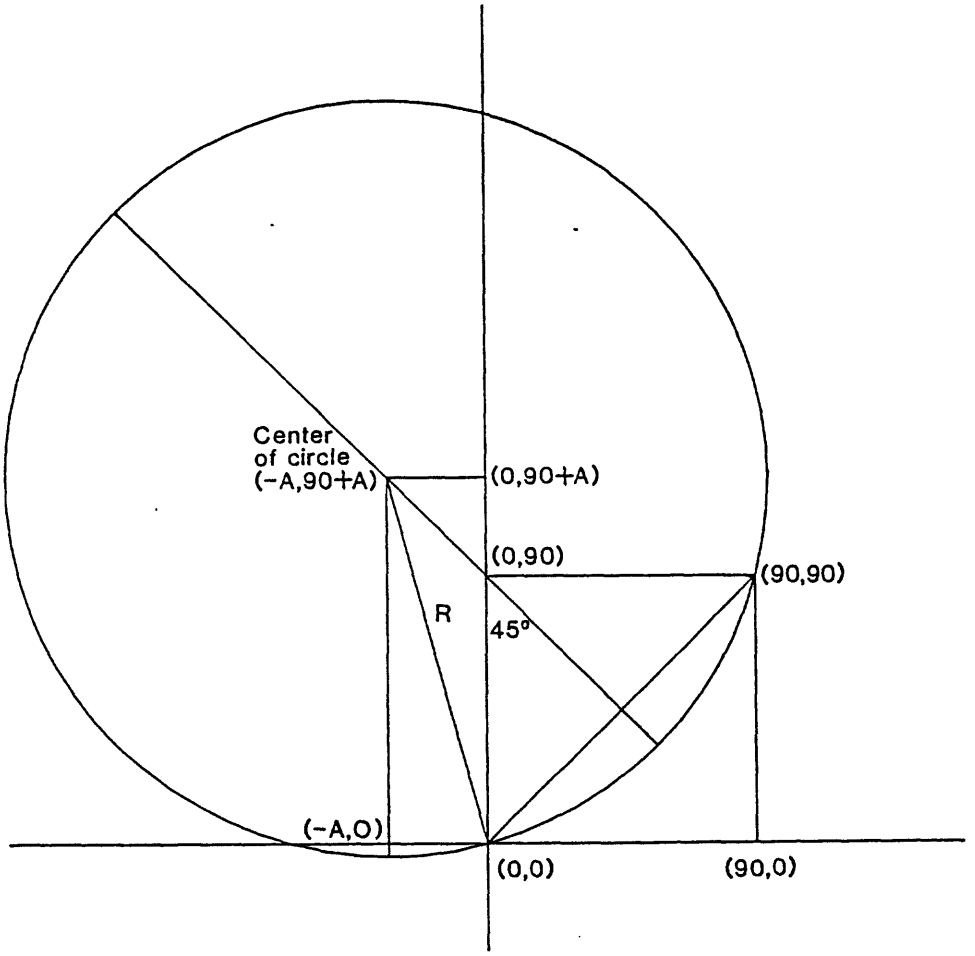

Figure 5. Geometry for determining the equation of circle.

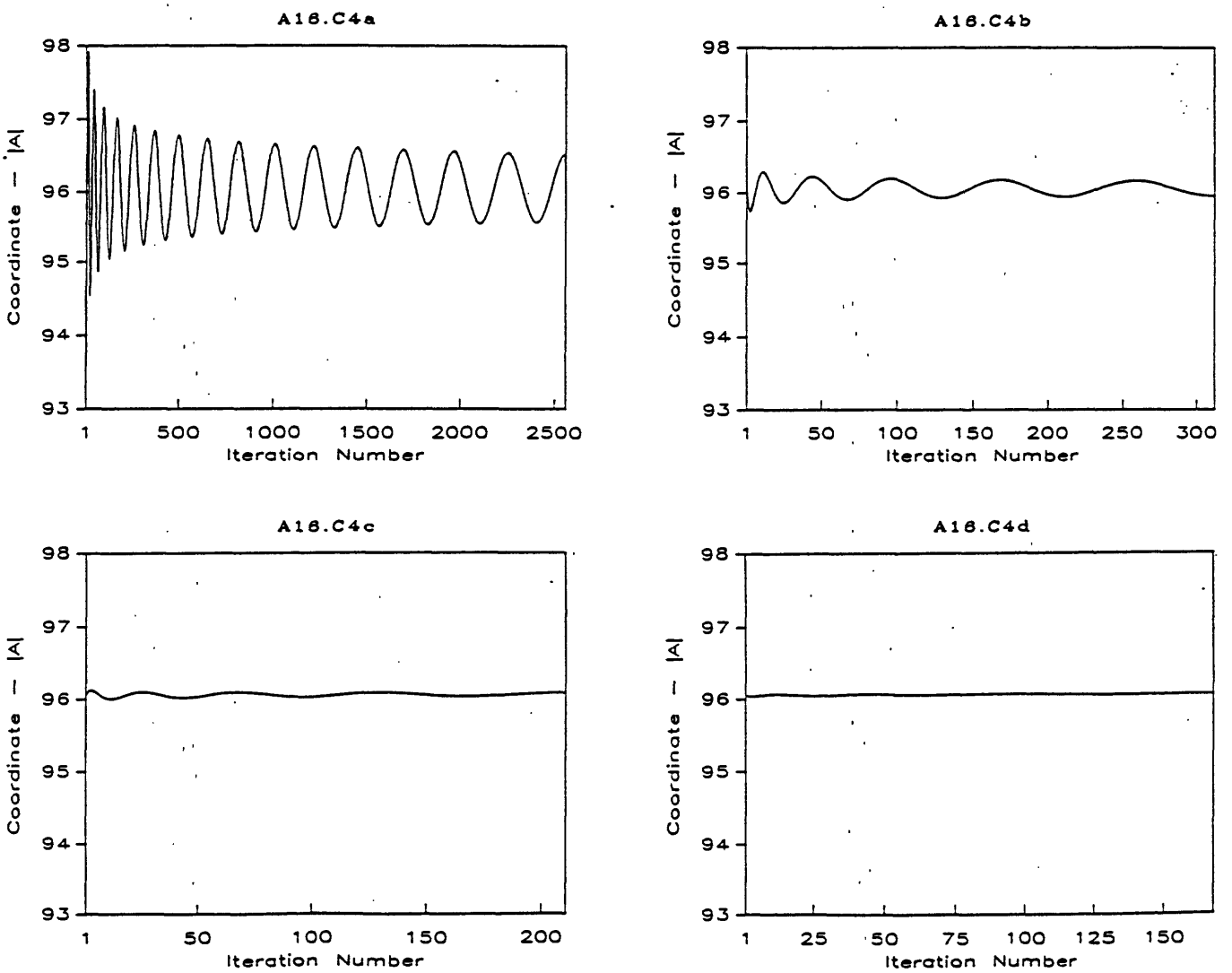

Figure 6. Plot of |A| (absolute value of x-coordinate) for each iteration of least-squares fit to arc of circle for 16 mm tubes at 4 °C. Only the first four computer runs are shown (labeled a, b, c, d). There is little change in succeeding runs from A16.C4d as can be seen from table 14.

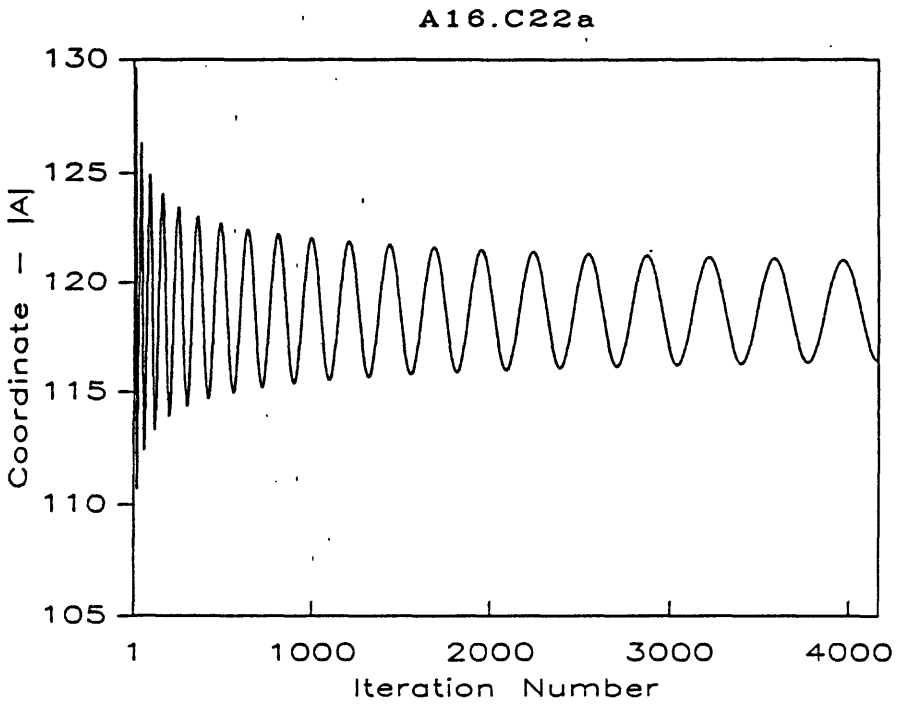

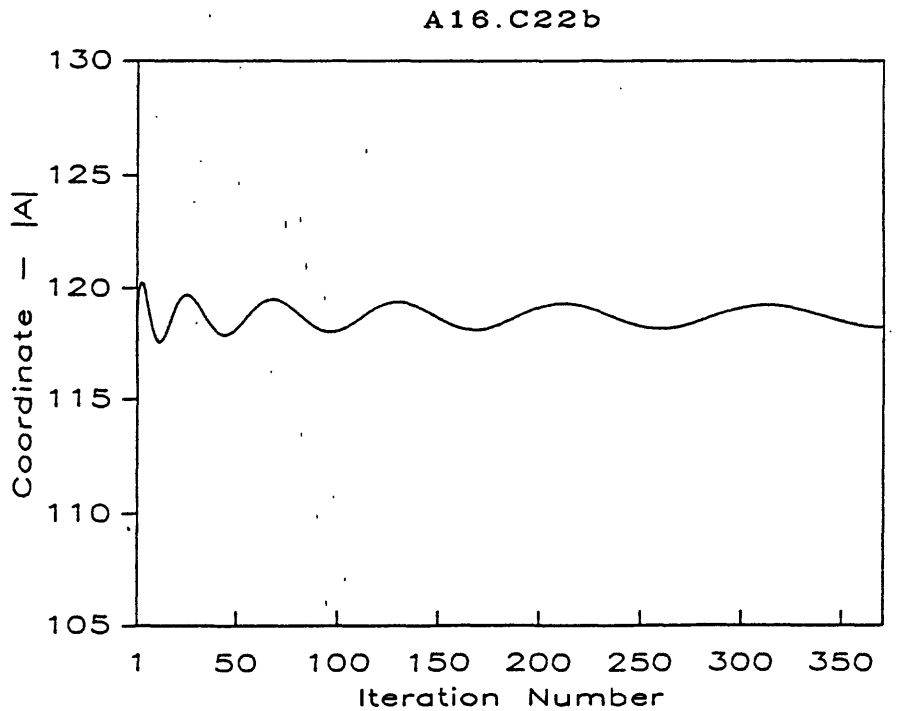

Figure 7. Plot of |A| (absolute value of x-coordinate) for each iteration of least-squares fit to arc of circle for 16 mm tubes at 22 °C. Only the results of the first two runs are shown (a and b). The remainder of the runs are similar to those shown in figure 6. Ranges, averages and ending value for A for each run, are listed in table 15.

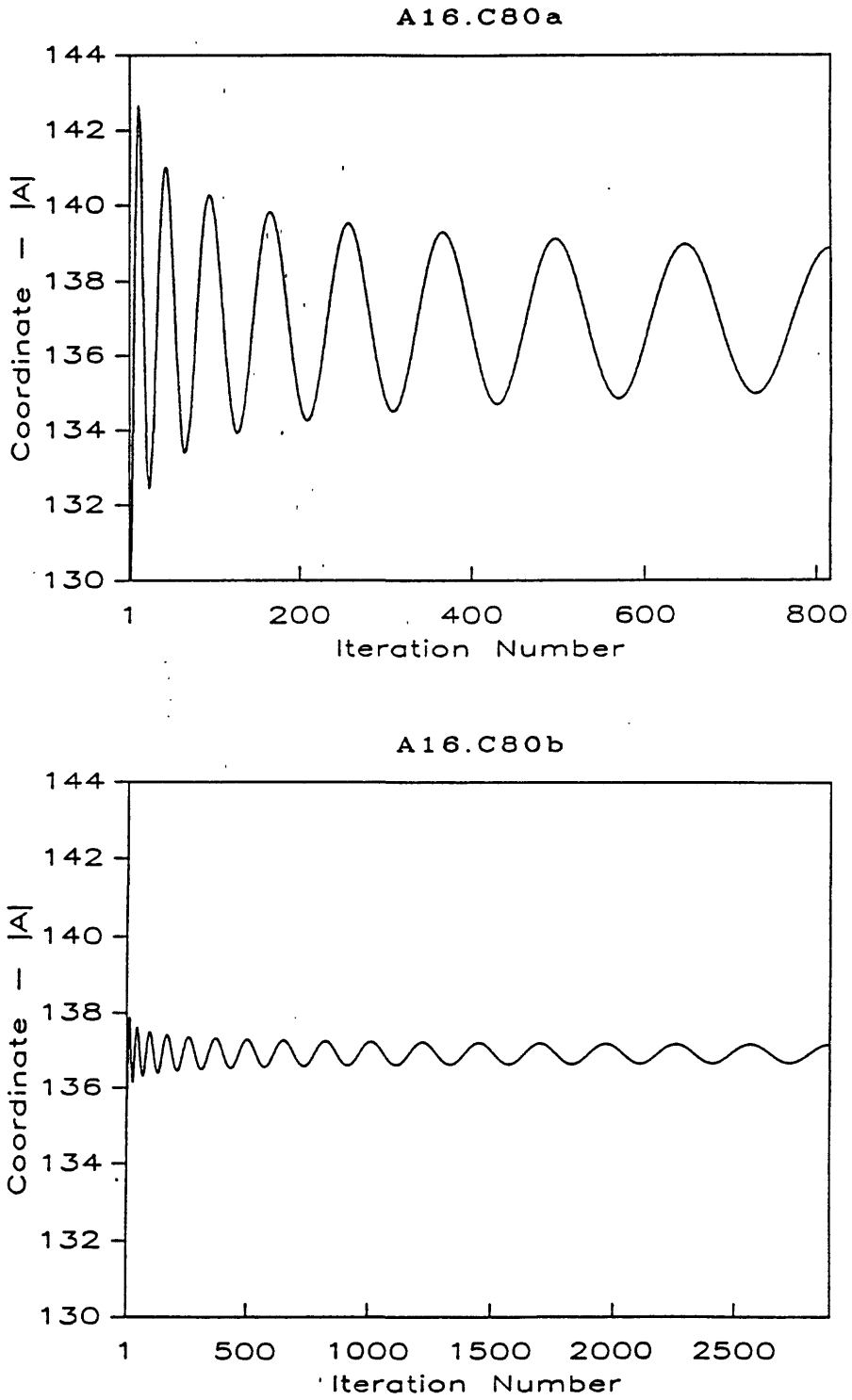

Figure 8. Plot of |A| (absolute value of x-coordinate) for each iteration of least-squares fit to arc of circle for 16 mm tubes at 80 °C. Only the results of the first two runs are shown (a and b). The remainder of the runs are similar to those shown in figure 6. Ranges, averages and ending value for A for each run are listed in table 16.

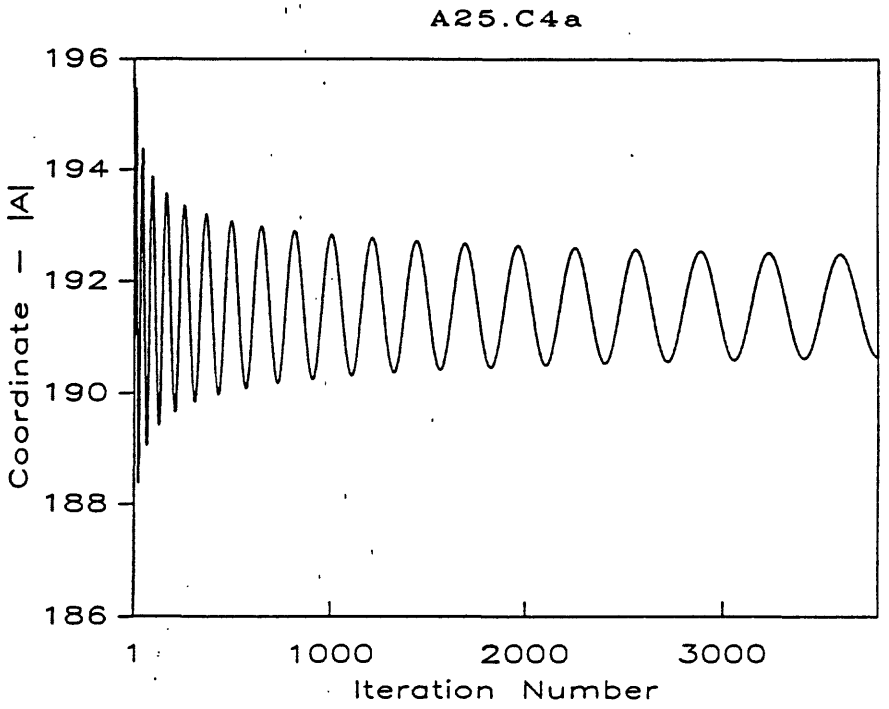

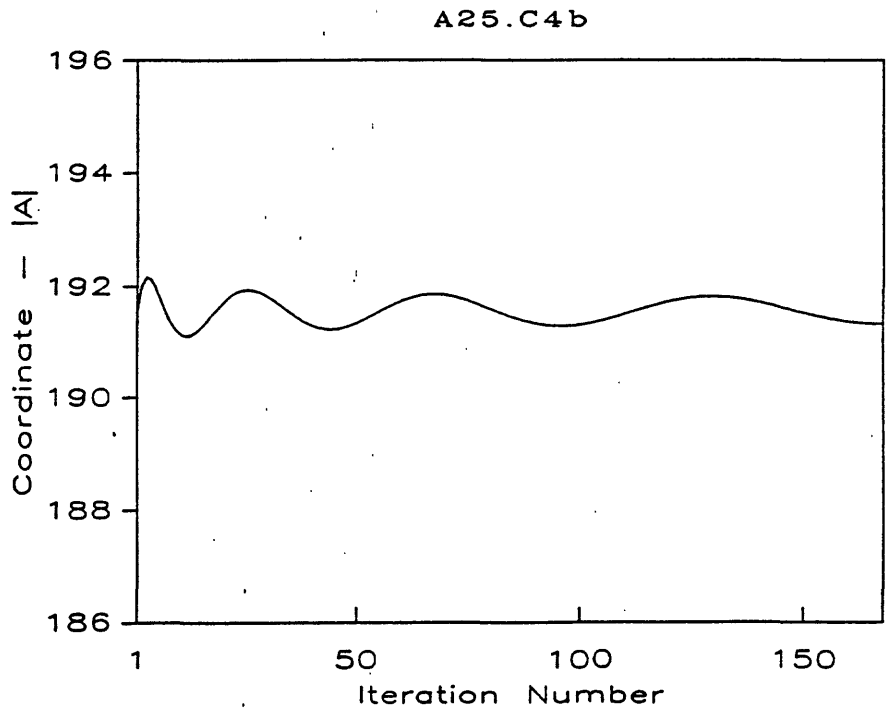

Figure 9. Plot of |A| (absolute value of x-coordinate) for each iteration of least-squares fit to arc of circle for 25 mm tubes at 4 °C. Only the results of the first two runs are shown (a and b). The remainder of the runs are similar to those shown in figure 6. Ranges, averages and ending value for A for each run are listed in table 17.

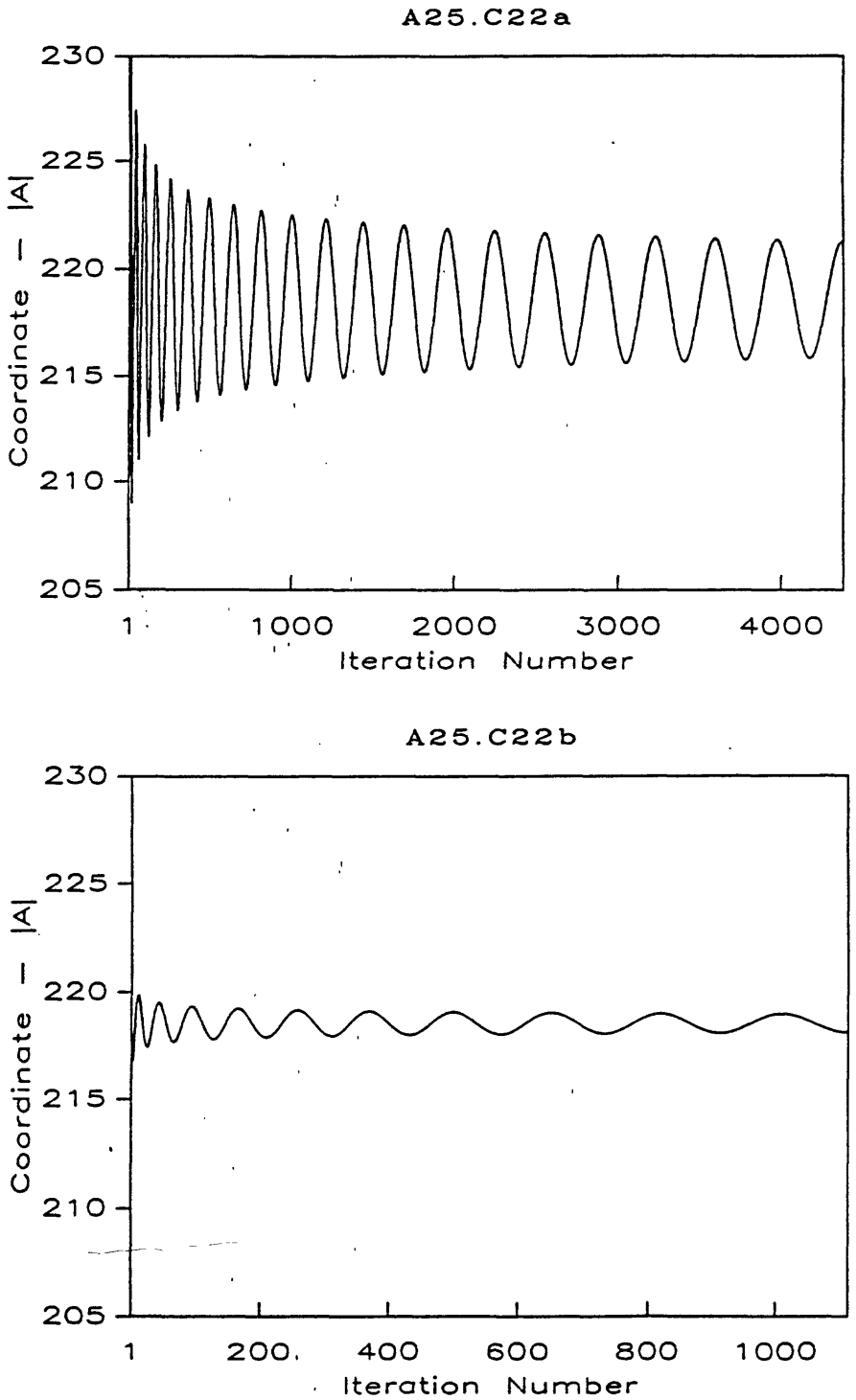

Figure 10. Plot of |A| (absolute value of x-coordinate) for each iteration of least-squares fit to arc of circle for 25 mm tubes at 22 °C. Only the results of the first two computer runs are shown (a and b). The remainder of the runs are similar to those shown in figure 6. Ranges, averages and ending value for A for each run are listed in table 18.

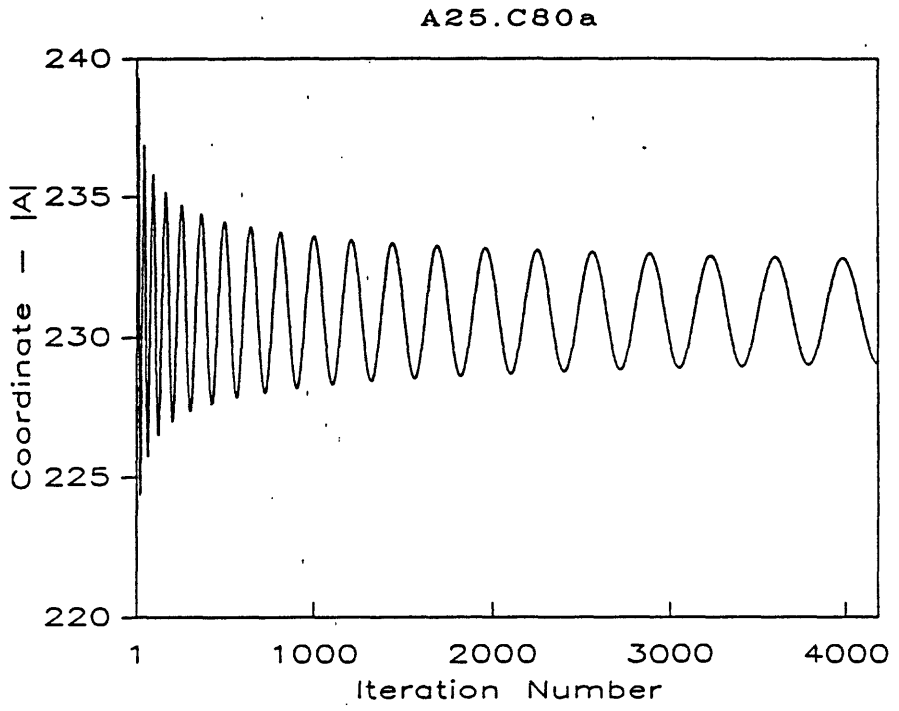

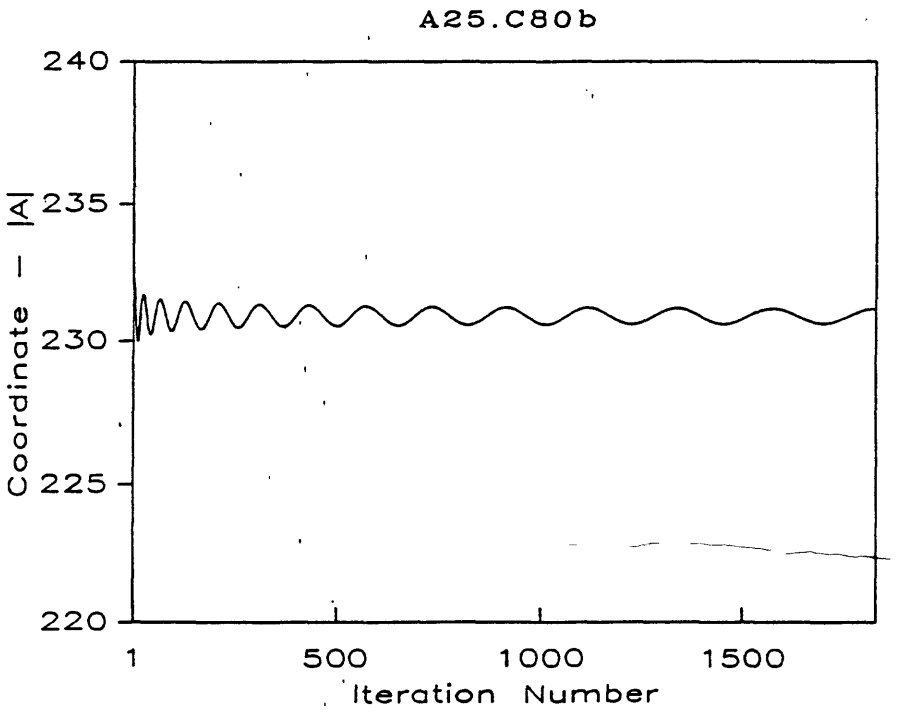

Figure 11. Plot of |A| (absolute value of x-coordinate) for each iteration of least-squares fit to arc of circle for 25 mm tubes at 80 °C. Only the results of the first two computer runs are shown (a and b). The remainder of the runs are similar to those shown in Figure 6. Ranges, averages, and ending value for A for each run are listed in Table 19.

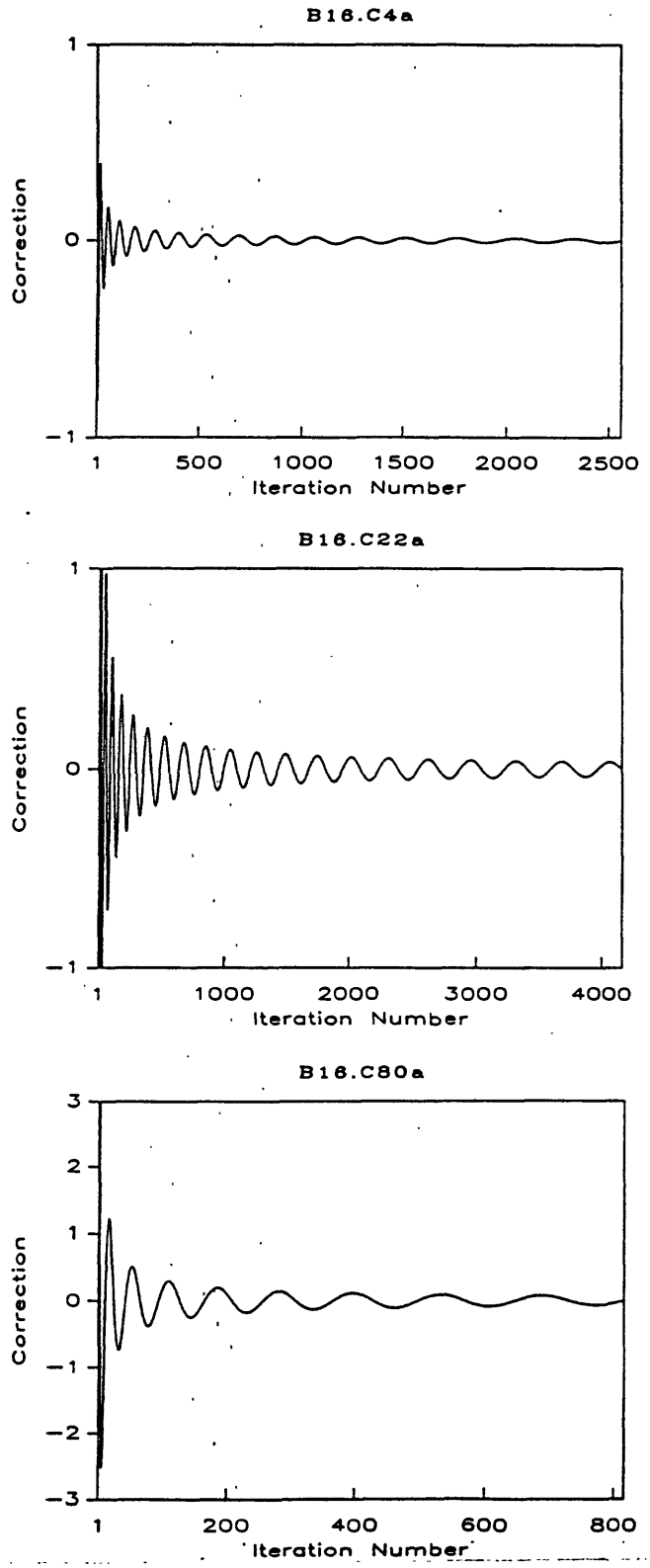

Figure 12. Plot of correction, B of equation 14, for each iteration for the first computer run of the 16 mm tubes at temperatures of 4°, 22°, and 80 °C. The value of B at the first iteration usually was significantly larger than the range shown and the scale was truncated in order to present the details of later iterations.

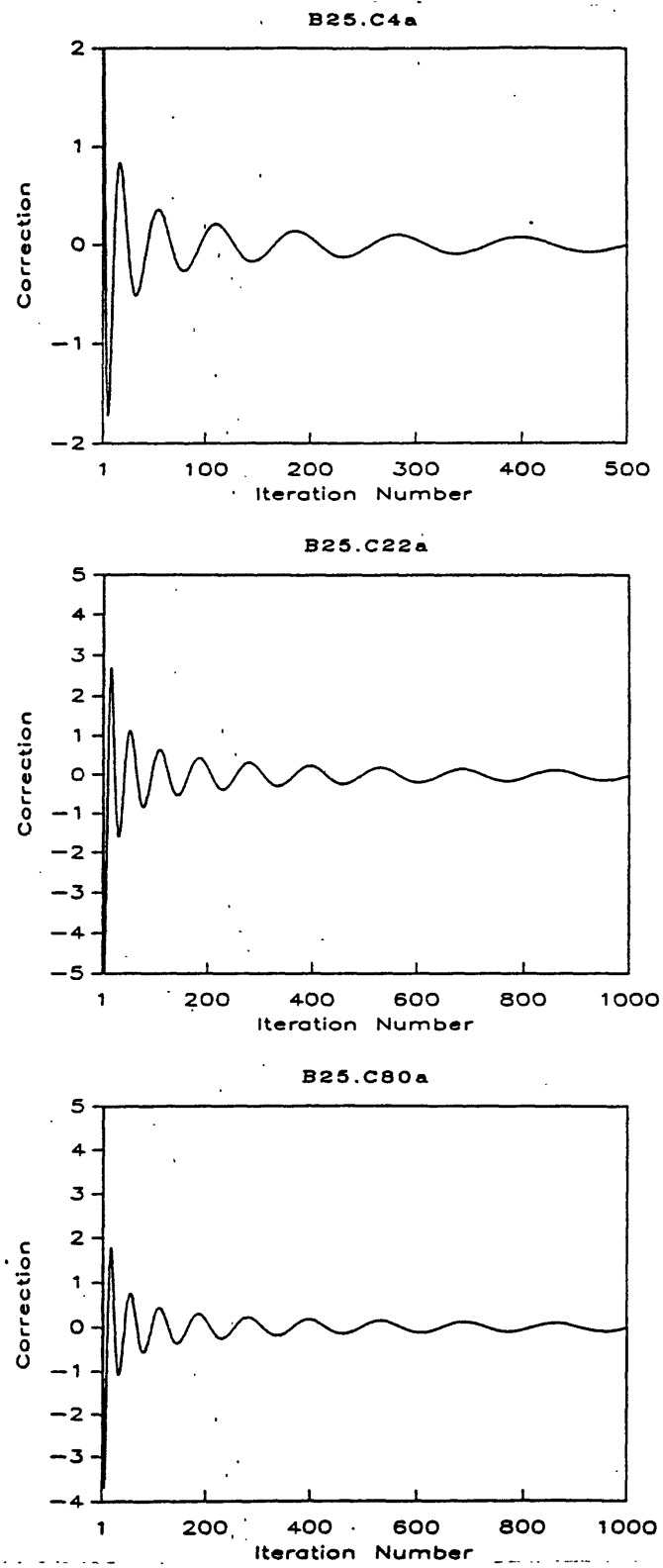

Figure 13. Plot of correction, B of equation 14, for each iteration for the first computer run of the 25 mm tubes at temperatures of 4°, 22°, and 80 °C. The value of B at the first iteration usually was significantly larger than the range shown and the scale was truncated in order to present the details of later iterations.

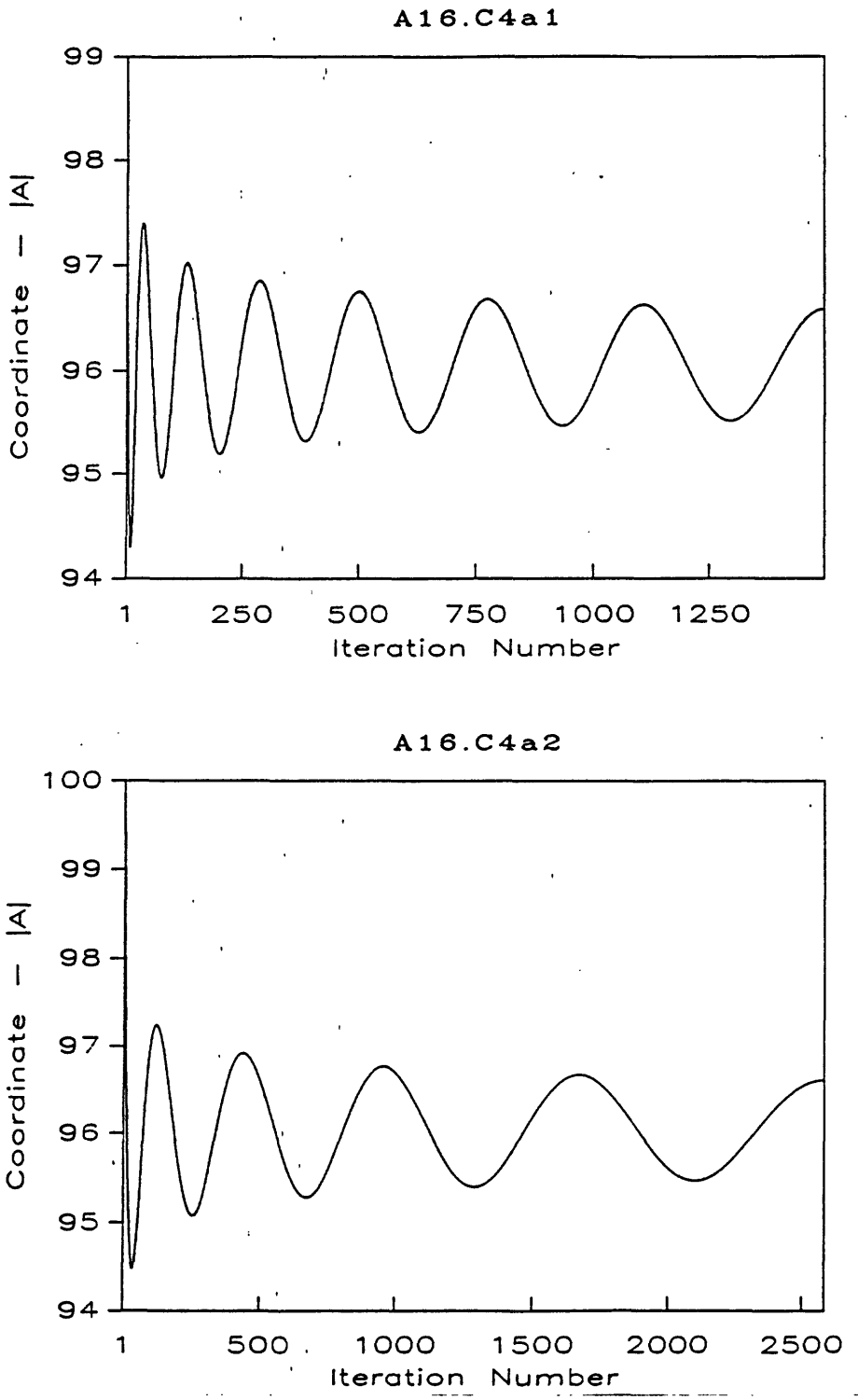

Figure 14. Plot of |A| (absolute value of x-coordinate) of arc of circle for 16 mm tubes at 4 °C. Shown are the first computer runs. For A16.C4a1 the corrections, B of equation 14, were divided by 3 while those for A16.C4a2 were divided by 10. Dividing by 3 reduced the number of iteration while dividing by 10 did not. Frequency content of A16.C4a2, however, was reduced when compared to A16.C4a of Figure 6.

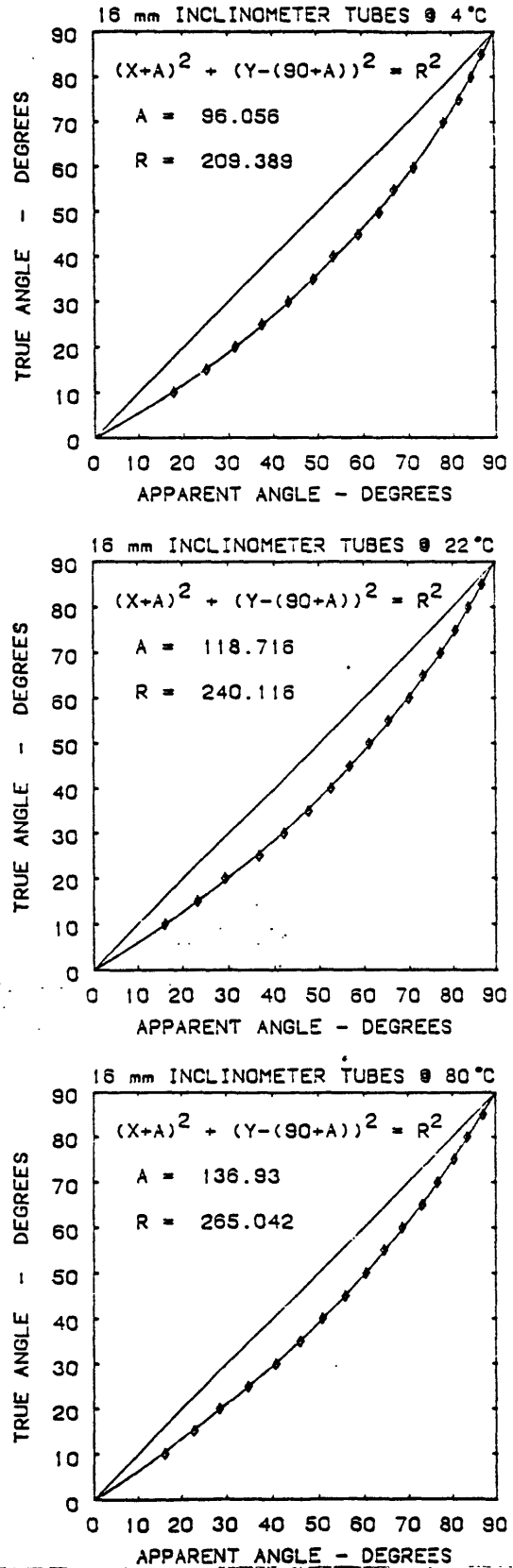

Figure 15. True versus apparent angle in degrees for 16 mm tubes at 4°, 22°, and 80 °C. Diamonds (◇) are the measured points. Curved line is the arc of a circle represented by the equation of a circle with constants A and R for each temperature. The diagonal straight line is the curve if there were no capillarity.

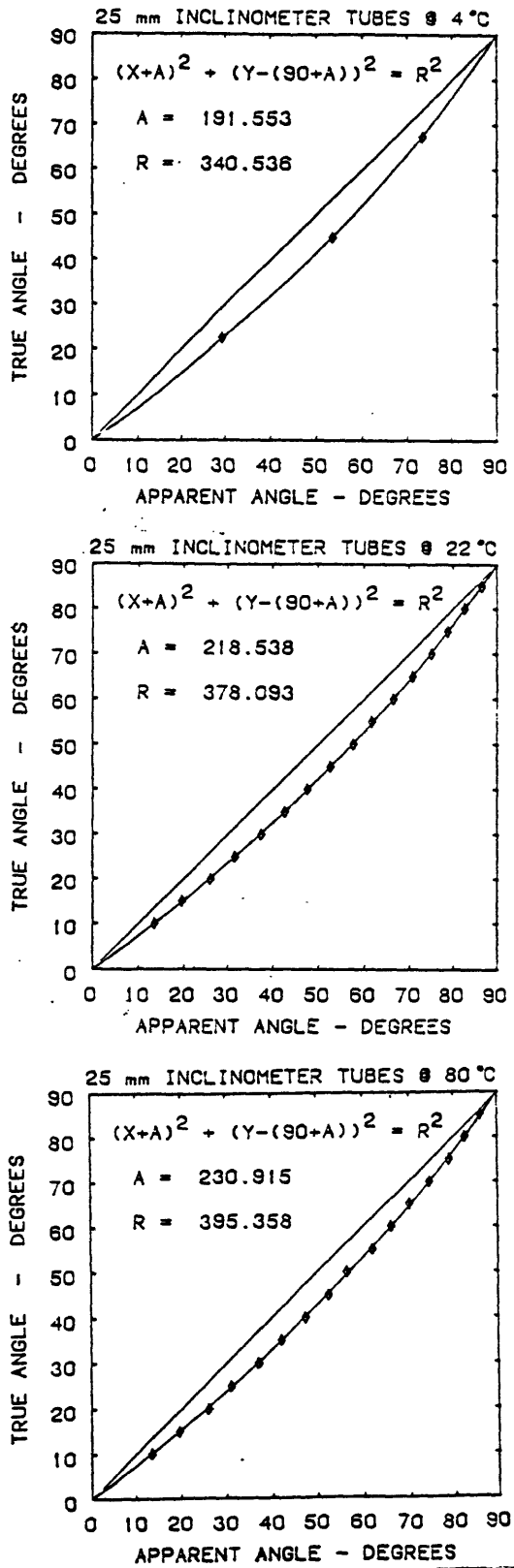

Figure 16. True versus apparent angle in degrees for 25 mm tubes at 4°, 22°, and 80 °C. Diamonds (◇) are the measured points. Curved line is arc of a circle represented by the equation with constants A and R for each temperature. The diagonal straight line is the curve if there were no capillarity.

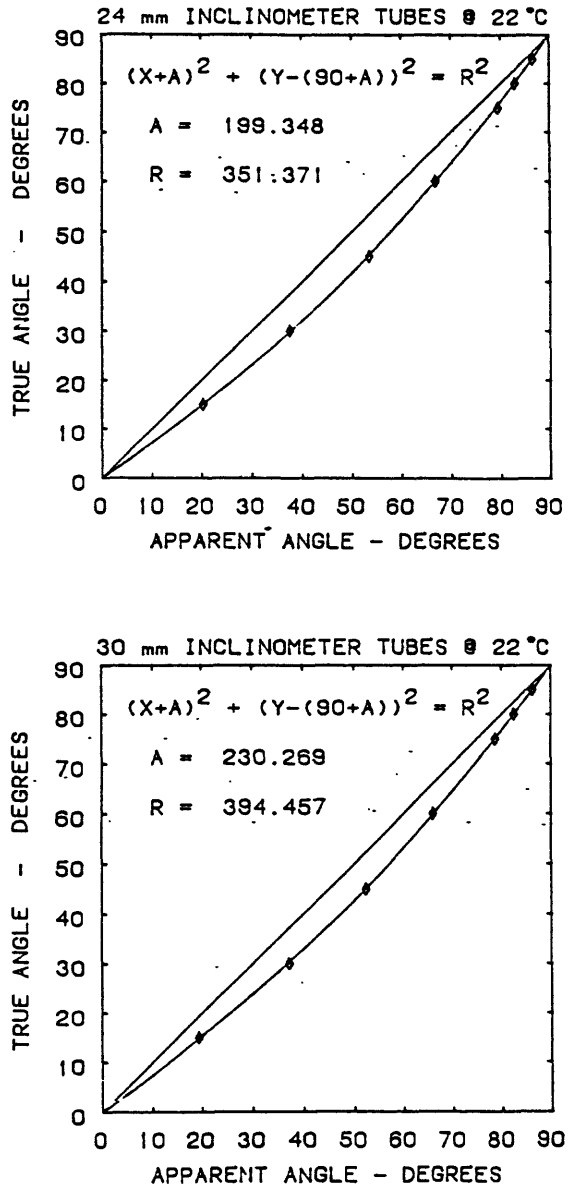

Figure 17. True versus apparent angle in degrees for 24- and 30-mm tubes from Cumming (1951, p. 344). Diamonds (◇) are measured points. Temperature of measurement is unknown but assumed to be near room temperature (≈ 22 °C). Curved line is arc of circle represented by least-squares equation with constants A and R. The diagonal straight line is the curve if there were no capillarity.

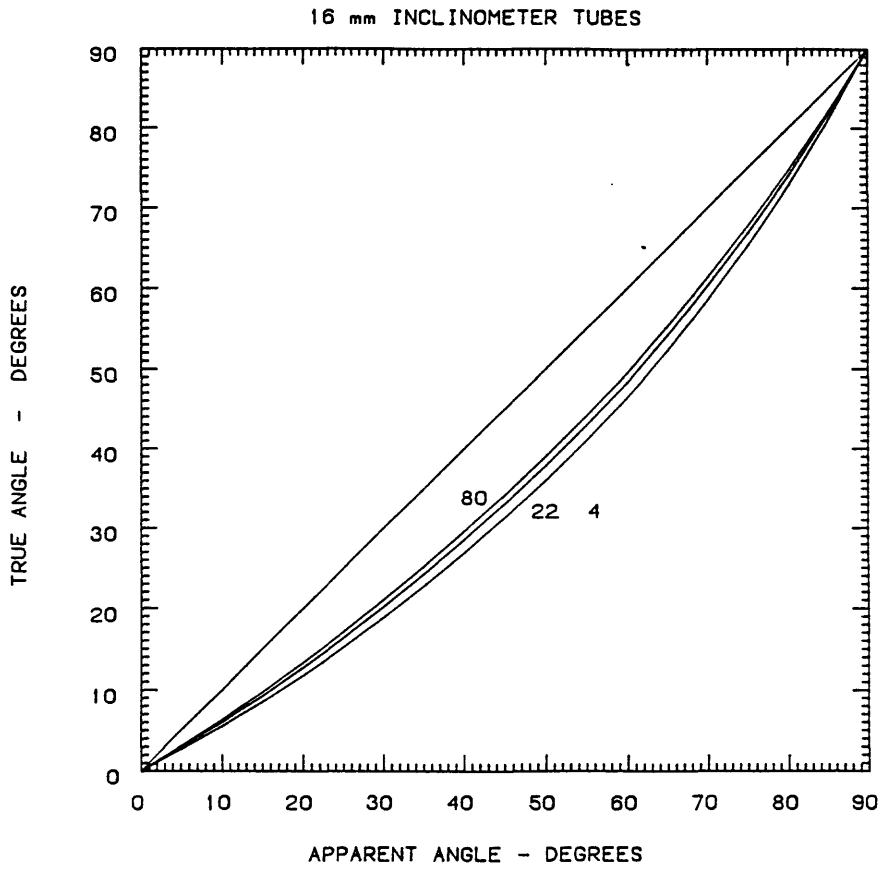

Figure 18. True versus apparent angle in degrees of the three least-squares fitted curves shown in Figure 15. The labled curves are for temperatures at 4°, 22°, and 80 °C. The diagonal, straight line is the curve if there were no capillarity.

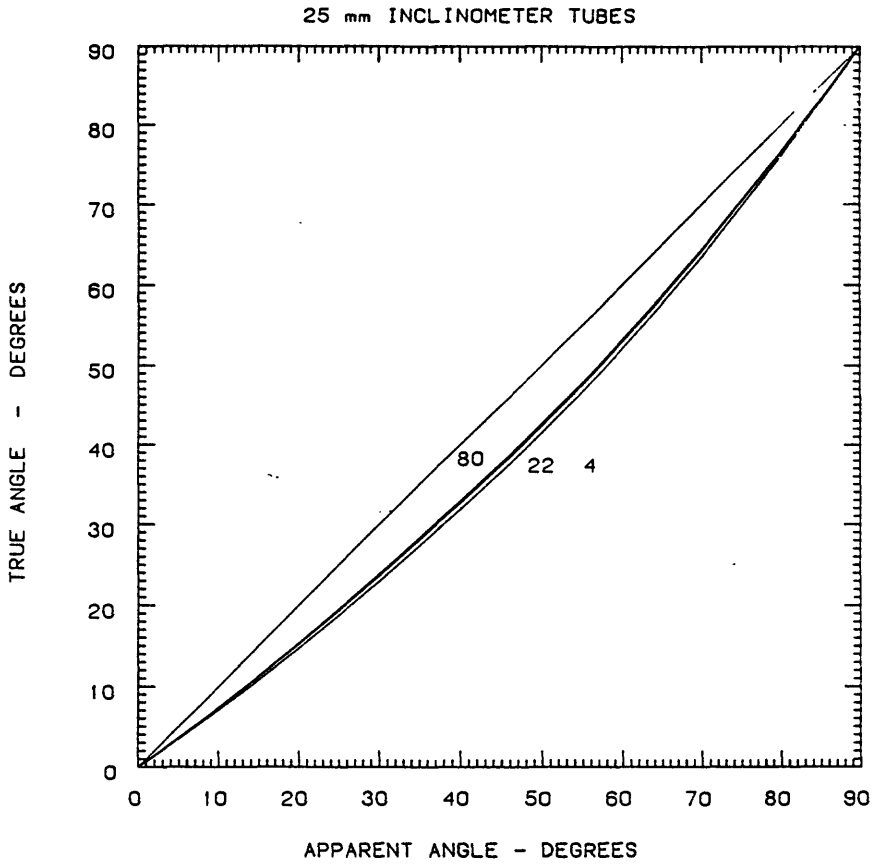

Figure 19. True versus apparent angle in degrees of the three least-squares fitted curves shown in Figure 16. The labeled curves are for temperatures at 4°, 22°, and 80 °C. The diagonal, straight line is the curve if there were no capillarity.

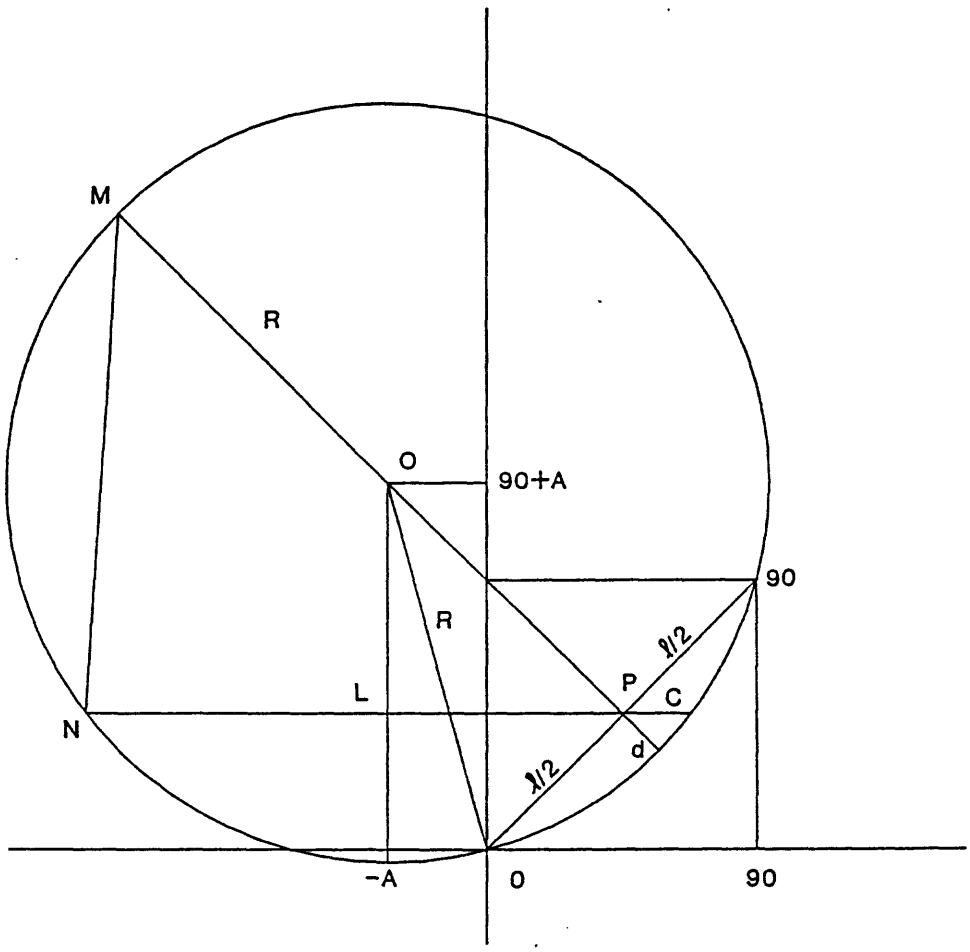

Figure 20. Geometry used in the derivation of equation 89. The center of the circle is at $(-A, 90 + A)$. C is the difference between the true and apparent angle in degrees, R is the radius of the circle, $R^2 = A^2 + (90+A)^2$, d is the distance along a radius at 45 degrees from the circle to line $\overline{\emptyset \cdot P \cdot 90}$ (line of no capillarity), the apparent angle (0 through 90) is on the abscissa, the true angle (0 through 90) is on the ordinate, and ℓ is the length of the diagonal, no capillarity line which is $90\sqrt{2}$.

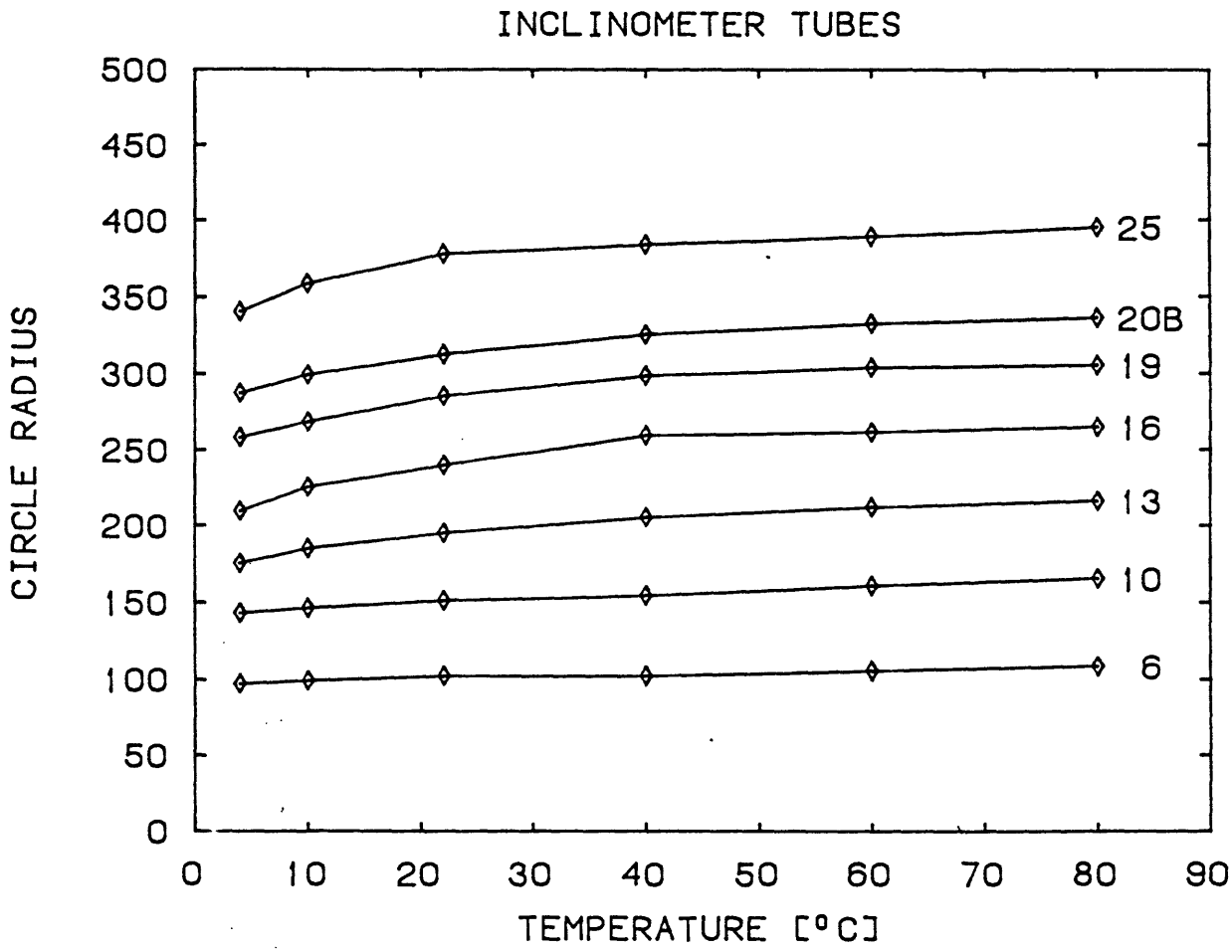

Figure 21. Plot of circle radius against temperature for the tubes used in this study. The numbers, 6 through 25, are the nominal tube diameters in mm. 20B are borosilicate tubes. Remainder of tubes are soda-lime glass. $(\partial R/\partial T)_D$ is positive and nearly constant for all tube diameters (D) at temperatures above 40 °C. Below 4 °C the derivative is not constant with the non-linearity increasing with tube diameter.

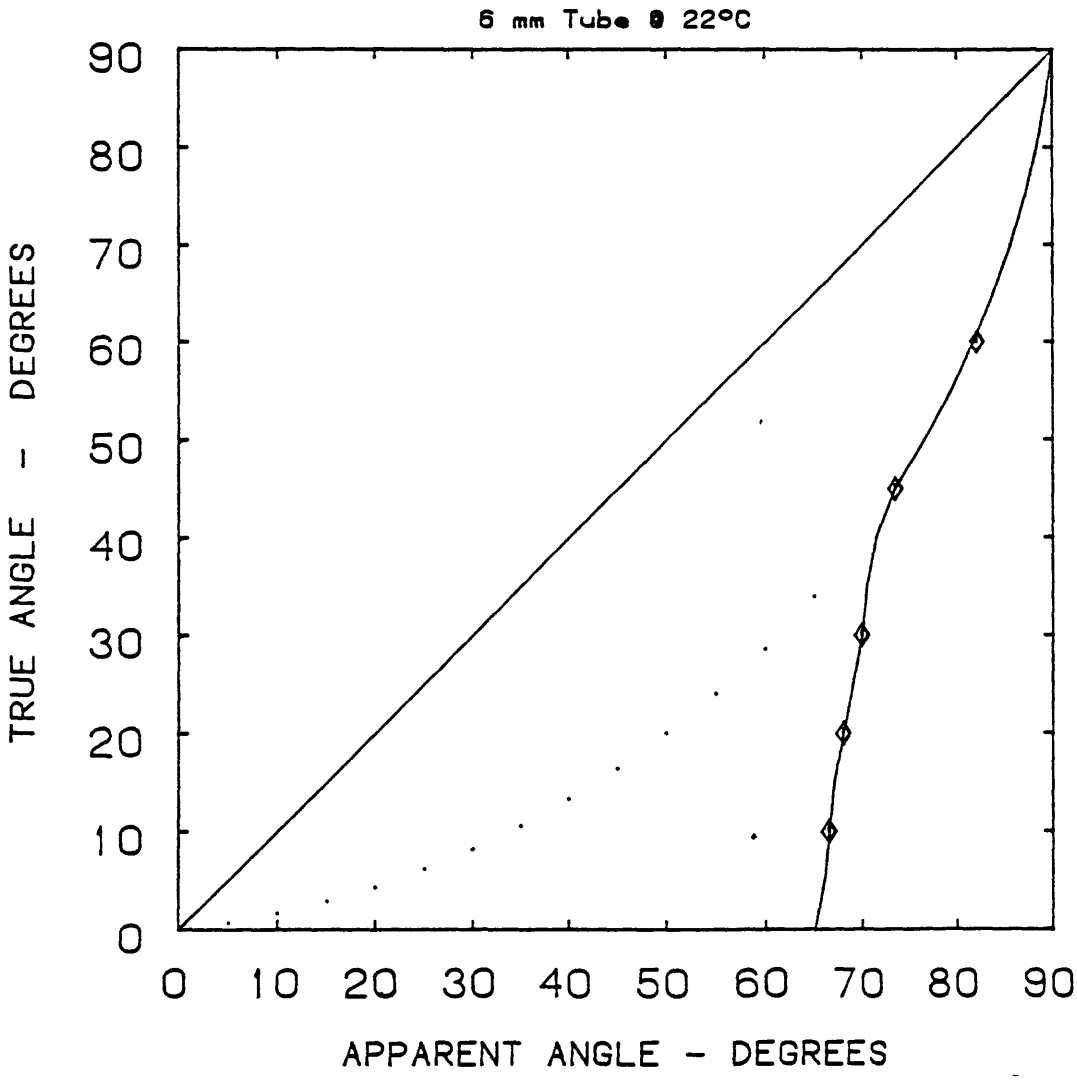

Figure 22. Departure of the apparent angle from circle for 6 mm tubes at 22 °C below 45 degrees true angle. Dots are arc of circle. Diamonds (◇) are measurement points. Values of data points listed in Table 32.

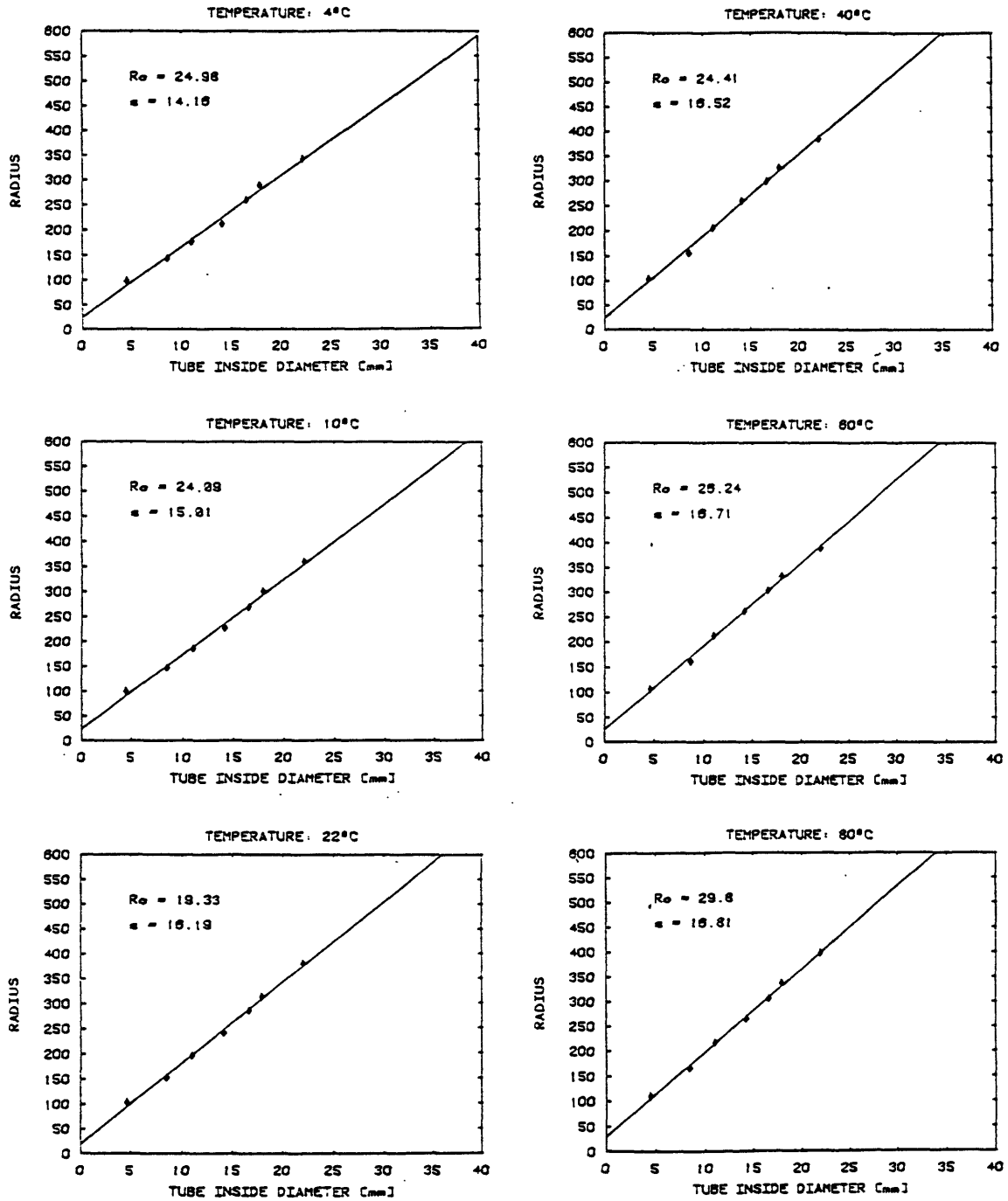

Figure 23. Circle radius (R) versus inside tube diameter (D) at constant temperature for all tubes used in this study. Data points ($\diamond$) for each temperature were fit with a least-squares straight line ($R = R_o + s \times D$). R_o-intercept at zero tube diameter; s-slope.

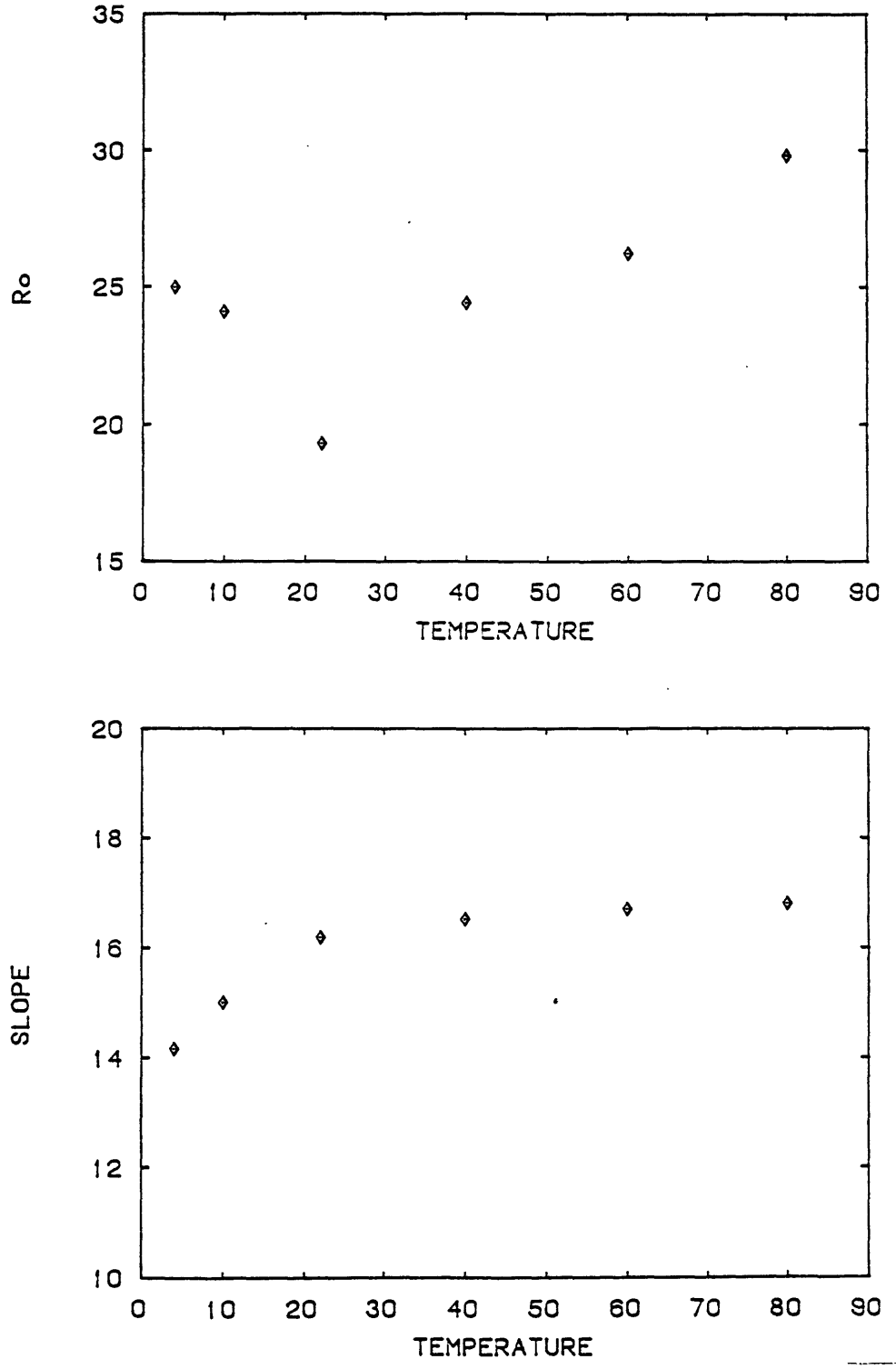

Figure 24. Intercepts (R_o) and slopes (s) from figure 23. Intercepts are not considered physically significant since the minimum R_o is 90. The slopes are approaching an asymptote as suggested by Figure 21.

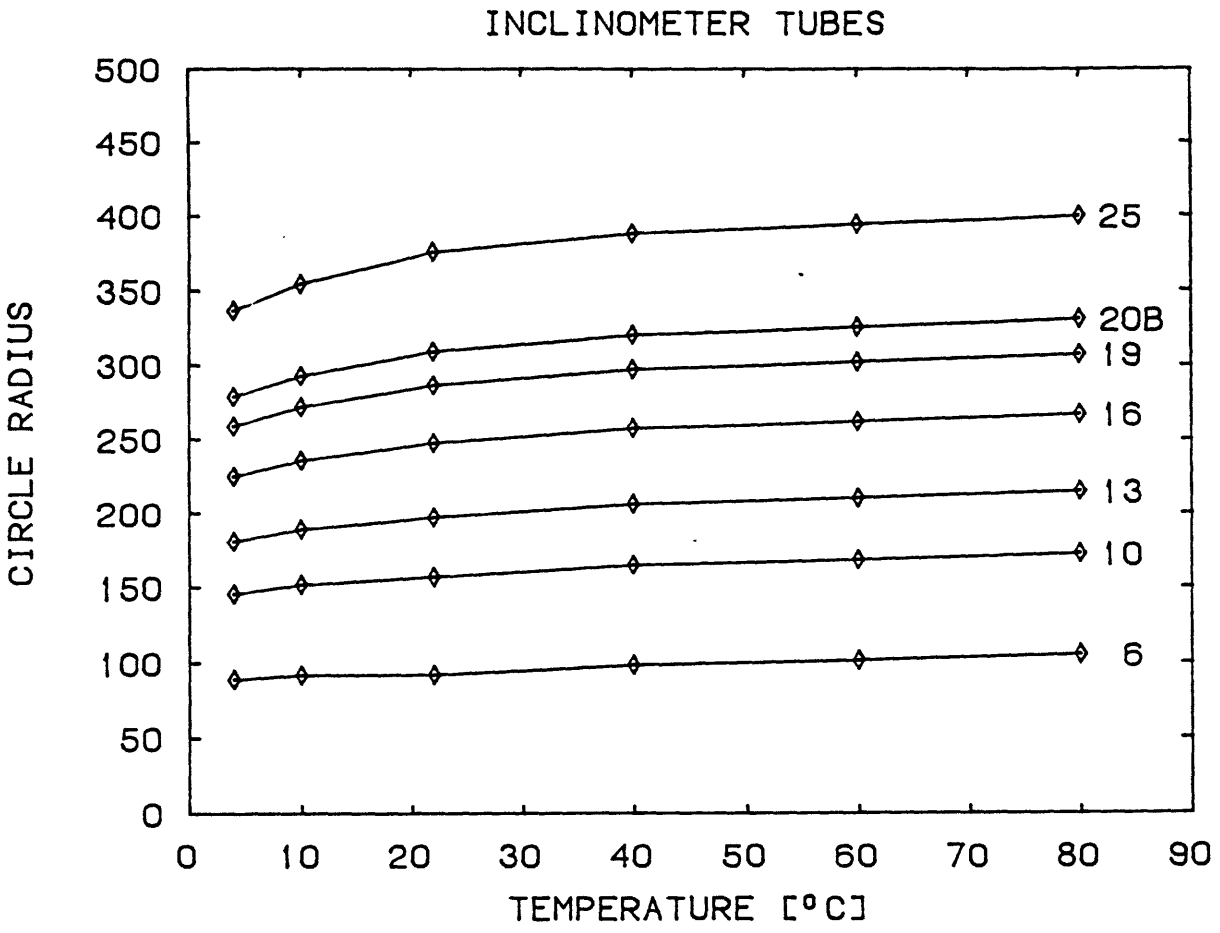

Figure 25. Data from Figure 21 corrected by straight-line equations (Figure 23; Table 33). The straight line corrects the larger diameter tubes producing a smoother curve, whereas the smallest tubes (6 mm) are more irregular.

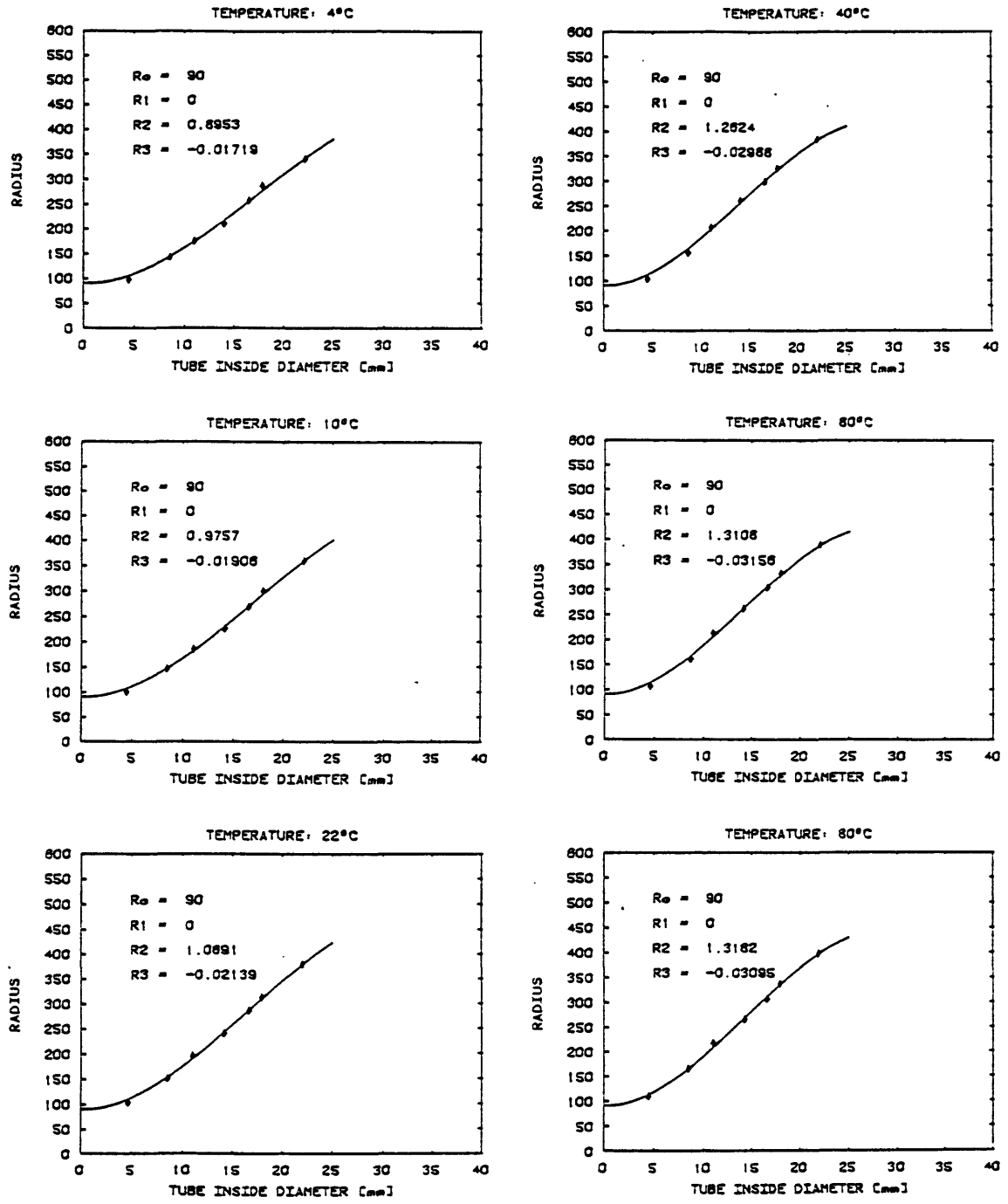

Figure 26. Circle radius (R) versus inside tube diameter (D) at constant temperature for all tubes used in this study. Data points ($\diamond$) were fit using a least squares cubic equation ($R = R_o + R1 \times D + R2 \times D^2 + R3 \times D^3$) constrained to pass through radius 90 (R_o) with $(\partial R/\partial D)_T = 0$ at $D = 0$ ($R1 = 0$).

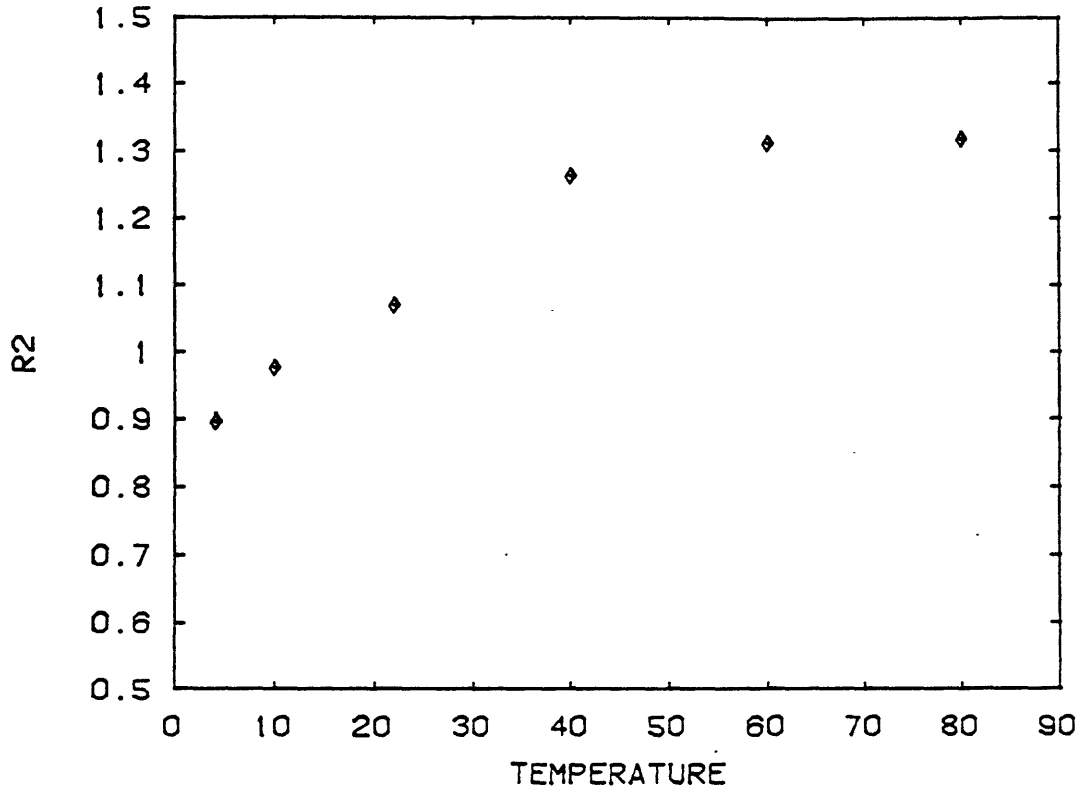

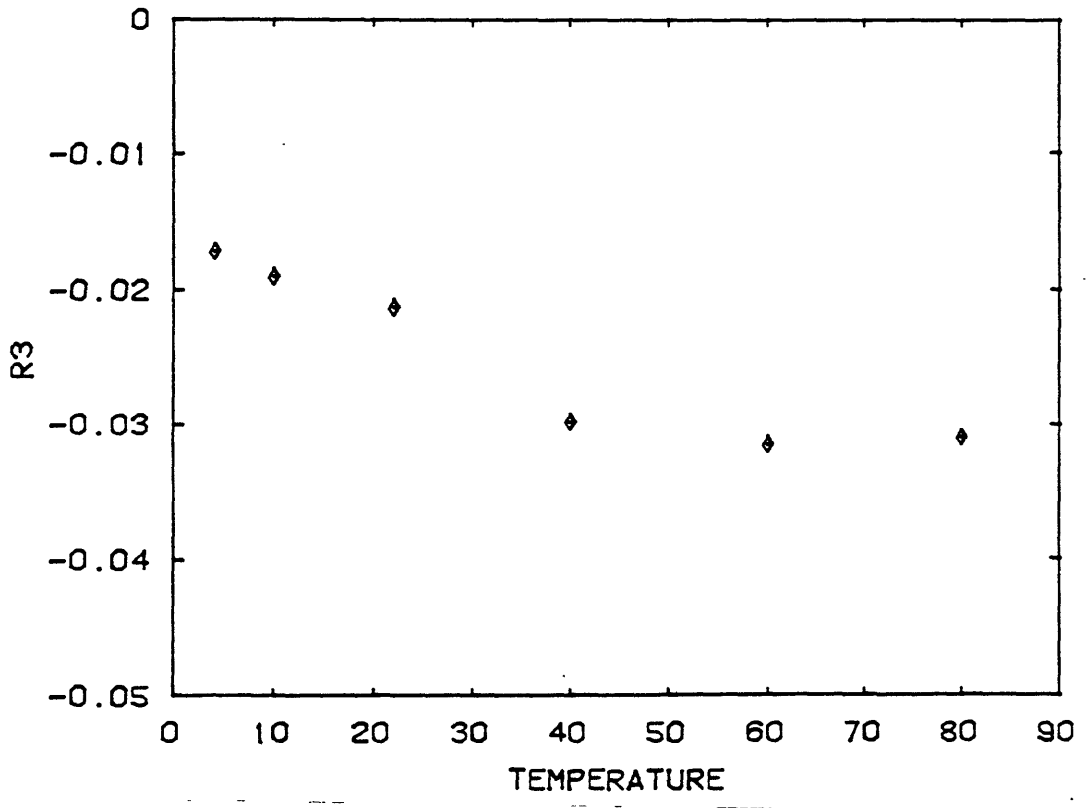

Figure 27. Values of R2 and R3 (Figure 26; Table 33) tend to approach asymptotes at temperaures above 40 °C.

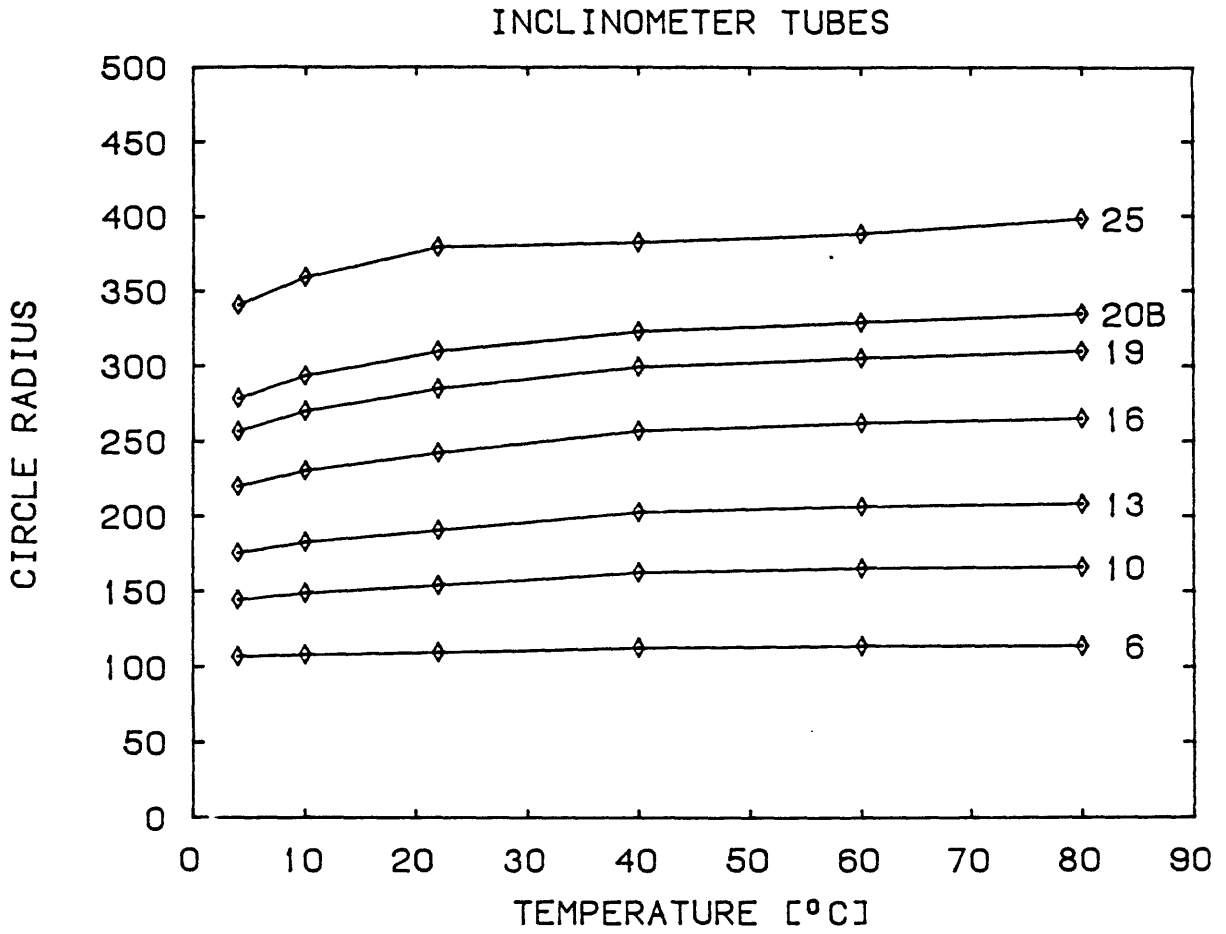

Figure 28. Plot of Figure 21 corrected by least-squares cubic curves of Figure 26 (Table 34). Compared to Figure 25 curves are smoother at small tube diameters but more irregular for 25 mm nominal tubes.

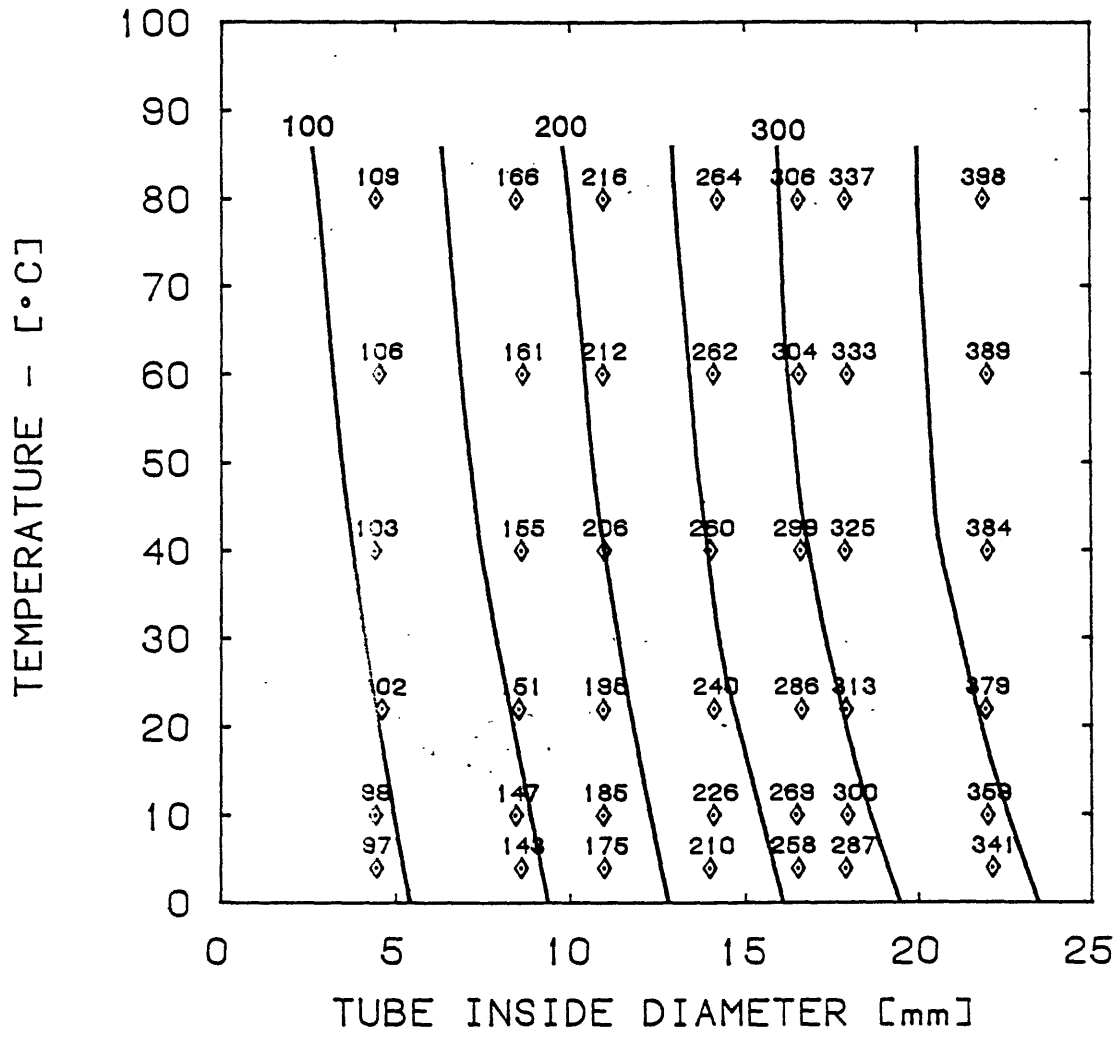

Figure 29. Generalized contours of circle radius against temperature and inside tube diameter. Data points were machine contoured and then smoothed by hand. Circle radii increase by the greatest amount at low temperatures and large diameter (see Figure 21).

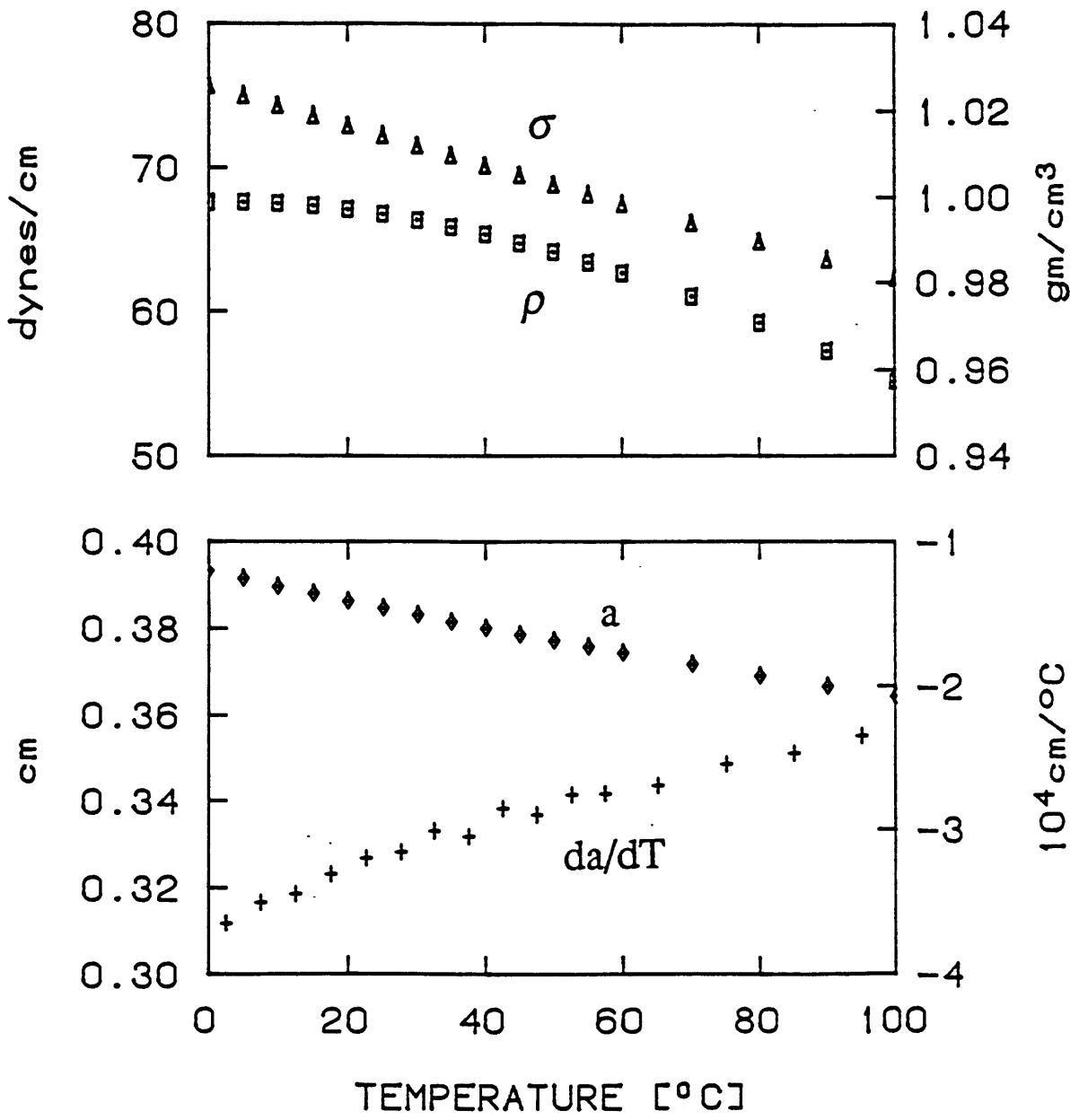

Figure 30. Variation of surface tension (σ), density (ρ), capillary constant (a) and da/dT with temperature. σ is from Partington (1951, p.192) and ρ is from Keenan, *et al.* (1969, Table 1). a and da/dT have been calculated from them. Deviations from smooth curves are a consequence of the number of significant figures tabulated.

REFERENCES

Adam, N.K., 1941, The physics and chemistry of surfaces, 3rd ed.: Oxford University Press, London, 435 p.

Adamson, A.W., 1967, Physical chemistry of surfaces, 2nd ed.: John Wiley and Sons, New York, 747 p.

Apostol, T.M., 1957, Mathematical analysis, a modern approach to advanced calculus: Addison-Wesley Publishing Company, Reading, Massachusetts, 559 p.

Benoit, W.R., 1984, Initial results from drillholes PLV-1 and PLV-2 in the western moat of the Long Valley caldera: Geothermal Resources Council, Transactions, v.8, p.397-402.

Cumming, J.D., 1951, Diamond drill handbook: J.K. Smit & Sons of Canada, Toronto, 501 p.

Cumming, J.D. and Wicklund, A.P., 1980, Diamond drill handbook, 3rd ed.: J.K. Smit, Toronto, 547 p.

Dean, J.A., ed., 1985, Lange's handbook of chemistry, 13th ed.: McGraw-Hill Book Company, New York, 1856 p.

Dorsey, N.E., 1968, Properties of ordinary water-substance: Hafner Publishing Company, new York, 673 p.

Eves, Howard, 1963, A survey of geometry: Allyn and Bacon, Boston, 489 p.

Hald, A., 1952, Statistical theory with engineering applications: John Wiley & Sons, New York, 783 p.

Hoel, P.G., 1962, Introduction to mathematical statistics, 3rd ed.: John Wiley & Sons, New York, 428 p.

Keenan, J.H., Keys, F.G., Hill, P.G., and Moore, J.G., 1969, Steam tables, thermodynamic properties of water including vapor, liquid, and solid phases: John Wiley & Sons, New York, 162 p.

Kimble Glass, Inc., 1988, Kimble, science products catalog K-88, Vineland, New Jersey, 325 p.

Landau, L.D., and Lifshitz, E.M., 1959, Fluid mechanics, Trans. from the Russian by J.B. Sykes and W.H. Reid: Pergamon Press, New York, 536 p.

Nielsen, K.L., 1964, Methods in numerical analysis, 2nd ed.: The MacMillan Company, New York, 408 p.

Olsen, H.W., 1965, Deviations from Darcy's law in saturated clays: Soil Science Society of America Proceedings, v.29(2), p.135-140.

Partington, J.R., 1951, An advanced treatise on physical chemistry, v.2: Logmans, Green and Company, London, 488 p.

Peele, Robert, 1941, Mining engineers' handbook, with collaboration of John A. Church, 3rd ed., v.1: John Wiley & Sons, Inc., New York, 1313 p.

Ratcliffe, E.H., 1963, A survey of most probable values for the thermal conductivity of glasses between about –150 and 100 °C, including new data on twenty-two glasses and a working formula for the calculation of conductivity from composition: Glass Technology, v. 4(4), p. 113-128.

Rayleigh, Lord, 1916, On the theory of the capillary tube: Proceedings of the Royal Society of London, Series A, v. 92, p. 184-195.

Reid, R.C. and Sherwood, T.K., 1966, The properties of gases and liquids, 2nd ed.: McGraw-Hill Book Company, New York, 646 p.

Staley, W.W., 1964, Introduction to mine surveying, 2nd ed.: Stanford University Press, Stanford, California, 303 p.

Taylor, A.E., 1955, Advanced calculus: Blaisdell Publishing Company, New York, 786 p.

Thomas, G.B.,Jr., 1960, Calculus and Analytic Geometry, 3rd ed.: Addison-Wesley Publishing Company, Reading, Massachusetts, 1010 p.

Urban, T.C., Diment, W.H. and Sorey, M.L., 1987, Hydrothermal regime of the southwest moat of Long Valley caldera, Mono County, California, and its relation to seismicity – New evidence from the Shady Rest borehole (RDO8): Geothermal Resources Council, Transactions, v.11, p.391-400.

Washburn, E.W., ed., 1928, International critical tables of numerical data, physics, chemistry and technology, v.4: McGraw-Hill Book Company, New York, 481p.

Wolberg, J.R., 1967, Prediction analysis: D. Van Nostrand Company, Princeton, 291 p.

APPENDIX

C-language program for least-squares fit to arc of a circle with statistical analysis.

```
#include <stdio.h>
#include <math.h>

#define  PC  '\045'  /* ASCII % */
#define  ESC '\033'  /* ASCII escape */

main (argc,argv)  /* Inclinometer tube calibration - Program written 4/21/88  */
                  /* File input for calibration data */
      int argc;
      char *argv[];

{
      int k0 = 9;
      int i,n,ch;
      double x[19],a0;
      double y[19] = {90,85,80,75,70,65,60,55,50,45,40,35,30,
                  25,20,15,10,5,0};
      /* Statistics from Hoel[1962, p. 401-402] */
      double chi2[20] = {6.635,9.21,11.341,13.277,15.086,16.812,18.475,
                  20.09,21.666,23.209,24.725,26.217,27.688,29.141,30.578,
                  32,33.409,34.805,36.191,37.566};
      double stt[20] = {63.657,9.925,5.841,4.604,4.032,3.707,3.499,
                  3.355,3.25,3.169,3.106,3.055,3.012,2.977,2.947,2.921,
                  2.898,2.878,2.861,2.845};
      double chi2i,stti;
      double c[1][2] = {0,0};
      double b,f5,Fa,Fo,Li,Fx,r;
      double s1 = 0.5;
      double s2 = 0.5;
      double e0 = 1.0e-5;
      double s,s5,s6,a2,a3,y1[19],d[19],sf;
      int k = 0;
      double sqrt(), fabs(),floor();
      char title[80];
      FILE *fopen(),*fp;
      /* initialize messages */
      char *msg1 = "Student's t value for ";
      char *msg2 = " degrees of freedom and P=0.005 = ";
      char *msg3 = "Chi-squased value for ";
      char *msg4 = " degrees of freedom and P=0.01 = ";
      if (argc != 2)
                  error("Usage: incal 'filename' ", NULL);
      if ((fp = fopen(argv[1],"r")) == NULL)
                  error("incal: can't open %s",argv[1]);
      else {
                  fgets(title,80,fp);
                  fscanf(fp,"%f",&a0);
                  fscanf(fp,"%d",&n);
                  for(i = 0; i < n; i++) fscanf(fp,"%f",&x[i]);
      }
```

```
b =1.0;

if (n < 19) {
        for (i = 0; i < n; i++)  {
                fscanf(fp,"%f",&y[i]);
        if (y[i] == 45.0) k0 = i; }
        }

fclose(fp);

printf("Initial guess = %5.1f\n",a0);
printf("Is this OK? "); ch = getchar();
        if (ch != 'Y' && ch != 'y') { printf("New initial guess: ");
                scanf("%f",&a0); }

while (fabs(b) > e0)
{ ++k;
        for (i = 0; i < n; i++)
        {
        f5 = sqrt(a0*a0 + (90.0 + a0)*(90.0 + a0) -
                (x[i] + a0)*(x[i] + a0));
        Fa = -1.0 + (a0 + 90.0 - x[i])/f5;
        Fo = y[i] - 90.0 - a0 + f5;
        Fx = -(x[i]+a0)/f5;
        Li = s1*s1 + (Fx*s2)*(Fx*s2);
        c[0][0] = c[0][0] + Fa*Fa/Li;
        c[0][1] = c[0][1] + Fa*Fo/Li;
        }

b = c[0][1]/c[0][0];
a0 -= b;
}

a0 = floor(1000.0*a0 + 0.5)/1000.0;
r = floor(sqrt(a0*a0 + (90.0+a0)*(90.0+a0))*1000.0+0.5)/1000.0;

if (n-1 <= 20) { stti = stt[n-2]; chi2i = chi2[n-2]; }
else { printf("%s%2d%s",msg1,n-1,msg2); scanf("%f",&stti);
        printf("%s%2d%s",msg3,n-1,msg4); scanf("%f",&chi2i); }

s = 0.0;
for (i = 0; i < n; i++)
        { y1[i] = 90.0+a0-sqrt(a0*a0+(90.0+a0)*(90.0+a0)-
                (x[i]+a0)*(x[i]+a0));
        y1[i] = floor(10.0*y1[i]+0.5)/10.0;
        d[i] = y[i]-y1[i];
        s = s+d[i]*d[i]; }
s = sqrt(s/(n-1));
s = floor(10.0*s+0.5)/10.0;
```

```
        s5 = 0.0;
        for (i = 0;i < n; i++) {
                f5 = sqrt(a0*a0+(90.0+a0)*(90.0+a0)-(x[i]+a0)*(x[i]+a0));
                Fa = -1.0 + (a0+90.0-x[i])/f5;
                Fx = -(x[i]+a0)/f5;
                Li = s1*s1+(Fx*s2)*(Fx*s2);
                s5 = s5+(y[i]-y1[i])*(y[i]-y1[i])/Li; }
        s6 = s5;
        s5 = sqrt(s5/(n-1))*sqrt(1.0/c[0][0]);
        a2 = a0-stti*s5;
        a3 = a0+stti*s5;
                f5 = sqrt(a0*a0+(90.0+a0)*(90.0+a0)-(x[k0]+a0)*(x[k0]+a0));
                Fa = -1.0 + (a0+90.0-x[k0])/f5;
                sf = sqrt(Fa*Fa*s5*s5);
        printf("%c[2J%c[1;1H",ESC,ESC); /*clears screen & homes cursor*/
        printf("%s\n",title);
        printf(" Number of data points = %d\n\n",n);
        printf(" (x+a)^2 + (y-(90+a))^2 = r^2 \n");
        printf(" r^2 = a^2 + (90+a)^2 \n");
        printf(" a = %7.3f\n",a0);
        printf(" Uncertainty in a = %6.3f\n",s5);
        printf("%s%2d%s%6.3f\n",msg1,n-1,msg2,stti);
        printf(" 99%c confidence interval = %7.3f < a < %7.3f\n",PC,
                a2,a3);
        printf(" r = %7.3f\n",r);
        printf("%s%2d%s%6.3f\n",msg3,n-1,msg4,chi2i);
        printf(" S = %7.3f\n",s6);
        if (s6 < chi2i) printf(" THIS IS A GOOD FIT!\n");
                else printf(" NOT A GOOD FIT\n");
        printf(" d = %4.1f\n",s);
        printf(" Number of iterations = %d\n",k);
        printf(" Uncertainty of function at %2.0f true degrees = %5.3E\n",
                y[k0],sf);
        printf(" b = %e\n",b);
        for (i = 0; i < n; i++)
        printf("%5.1f(%4.1f)%c",d[i],y[i],(i%5==4 || i==n-1) ? '\n' : ' ');
}

error(s1,s2) /* Print error message and exit */
char *s1,*s2;
{
        printf(s1,s2);
        printf("\n");
        exit(1);
}
```